

---

# MULTI-FIDELITY METHODS FOR UNCERTAINTY PROPAGATION IN KINETIC EQUATIONS

Giacomo Dimarco, Liu Liu, Lorenzo Pareschi & Xueyu Zhu

---

**Abstract.** — The construction of efficient methods for uncertainty quantification in kinetic equations represents a challenge due to the high dimensionality of the models: often the computational costs involved become prohibitive. On the other hand, precisely because of the curse of dimensionality, the construction of simplified models capable of providing approximate solutions at a computationally reduced cost has always represented one of the main research strands in the field of kinetic equations. Approximations based on suitable closures of the moment equations or on simplified collisional models have been studied by many authors. In the context of uncertainty quantification, it is therefore natural to take advantage of such models in a multi-fidelity setting where the original kinetic equation represents the high-fidelity model, and the simplified models define the low-fidelity surrogate models. The scope of this article is to survey some recent results about multi-fidelity methods for kinetic equations that are able to accelerate the solution of the uncertainty quantification process by combining high-fidelity and low-fidelity model evaluations with particular attention to the case of compressible and incompressible hydrodynamic limits. We will focus essentially on two classes of strategies: multi-fidelity control variates methods and bi-fidelity stochastic collocation methods. The various approaches considered are analyzed in light of the different surrogate models used and the different numerical techniques adopted. Given the relevance of the specific choice of the surrogate model, an application-oriented approach has been chosen in the presentation.

---

**Key words and phrases.** — Kinetic equations, Boltzmann equation, uncertainty quantification, moment methods, hydrodynamical limits, multi-fidelity methods, surrogate models.

**Résumé.** — La construction de méthodes rapides pour la quantification de l'incertitude dans les équations cinétiques représente un défi en raison de la grande dimensionnalité des modèles qui impliquent souvent des coûts de calcul prohibitifs. D'autre part, précisément à cause de fléau de la dimension, la construction de modèles simplifiés capables de fournir des solutions approchées à un coût de calcul réduit a toujours représenté l'un des principaux axes de recherche dans le domaine des équations cinétiques. Des approximations basées sur des fermetures appropriées des équations des moments ou sur des modèles collisionnels simplifiés ont été étudiées par de nombreux auteurs. Dans le cadre de la quantification de l'incertitude, il est donc naturel utiliser tels modèles dans un cadre multi-fidélité où l'équation cinétique d'origine représente le modèle haute fidélité, et les modèles simplifiés définissent les modèles à basse fidélité. Ce travail passe en revue quelques résultats récents sur les méthodes multi-fidélité pour les équations cinétiques qui accélèrent la résolution du processus de quantification des incertitudes en combinant des évaluations de modèles haute fidélité et basse fidélité avec une attention particulière au cas des limites hydrodynamiques compressibles et incompressibles. Nous nous concentrerons essentiellement sur deux classes de stratégies : les méthodes des variables de contrôle multi-fidélité et les méthodes de collocation stochastique bi-fidélité. Les différentes approches sont analysées à la lumière des différents modèles simplifiés utilisés et des différentes techniques numériques adoptées. Compte tenu de la pertinence du choix spécifique du modèle de substitution simplifié, une approche orientée aux applications a été choisie dans la présentation.

## Contents

1. Introduction.....	2
2. Fidelity spectrum of kinetic models.....	5
3. Multi-fidelity control variate methods.....	14
4. Bi-fidelity stochastic collocation methods.....	49
5. Conclusions.....	73
References.....	75

## 1. Introduction

The Boltzmann equation is used to model a very large number of different phenomena ranging from rarefied gas flows such as those found in hypersonic aerodynamics, gases in vacuum technologies, or fluids inside microelectromechanical devices [15, 16], to the description of social and biological phenomena [64, 74]. For these reasons, the development of efficient and accurate numerical methods for solving kinetic equations and in particular the Boltzmann equation has experienced great commitment in the past to which contributed

many researchers working in different fields [9, 13, 31, 42, 43, 65, 70, 72, 104]. We refer to [20, 22, 71, 72, 88] for recent monographs, collections and surveys.

In spite of the vast amount of existing research on the approximation of Boltzmann and related equations, the study of kinetic equations with stochastic terms has been considered only in recent years [30, 41, 45, 53, 78, 84, 86, 87, 92, 108]. See in particular the recent collection [46] and the survey [69]. We refer also to [57, 67, 83, 87, 87] for related researches in computational fluid dynamics and hyperbolic conservation laws.

On the other hand, these uncertainties arise naturally in many problems where these models are frequently used. In particular, incomplete knowledge of the interaction mechanism between the particles, imprecise measurements of the initial and boundary data, and unknown details of the domain geometry or forcing terms represent problems that are nearly impossible to overcome in a fully deterministic environment. At the same time, modeling the impact of these uncertainties in the solution is critical to providing reliable results for decision and design processes in applications.

Most of the literature on quantification of uncertainties in kinetic equations is based on the use of Stochastic-Galerkin methods built via generalized Polynomial Chaos (gPC) expansions [19, 40, 45, 53, 92, 101, 108]. Only recently these problems have been analyzed in the framework of statistical sampling methods based on Monte Carlo (MC) techniques [23, 24, 26, 33, 41]. We also cite a related research direction where Monte Carlo sampling has been used in the physical space while the random space is still approximated through gPC expansions [3, 14, 78, 85].

In particular, when dealing with kinetic equations, non-intrusive sampling methods, such as MC sampling, have several advantages over an intrusive gPC approach, as they allow to be used in combination with existing deterministic numerical solvers designed to satisfy certain relevant physical properties [20, 22]. This permits also to use implementations via fast algorithms and parallelization techniques which are essential to reduce the computational complexity [21]. Furthermore, Monte Carlo methods are very effective when the probability distribution of the random inputs is not known analytically or lacks of regularity while the approaches based on stochastic orthogonal polynomials may be impossible to use or may produce low accurate results [33, 60, 102].

One of the challenges central to uncertainty quantification for kinetic equations is the simulation cost. Most of the existing algorithms are mainly developed based on the direct resolution of the main reference model, the so-called high-fidelity model. For many complex systems, in particular, the kinetic equations with multidimensional random inputs, an accurate high-fidelity deterministic simulation can be so time-consuming and memory demanding that only a few high-fidelity simulations can be afforded. Many stochastic algorithms

require repetitive implementations of the deterministic solver, the overall accurate stochastic simulation can be difficult and even computationally infeasible. However, there usually exist some approximate, less complex low-fidelity models which compared to the high-fidelity models, usually contain simplified physics and/or are simulated on a coarser physical mesh, and consequently, own a cheaper computational cost. Although their accuracy may not be high, the low-fidelity models are designed in such a way that they can resolve or capture certain important features of the underlying problem and produce reliable and qualitative predictions. Recently, there has been a surging interest in developing efficient uncertainty quantification algorithms by leveraging the strengths of multiple models where costs and fidelity, to be intended as the capacity of correctly describing the problem under consideration, vary. This approach is known in the literature as the multi-fidelity method [27, 79, 80].

In this work, we precisely survey several recent results about multi-fidelity methods for kinetic equations that accelerate the solution of the uncertainty quantification process based on stochastic samples by combining high-fidelity and low-fidelity model evaluations. This will be done through the introduction of multi-fidelity control variates techniques and bi-fidelity stochastic collocation approaches. The first class of methods uses the knowledge of the space spanned by one or more inexpensive low-fidelity models to improve the accuracy of the Monte Carlo solution at the high-fidelity level [23–25]. The choice of the low fidelity models follows the classical legacy of kinetic equations based on developing a hierarchy of reduced order models through suitable fluid-dynamics and diffusive scalings. Note that this requires the adoption of a suitable asymptotic-preserving solver for the high-fidelity model in order to take full advantage of the multiscale control variate [22].

However, the choice of the samples for the high fidelity solver remains arbitrary. The second methodology, is based on a simpler bi-fidelity setting where a single low-fidelity model is used to effectively inform the selection of representative points in the parameter space and then employ this information to construct accurate approximations to high-fidelity solutions [32, 55, 63, 105–107]. As a result, it does not necessarily require that the low-fidelity and high-fidelity to reside in the same physical space.

Consistent with the discussion above, the remainder of this survey is divided into two main parts. The first part addresses the construction of multi-fidelity Monte Carlo methods based on single or multiple control variates. The focus of this part will be primarily on the Boltzmann equation of rarefied gas dynamics [15, 23, 24]. The concepts will then be extended to the case of kinetic equations in the social and economic sciences where we also discuss how to couple the approach with direct simulation Monte Carlo solvers in the physical space [74, 76]. The second part will cover bi-fidelity approximations based on an appropriate choice of collocation nodes. Initially, the Boltzmann equation

of rarefied gas dynamics will still be discussed. Subsequently, the bi-fidelity approach will be extended to linear transport kinetic equations in the diffusive limit, both in the classical case of neutron transport [49, 54] and in the context of epidemiology [1, 6]. Some final remarks conclude this review.

## 2. Fidelity spectrum of kinetic models

The fidelity of the kinetic models can vary along a broad spectrum between low- and high-fidelity. This sections provide examples of kinetic models across the fidelity spectrum, while defining the benefits and limitations of each model. We first focus on the Boltzmann equation of rarefied gas dynamics (RGD), including in our discussion the related moment equations, their possible closures, and the Bhatnagar-Gross-Krook (BGK) approximation. We next illustrate the quasi-invariant limit for some homogeneous Boltzmann equation of interest in the socio-economic sciences. Finally, we consider kinetic equations of linear transport in the diffusion limit both in the case of classical neutron transport and in recent applications in epidemiology. In Table 1 we summarized the various low- and high-fidelity models.

TABLE 1. Fidelity spectrum of different kinetic models

High-fidelity	Low-fidelity	Application
Homogeneous Boltzmann	- Maxwellian steady state - Homogeneous BGK	Trend to equilibrium
Full Boltzmann	- Euler equations - Navier-Stokes equations - Full BGK	Rarefied gas dynamics
Boltzmann-type models	- Mean-field steady state - Mean-field limit	Socio-economy
Linear transport	- Diffusion limit - Goldstein-Taylor model	Neutron transport
Compartmental transport	- Reaction-diffusion limit - Two-velocity models	Epidemiology

**2.1. The Boltzmann equation of rarefied gas dynamics.** — We consider kinetic equations of the general form [15, 23]

$$(1) \quad \partial_t f + v \cdot \nabla_x f = \frac{1}{\varepsilon} Q(f, f),$$

where  $f = f(z, x, v, t)$ ,  $t \geq 0$ ,  $x \in \mathcal{D} \subseteq \mathbb{R}^{d_x}$ ,  $v \in \mathbb{R}^{d_v}$ ,  $d_x, d_v \geq 1$ , and  $z \in \Omega \subseteq \mathbb{R}^{d_z}$ ,  $d_z \geq 1$ , is a random variable. In (1) the parameter  $\varepsilon > 0$  is the Knudsen number and the particular structure of the interaction term  $Q(f, f)$  depends on the kinetic model considered. The most famous example is represented by the nonlinear Boltzmann equation of rarefied gas dynamics

$$(2) \quad Q(f, f) = \int_{S^{d_v-1} \times \mathbb{R}^{d_v}} B(v, v_*, \omega, z) (f' f'_* - f f_*) dv_* d\omega$$

where  $d_v \geq 2$  and

$$(3) \quad v' = \frac{1}{2}(v + v_*) + \frac{1}{2}(|v - v_*|\omega), \quad v'_* = \frac{1}{2}(v + v_*) - \frac{1}{2}(|v - v_*|\omega).$$

We consider the variable hard sphere (VHS) case with

$$(4) \quad B(v, v_*, \omega, z) = b(z)|v - v_*|^\alpha, \quad -d_v < \alpha \leq 1.$$

The Boltzmann operator  $Q(f, f)$  is such that the local conservation properties are satisfied, i.e.

$$(5) \quad \int_{\mathbb{R}^{d_v}} \phi(v) Q(f, f) dv =: \langle \phi Q(f, f) \rangle = 0,$$

where  $\phi(v) = (1, v, |v|^2/2)^T$  are the collision invariants. In addition, the operator satisfies the entropy inequality

$$(6) \quad \frac{d}{dt} H(f) = \int_{\mathbb{R}^{d_v}} Q(f, f) \log f dv \leq 0, \quad H(f) = \int_{\mathbb{R}^{d_v}} f \log f dv.$$

As a consequence, the functions such that  $Q(f, f) = 0$  are local Maxwellian equilibrium functions

$$(7) \quad f^\infty(\rho, u, T) = \frac{\rho}{(2\pi T)^{d_v/2}} \exp\left(\frac{-|u - v|^2}{2T}\right),$$

where  $\rho, u, T$  are the density, mean velocity and temperature of the gas in the  $x$ -position and at time  $t$  defined as

$$(8) \quad (\rho, \rho u, E)^T = \langle \phi f \rangle, \quad T = \frac{1}{d_v \rho} (E - \rho |u|^2).$$

Integrating now (1) against the collision invariants in the velocity space leads to the following set of non closed conservations laws

$$(9) \quad \partial_t \langle \phi f \rangle + \operatorname{div}_x \langle v \otimes \phi f \rangle = 0.$$

Close to fluid regimes, the mean free path between collisions, and therefore the Knudsen number, is very small (see Figure 1). In this situation, passing to the limit  $\varepsilon \rightarrow 0$  we formally obtain  $Q(f, f) = 0$  from (1) and so  $f = f^\infty$ . Thus,

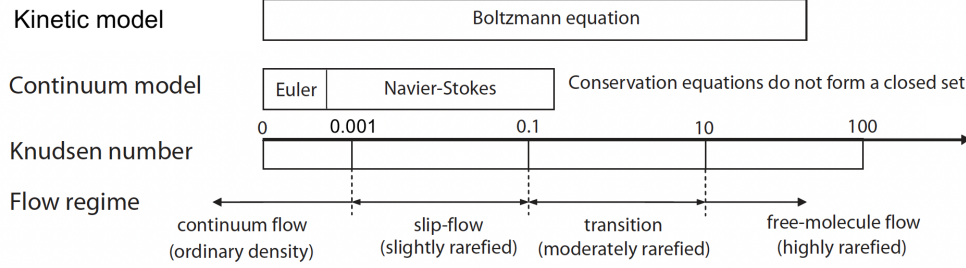


FIGURE 1. The different scales of the Boltzmann equation in rarefied gas dynamics and the corresponding reduced order models

at least formally, we recover the closed hyperbolic system of compressible Euler equations

$$(10) \quad \partial_t U + \nabla_x \cdot \mathcal{F}(U) = 0$$

with  $U = \langle \phi f^\infty \rangle = (\rho, \rho u, E)^T$  and

$$\mathcal{F}(U) = \langle v \otimes \phi f^\infty \rangle = \begin{pmatrix} \rho u \\ \rho u \otimes u + pI \\ Eu + pu \end{pmatrix},$$

$$p = \rho T, \quad T = \frac{1}{3} \left( \frac{2E}{\rho} - |u|^2 \right),$$

where  $I$  is the identity matrix. For small but non zero values of the Knudsen number, the evolution equation for the moments can be derived by the so-called Chapman-Enskog expansion [15]. This originates the compressible Navier-Stokes equations as a second order approximation with respect to  $\varepsilon$  to the solution of the Boltzmann equation

$$(11) \quad \partial_t U + \nabla_x \cdot \mathcal{F}(U) = \varepsilon \nabla_x \cdot \mathcal{D}(\nabla_x U)$$

with

$$(12) \quad \mathcal{D}(\nabla_x U) = \begin{pmatrix} 0 \\ \mu \tau(u) \\ \kappa \nabla_x T + \mu \tau(u) \cdot u \end{pmatrix},$$

$$(13) \quad \tau(u) = \frac{1}{2} (\nabla_x u + (\nabla_x u)^T) - \frac{2}{3} \operatorname{div}_x u I,$$

with the viscosity  $\mu$  and the thermal conductivity  $\kappa$  defined according to the Boltzmann operator [15]. The Prandtl number in this setting is defined as the ratio  $Pr = 5\mu/(2\kappa)$ .

A simplified kinetic model is obtained by replacing (2) by a relaxation operator towards the local Maxwellian state. This model is usually referred to as BGK model since its introduction by Bhatnagar, Gross and Krook [8]

$$(14) \quad Q(f)(v) = \nu(f^\infty[f] - f).$$

In (14) the function  $M[f]$  is the local Maxwellian and  $\nu$ , in general, is proportional to the density and depends on the temperature  $\nu(\rho, T)$ . For instance, a frequently used law is given by  $\nu = C\rho T^{1-\eta}$ , where  $C > 0$  is a constant and  $\eta$  is the exponent of the viscosity law of the gas [58]. Conservation of mass, momentum and energy as well as Boltzmann's H-theorem are readily satisfied and the equilibrium solutions are Maxwellians. Furthermore, the model has the correct fluid dynamic limit, since as  $\varepsilon \rightarrow 0$  formally the moments  $\rho$ ,  $\rho u$ , and  $E$  satisfy the compressible Euler equations (10). However, this model exhibits some unphysical features, such as an unrealistic Prandtl number  $Pr = 1$ . The correct Navier-Stokes limit (11) can be recovered using more sophisticated BGK models such as the Ellipsoidal Statistical BGK (ES-BGK) models [39].

The Boltzmann equation (1) and its low-fidelity counterparts such as the BGK equation (14) and the compressible Euler (10) and Navier-Stokes (11) systems will be employed as leading examples both for the development of the control variate multi-fidelity methods in Section 3 as well as in the case of the stochastic collocation bi-fidelity approach in Section 4.

**2.2. Kinetic models for the social sciences.** — Recently, Boltzmann-type models have also become quite popular for describing binary dynamics between agents, representing individuals interacting in a society (see [74] for an introduction to the topic). In presence of uncertainties, the pair of interacting agents is characterized by the pre-interaction states  $v, w \in V \subseteq \mathbb{R}$  and the post-interaction states  $v', w' \in V$  obtained as follows [26, 76]

$$(15) \quad \begin{aligned} v' &= v + \gamma[(p_1(z) - 1)v + q_1(z)w] + D(v, z) \eta, \\ w' &= w + \gamma[p_2(z)v + (q_2(z) - 1)w] + D(w, z) \eta^*, \end{aligned}$$

where  $\gamma > 0$  is a given constant,  $p_i, q_i$ ,  $i = 1, 2$ , are suitable interaction functions depending on a random variable  $z \in \Omega \subseteq \mathbb{R}^{d_z}$ . Furthermore,  $\eta$  and  $\eta^*$  are i.i.d. random variables with zero mean and variance  $\sigma^2$ . The function  $D(\cdot, z)$  defines the local relevance of the diffusion.

Introducing the distribution function  $f = f(t, w, z)$ , its evolution is given in terms of the Boltzmann-type equation

$$(16) \quad \begin{aligned} & \frac{d}{dt} \int_V f(t, w, z) \varphi(w) dw \\ &= \frac{1}{2} \left\langle \iint_{V^2} (\varphi(w') + \varphi(v') - \varphi(w) - \varphi(v)) f(t, w, z) f(t, v, z) dw dv \right\rangle_\eta \end{aligned}$$



being  $\varphi : V \rightarrow \mathbb{R}$  any observable quantity which may be expressed as a function of the microscopic state  $w$  of the agents. The symbol  $\langle \cdot \rangle_\eta$  denotes the expectation with respect to  $\eta$ . Taking  $\varphi(w) = 1$  is easily seen that the number of agents is conserved in time.

In contrast to the classical Boltzmann case (1), the equilibrium states of the socio-economic Boltzmann models like (16) are often unknown. A way to achieve some insight into the long time behavior of such systems is to consider the quasi-invariant interaction limit [73, 74, 99]. To that aim, given a small parameter  $\varepsilon > 0$ , let us introduce the scaling

$$(17) \quad \gamma \rightarrow \varepsilon, \quad \sigma \rightarrow \sqrt{\varepsilon}\sigma, \quad t \rightarrow \varepsilon t,$$

and denote by  $f_\varepsilon(t, w, z)$  the scaled distribution. Thus, small values of  $\varepsilon$  correspond to the case in which elementary interactions (15) produce minimal modification of  $v$  and  $w$  and, at the same time, the frequency of such interactions increases like  $1/\varepsilon$ . Then, the distribution  $f_\varepsilon$  is solution to

$$(18) \quad \frac{d}{dt} \int_V \varphi(w) f_\varepsilon(t, w, z) dw = \frac{1}{2\varepsilon} \left\langle \iint_{V^2} (\varphi(w') + \varphi(v') - \varphi(v) - \varphi(w)) f_\varepsilon(t, w, z) f_\varepsilon(t, v, z) dw dv \right\rangle_\eta.$$

Now, for small values of  $\varepsilon$  using a Taylor expansion of the interactions it can be shown that in the limit  $\varepsilon \rightarrow 0$ ,  $f_\varepsilon$  converges, up to subsequences, to a distribution function  $\tilde{f} = \tilde{f}(t, w, z)$  which is weak solution to the following Fokker-Planck equation

$$(19) \quad \begin{aligned} \partial_t \tilde{f}(t, w, z) + \partial_w \left[ \left( \int_V P(v, w, z) \tilde{f}(t, v, z) dv \right) \tilde{f}(t, w, z) \right] \\ = \frac{\sigma^2}{2} \partial_w^2 (D^2(w, z) \tilde{f}(t, w, z)), \end{aligned}$$

where

$$P(v, w, z) = \frac{1}{2} [(p_1(z) + q_2(z) - 2)w + (p_2(z) + q_1(z))v]$$

provided that suitable boundary conditions are taken for  $w \in \partial V$ .

We shortly present now two socio-economic models used in the rest of the survey as examples for developing our multi-fidelity Monte Carlo methods. The first is an opinion formation model where we set  $V = [-1, 1]$  and the binary interaction rules read [2, 74, 75]

$$(20) \quad \begin{aligned} v' &= v + \varepsilon p(|w - v|, z)(w - v) + D(v)\eta, \\ w' &= w + \varepsilon p(|v - w|, z)(v - w) + D(w)\eta, \end{aligned}$$

where the function  $0 \leq p(|v - w|, z) \leq 1$  weights the compromise tendency with respect to the relative opinion  $|v - w|$ . In the quasi-invariant limit, the

following model is obtained

$$\begin{aligned} \partial_t \tilde{f}(t, w, z) + \partial_w \left[ \left( \int_V p(|v-w|, z) (v-w) \tilde{f}(t, v, z) dv \right) \tilde{f}(t, w, z) \right] \\ = \frac{\sigma^2}{2} \partial_w^2 (D^2(w, z) \tilde{f}(t, w, z)). \end{aligned}$$

If  $p(|v-w|, z) = p(z)$  in (20),  $D(w, z) = 1 - w^2$ , and we consider uncertainties in the initial distribution, the steady state distribution of the Fokker-Planck model reads

$$(21) \quad \tilde{f}_\infty(w, z) = C(z) (1+w)^{-2+\frac{p(z)m(z)}{2\sigma^2}} \times \\ (1-w)^{-2-\frac{p(z)m(z)}{2\sigma^2}} \exp \left\{ -\frac{p(z)(1-m(z)w)}{\sigma^2(1-w^2)} \right\},$$

where  $C(z)$  is a normalization factor such that  $\int_V \tilde{f}_\infty(w, z) dw = 1$ . Other form of equilibrium distribution can be determined as well [75].

For example the choice  $D(w) = \sqrt{1-w^2}$  produce a Beta-type steady state of the form

$$(22) \quad \tilde{f}_\infty(w, z) = 2^{1-\frac{2}{\sigma^2}} \frac{1}{B\left(\frac{1+m(z)}{\sigma^2}, \frac{1-m(z)}{\sigma^2}\right)} (1+w)^{\frac{1+m(z)}{\sigma^2}-1} (1-w)^{\frac{1-m(z)}{\sigma^2}-1},$$

where  $B(\cdot, \cdot)$  is the Beta function. We refer to [75] for a detailed discussion.

The second example, known as the Cordier-Pareschi-Toscani (CPT) model [18, 74] for wealth exchanges between agents composing a simple economy. The wealth variable is here allowed to take values on the positive half line therefore  $V = \mathbb{R}^+$ . The binary interactions with reference to (15) are such that  $p_1 = q_2 = q(z)$  and  $p_2 = q_1 = \lambda(z)$  with  $q(z) = 1 - \lambda(z)$ . We also consider  $D(w, z) = w$ . The uncertain parameter  $\lambda(z) \in (0, 1)$  determines the proportion of wealth that a single agents wants to invest, the quantity  $1 - \lambda(z)$  is the so-called saving propensity. Thus, the binary scheme for wealth exchanges reads

$$(23) \quad \begin{aligned} v' &= (1 - \varepsilon\lambda(z))v + \varepsilon\lambda(z)w + v\eta \\ w' &= (1 - \varepsilon\lambda(z))w + \varepsilon\lambda(z)v + w\eta. \end{aligned}$$

The corresponding mean field model reads

$$\partial_t \tilde{f}(t, w, z) + \lambda(z) \partial_w \left[ (m_{\tilde{f}}(z) - w) \tilde{f}(t, w, z) \right] = \frac{\sigma^2}{2} \partial_w^2 (w^2 \tilde{f}(t, w, z)),$$

If we assume that there is no uncertainty in the initial conditions, following [74] the equilibrium state can be computed and reads

$$(24) \quad \tilde{f}_\infty(w, z) = \frac{(\mu(z) - 1)^{\mu(z)}}{\Gamma(w) w^{1+\mu(z)}} \exp \left( -\frac{(\mu(z) - 1)m_{\tilde{f}}(z)}{w} \right),$$

where  $\Gamma(\cdot)$  denotes the Gamma function and  $\mu(z) = 1 + 2\lambda(z)/\sigma^2$ . We refer to Section 3.6 for applications of control variate strategies based on the mean-field equilibrium states (21) and (24) or on the full mean-field system (19).

**2.3. Linear transport equations.** — Another class of kinetic models that will be considered in the sequel are the linear transport equation under diffusive scaling and with random parameters [45, 49, 54]. Let  $f(t, x, v, z)$  be the probability density distribution of particles at time  $t > 0$ , position  $x \in \mathcal{D} \subseteq \mathbb{R}$ , and with  $v \in [-1, 1]$  the cosine of the angle between the particle velocity and its position. In particular, we consider in our discussion the case of random scattering coefficients  $\sigma(x, z)$  with  $z \in \Omega \subseteq \mathbb{R}^{d_z}$  a random vector. The time evolution of the distribution function  $f$  is governed by the following linear transport equation under diffusive scaling

$$(25) \quad \varepsilon \partial_t f + v \partial_x f = \frac{\sigma(x, z)}{\varepsilon} \left[ \frac{1}{2} \int_{-1}^1 f(v') dv' - f \right],$$

where  $\varepsilon$  is the Knudsen number. In order to shed light on the link between the kinetic equation and its diffusive limit, we first split (25) into two equations for  $v > 0$

$$(26) \quad \begin{aligned} \varepsilon \partial_t f(v) + v \partial_x f(v) &= \frac{\sigma(x, z)}{\varepsilon} \left[ \frac{1}{2} \int_{-1}^1 f(v') dv' - f(v) \right], \\ \varepsilon \partial_t f(-v) - v \partial_x f(-v) &= \frac{\sigma(x, z)}{\varepsilon} \left[ \frac{1}{2} \int_{-1}^1 f(v') dv - f(-v) \right]. \end{aligned}$$

where we omitted for brevity the dependence from  $(t, x, z)$  in the kinetic density. By using now the so-called even-odd decomposition [48], we introduce then the relative even and odd parities

$$(27) \quad \begin{aligned} r(t, x, v, z) &= \frac{1}{2} [f(t, x, v, z) + f(t, x, -v, z)], \\ j(t, x, v, z) &= \frac{1}{2\varepsilon} [f(t, x, v, z) - f(t, x, -v, z)]. \end{aligned}$$

Thanks to the above reformulation, the system (26) can then be recast in the following form:

$$(28) \quad \begin{cases} \partial_t r + v \partial_x j = \frac{\sigma(x, z)}{\varepsilon^2} (\rho - r), \\ \partial_t j + \frac{v}{\varepsilon^2} \partial_x r = -\frac{\sigma(x, z)}{\varepsilon^2} j, \end{cases}$$

where

$$(29) \quad \rho(t, x) = \int_0^1 r dv.$$

Now the formal passage to the limit is easily obtained. In fact, as  $\varepsilon \rightarrow 0$ , the system (28) yields

$$r = \rho, \quad j = -\frac{v}{\sigma(x, z)} \partial_x \rho.$$

Substituting back this limit it into the same system (28) and integrating over  $v$ , one gets the limiting diffusion equation [4, 49]

$$(30) \quad \begin{cases} j = -\frac{v}{\sigma(x, z)} \partial_x \rho, \\ \partial_t \rho = \partial_x \left[ \frac{1}{3\sigma(x, z)} \partial_x \rho \right]. \end{cases}$$

The neutron transport equation (25) and its low-fidelity diffusive limit (30) are employed in Section 2.3 to design efficient bi-fidelity approximations, together with a different low-fidelity models given by the Goldstein-Taylor model [54, 74].

**2.4. Kinetic models in epidemiology.** — We consider the development of hyperbolic transport models for the propagation in space of an epidemic phenomenon described by a classical compartmental dynamics [1, 5, 10]. The model is based on a kinetic description with discrete velocities of the spatial movement and interactions of a population of susceptible, infected and recovered individuals. The model is constructed in such a way that a diffusive behavior of the spread can be recovered in a suitable limit similar to the one described in Section 2.3. In the considered framework, the distributions of individuals at position  $x \in \mathcal{D} \subseteq \mathbb{R}$  at time  $t$  moving with velocity  $v \in [-1, 1]$  are then denoted by

$$f_S = f_S(x, v, t, z), \quad f_I = f_I(x, v, t, z), \quad f_R = f_R(x, v, t, z).$$

These quantities represent, respectively, the fraction of susceptible individuals  $S$  (who may be infected by the disease), the fraction of infected individuals  $I$  (who may transmit the disease) and removed individuals  $R$  (healed or died due to the disease). We assume to have a population without an a-priori immunity and we neglect the vital dynamics represented by births and deaths due to the time scale considered. The densities for  $S$ ,  $I$  and  $R$  are given by

$$(31) \quad \begin{aligned} S(x, t, z) &= \int_{-1}^1 f_S(x, v, t, z) dv \\ I(x, t, z) &= \int_{-1}^1 f_I(x, v, t, z) dv \\ R(x, t, z) &= \int_{-1}^1 f_R(x, v, t, z) dv. \end{aligned}$$

In this setting, the distribution functions satisfy the epidemic transport equations

$$(32) \quad \begin{aligned} \frac{\partial f_S}{\partial t} + \frac{\partial(v_S f_S)}{\partial x} &= -F(f_S, I) + \frac{1}{\tau_S} \left( \frac{S}{2} - f_S \right) \\ \frac{\partial f_I}{\partial t} + \frac{\partial(v_I f_I)}{\partial x} &= F(f_S, I) - \gamma f_I + \frac{1}{\tau_I} \left( \frac{I}{2} - f_I \right) \\ \frac{\partial f_R}{\partial t} + \frac{\partial(v_R f_R)}{\partial x} &= \gamma f_I + \frac{1}{\tau_R} \left( \frac{R}{2} - f_R \right), \end{aligned}$$

where  $v_S = \lambda_S(x)v$ ,  $v_I = \lambda_I(x)v$ ,  $v_R = \lambda_R(x)v$  with  $\lambda_S, \lambda_I, \lambda_R \geq 0$  take into account the heterogeneities of geographical areas, thus are chosen dependent on the spatial location. The quantity  $\gamma = \gamma(x, z)$  is the recovery rate of infected, and the transmission of infection is governed by an incidence function  $F(\cdot, I)$  modeling the transmission of the disease [38]

$$(33) \quad F(g, I) = \beta \frac{gI^p}{1 + \kappa I},$$

with the classic bi-linear case corresponding to  $p = 1$ ,  $\kappa = 0$ . Finally,  $\tau_S, \tau_I, \tau_R$  represent the relaxation frequencies playing the role of the Knudsen number  $\varepsilon$  introduced in Section 2.3 when discussing the linear transport equation in the diffusive scaling. In this model, the reproduction number for the system (32) is given by

$$(34) \quad R_0(t, z) = \frac{\int_{\mathcal{D}} F(S, I) dx}{\int_{\mathcal{D}} \gamma(x, z) I(x, t, z) dx} \geq 1.$$

This quantity describes the space averaged instantaneous variation of the number of infected individuals at time  $t > 0$ . Now, with the scope of deriving a possible surrogate/low-fidelity model approaching the high fidelity model described by system (32), we introduce the flux functions

$$(35) \quad \begin{aligned} J_S &= \lambda_S \int_{-1}^1 v f_S(x, v, t, z) dv, \\ J_I &= \lambda_I \int_{-1}^1 v f_I(x, v, t, z) dv, \\ J_R &= \lambda_R \int_{-1}^1 v f_R(x, v, t, z) dv. \end{aligned}$$

We integrate then the system (32) over  $v$  and obtain the following equations for the macroscopic densities

$$(36) \quad \begin{aligned} \frac{\partial S}{\partial t} + \frac{\partial J_S}{\partial x} &= -F(S, I) \\ \frac{\partial I}{\partial t} + \frac{\partial J_I}{\partial x} &= F(S, I) - \gamma I \\ \frac{\partial R}{\partial t} + \frac{\partial J_R}{\partial x} &= \gamma I. \end{aligned}$$

The above system is not closed since the flux functions depend upon the distribution functions values. However, by introducing now the so-called diffusion coefficients that characterize the diffusive transport mechanism of susceptible, infected and removed

$$(37) \quad D_S = \frac{1}{3}\lambda_S^2\tau_S, \quad D_I = \frac{1}{3}\lambda_I^2\tau_I, \quad D_R = \frac{1}{3}\lambda_R^2\tau_R,$$

one can pass to the limit  $\tau_J \rightarrow 0$ ,  $J = S, I, R$  while keeping the diffusive coefficients finite. This permits to get the following diffusion system characterizing a possible low fidelity model for the spread of a disease

$$(38) \quad \begin{aligned} \frac{\partial S}{\partial t} &= -F(S, I) + \frac{\partial}{\partial x} \left( D_S \frac{\partial S}{\partial x} \right) \\ \frac{\partial I}{\partial t} &= F(S, I) - \gamma I + \frac{\partial}{\partial x} \left( D_I \frac{\partial I}{\partial x} \right) \\ \frac{\partial R}{\partial t} &= \gamma I + \frac{\partial}{\partial x} \left( D_R \frac{\partial R}{\partial x} \right). \end{aligned}$$

In Section 4.4 we will discuss strategies for quantifying uncertainty for the above model while also introducing an alternative low-fidelity model based on a simpler two-velocity dynamic [6, 7].

### 3. Multi-fidelity control variate methods

This part introduces the multi-fidelity control variate methods for the Boltzmann equation of gas dynamic introduced in Section 2.1 and then discusses its extension to the kinetic models in the social sciences presented in Section 2.2.

**3.1. Some notations and definitions.** — First we introduce some notations and assumptions that will be used in the sequel of the section. If  $z \in \Omega$  is distributed as  $p(z)$  we denote the expected value of any *quantity of interest* expressed as a functional  $q[f](z, x, v, t)$  by

$$(39) \quad \mathbb{E}[q[f]](x, v, t) = \int_{\Omega} q[f](z, x, v, t)p(z)dz,$$

and its variance by

$$(40) \quad \text{Var}(q[f])(x, v, t) = \int_{\Omega} (q[f](z, x, v, t) - \mathbb{E}[q[f]](x, v, t))^2 p(z) dz.$$

As quantity of interest, in addition to  $q[f] = f$ , another natural choice is represented by  $q[f] = \langle \phi, f \rangle$ , the moments of the distribution function. In the latter case the dependence on  $v$  is dropped in the previous definitions.

We also introduce the following  $L^p$ -norm with polynomial weight [82, 90]

$$(41) \quad \|f(z, \cdot, t)\|_{L_s^p(\mathcal{D} \times \mathbb{R}^{d_v})}^p = \int_{\mathcal{D} \times \mathbb{R}^{d_v}} |f(z, x, v, t)|^p (1 + |v|)^s dv dx.$$

Next, for a random variable  $Z$  taking values in  $L_s^p(\mathcal{D} \times \mathbb{R}^{d_v})$ , we define

$$(42) \quad \|Z\|_{L_s^p(\mathcal{D} \times \mathbb{R}^{d_v}; L^2(\Omega))} = \|\mathbb{E}[Z^2]^{1/2}\|_{L_s^p(\mathcal{D} \times \mathbb{R}^{d_v})}.$$

The above norm, in general, differs from a more classical norm used in the context of uncertainty quantification for hyperbolic conservation laws. This latter often reads

$$(43) \quad \|Z\|_{L^2(\Omega; L_s^p(\mathcal{D} \times \mathbb{R}^{d_v}))} = \mathbb{E} \left[ \|Z\|_{L_s^p(\mathcal{D} \times \mathbb{R}^{d_v})}^2 \right]^{1/2},$$

which has been used for example in [60]. Note, in particular that by Jensen inequality [89], we have

$$(44) \quad \|Z\|_{L_s^p(\mathcal{D} \times \mathbb{R}^{d_v}; L^2(\Omega))} \leq \|Z\|_{L^2(\Omega; L_s^p(\mathcal{D} \times \mathbb{R}^{d_v}))}.$$

Let also observe that for  $p = 2$  the two norms (42) and (43) coincide. In the sequel, we will consider in our analysis the norm (42) with  $p = 1$ . The extension of the results shown about the control variate approach to norm (43) for  $p = 1$  typically requires  $Z$  to be compactly supported (see [23, 59, 60] for further details).

We assume that the model (1) is solved in the phase-space by means of deterministic methods and that the following estimate is satisfied (see [22, 23, 61, 90, 93])

$$(45) \quad \|f(\cdot, t^n) - f_{\Delta x, \Delta v}^n\|_{L_2^1(\mathcal{D} \times \mathbb{R}^{d_v})} \leq C (\Delta x^{q_1} + \Delta v^{q_2}),$$

with  $C$  a positive constant which depends on time and on the initial data, and  $f_{\Delta x, \Delta v}^n$  the computed approximation of the deterministic solution  $f(x, v, t)$  at time  $t^n$  on the mesh  $\Delta x$  and  $\Delta v$ . The positive integers  $q_1$  and  $q_2$  characterize the accuracy of the discretizations in the phase-space and, for simplicity, we ignored the errors due to the time discretization and to the truncation of the velocity domain in the deterministic solver. We refer to [22] for details about the numerical discretization of a kinetic equation of the form (1). In the sequel, if not otherwise stated, in the numerical examples we will make use of the fast spectral method [29, 61] combined with finite volumes WENO solvers

in space [44]. The time discretization is performed by suitable asymptotic-preserving techniques [22].

**3.2. Monte Carlo sampling method.** — Before discussing the multi-fidelity approach, we first recall the standard Monte Carlo method for the estimation of the uncertainties when computing the solution of a kinetic equation of the type (1) with random initial data  $f(z, x, v, 0) = f_0(z, x, v)$ . To avoid unnecessary difficulties, we will mainly restrict to the case of a one-dimensional random input  $d_z = 1$  distributed as  $p(z)$ , the extension to multidimensional setting being straightforward.

The simplest Monte Carlo (MC) sampling method for UQ is described in Algorithm 1.

---

**Algorithm 1:** Monte Carlo sampling method

---

1. **Sampling:** Sample  $M$  independent identically distributed (i.i.d.) initial data  $f_0^k$ ,  $k = 1, \dots, M$  from the random initial data  $f_0$  and approximate these over the grid.
2. **Solving:** For each realization  $f_0^k$ , the underlying kinetic equation (1) is solved numerically by a deterministic solver. We denote the solutions at time  $t^n$  by  $f_{\Delta x, \Delta v}^{k,n}$ ,  $k = 1, \dots, M$ , where  $\Delta x$  and  $\Delta v$  characterizes the discretizations in  $x$  and  $v$ .
3. **Estimating:** Estimate the expected value of the random solution field with the sample mean of the approximate solution

$$(46) \quad E_M[f_{\Delta x, \Delta v}^n] = \frac{1}{M} \sum_{k=1}^M f_{\Delta x, \Delta v}^{k,n}.$$


---

Similarly to the case of the expectation, higher order statistical moments can be computed as well. The above algorithm present several advantages:

- i) Straightforward to implement in any existing deterministic or stochastic solver for the particular kinetic equation.
- ii) It operates in a *post-processing* setting, the only data interaction between different samples is in step 3, when ensemble averages are computed.
- iii) It is non-intrusive and easily parallelizable.

Concerning the error analysis, starting from the fundamental estimate [12, 56]

$$(47) \quad \mathbb{E} [(\mathbb{E}[f] - E_M[f])^2] \leq C \text{Var}(f) M^{-1},$$

one can obtain the typical error bound which is summarized by the following proposition (see [23, 59, 60] for more details).



**Proposition 3.1.** — Consider a deterministic scheme satisfying (45) for equation (1) with random sufficiently regular initial data  $f(z, x, v, 0) = f_0(z, x, v)$ . Then, the Monte Carlo estimate (46) satisfies the error bound (48)

$$\|\mathbb{E}[f](\cdot, t^n) - E_M[f_{\Delta x, \Delta v}^n]\|_{L^1_2(\mathcal{D} \times \mathbb{R}^{d_v}; L^2(\Omega))} \leq C \left( \sigma_f M^{-1/2} + \Delta x^{q_1} + \Delta v^{q_2} \right),$$

where  $\sigma_f = \|\text{Var}(f)^{1/2}\|_{L^1_2(\mathcal{D} \times \mathbb{R}^{d_v})}$ ,  $\text{Var}(f) = \mathbb{E}[(\mathbb{E}[f] - f)^2]$  and the constant  $C = C(T, f_0) > 0$  depends on the final time  $T$  and the initial data  $f_0$ .

Once an error estimate is given, it is possible to equilibrate the discretization and the sampling errors in the a-priori estimate taking  $M = \mathcal{O}(\Delta x^{-2q_1})$  and  $\Delta x = \mathcal{O}(\Delta v^{q_2/q_1})$ . This means that in order to have comparable errors the number of samples should be extremely large, especially when dealing with high order deterministic discretizations. As a consequence, the Monte Carlo approach may result very expensive in practical applications.

**Remark 3.1.** — The previous Monte Carlo method can be improved using standard variance reduction techniques such as stratified sampling and importance sampling methods. We refer to [12, 68, 80] for more details.

**3.3. Multi-Scale Control Variate (MSCV) method.** — We survey here the MSCV approach recently introduced in [23]. The main idea of the method is to reduce the variance of standard Monte Carlo estimators using as control variate different low-fidelity models at the various scales introduced by the Knudsen number. In the following we will refer to this type of approach that uses a high-fidelity model and a single low-fidelity model as the *bi-fidelity* case.

**3.3.1. The space homogeneous case.** — For sake of clarity, we first illustrate the method when applied to the solution of a kinetic equation of the type (1) with deterministic interaction operator  $Q(f, f)$  and random initial data  $f(z, x, v, 0) = f_0(z, x, v)$  in a homogeneous setting

$$(49) \quad \frac{\partial f}{\partial t} = Q(f, f),$$

where  $f = f(z, v, t)$ . Let observe that without loss of generality, we have fixed here  $\varepsilon = 1$ , since in the space homogeneous case the only temporal scale is the collisional one. Under suitable assumptions, one can show that  $f(z, v, t)$  exponentially decays [96–99] to the unique steady state  $f^\infty(z, v)$  such that  $Q(f^\infty, f^\infty) = 0$  which satisfies

$$(50) \quad \langle \phi f_0 \rangle = \langle \phi f^\infty \rangle = (\rho, \rho u, E)^T.$$

The error of the standard Monte Carlo estimator reads now

$$(51) \quad \|\mathbb{E}[f] - E_M[f]\|_{L^1_2(\mathcal{D} \times \mathbb{R}^{d_v}; L^2(\Omega))} = \sigma_f M^{-1/2}.$$

Thus, a first variance reduction strategy is obtained by splitting the expected value of the solution as

$$\begin{aligned}
 \mathbb{E}[f](v, t) &= \int_{\Omega} f(z, v, t) p(z) dz \\
 (52) \quad &= \int_{\Omega} f^{\infty}(z, v) p(z) dz + \int_{\Omega} (f(z, v, t) - f^{\infty}(z, v)) p(z) dz \\
 &= \mathbb{E}[f^{\infty}](v) + \mathbb{E}[f - f^{\infty}](v, t),
 \end{aligned}$$

and exploiting the fact that  $\mathbb{E}[f^{\infty}]$  can be evaluated with arbitrary accuracy at a negligible cost (for example using a very fine grid of samples) since it does not depend on the solution computed at each time step. Now, if we use (52) and estimate

$$(53) \quad \mathbb{E}[f] \approx \mathbb{E}[f^{\infty}] + E_M[f - f^{\infty}]$$

we obtain an error of the type

$$\|\mathbb{E}[f](\cdot, t) - \mathbb{E}[f^{\infty}](\cdot) - E_M[f - f^{\infty}](\cdot, t)\|_{L^1_2(\mathbb{R}^{d_v}; L^2(\Omega))} = \sigma_{f-f^{\infty}} M^{-1/2}.$$

Since the non equilibrium part  $f - f^{\infty}$  goes to zero in time exponentially fast, then also its variance goes to zero, which means that for long times estimate (53) becomes exact and depends only on the accuracy of the evaluation of  $\mathbb{E}[f^{\infty}]$ .

The above argument can be generalized by considering a time dependent approximation of the solution  $\tilde{f}(z, v, t)$ , whose evaluation is significantly cheaper than computing  $f(z, v, t)$ , such that  $\langle(\phi \tilde{f})\rangle = \langle\phi f\rangle$  for some moments and that  $\tilde{f}(z, v, t) \rightarrow f^{\infty}(z, v)$  as  $t \rightarrow \infty$ . For example, one can consider to use the BGK approximation (14) which in this simple case can be exactly solved giving the following expression

$$(54) \quad \tilde{f}(z, v, t) = e^{-\nu t} f_0(z, v) + (1 - e^{-\nu t}) f^{\infty}(z, v).$$

Then we have

$$(55) \quad \mathbb{E}[\tilde{f}](v, t) = e^{-\nu t} \mathbf{f}_0(v) + (1 - e^{-\nu t}) \mathbf{f}^{\infty}(v),$$

where  $\mathbf{f}_0 = \mathbb{E}[f_0(\cdot, v)]$  and  $\mathbf{f}^{\infty} = \mathbb{E}[f^{\infty}](v)$  or accurate approximations of the same quantities.

Using the same estimator (53)

$$(56) \quad \mathbb{E}[f] \approx \mathbb{E}[\tilde{f}] + E_M[f - \tilde{f}]$$

gives the following estimate for the error

$$\|\mathbb{E}[f](\cdot, t) - \mathbb{E}[\tilde{f}](\cdot) - E_M[f - \tilde{f}](\cdot, t)\|_{L^1_2(\mathbb{R}^{d_v}; L^2(\Omega))} = \sigma_{f-\tilde{f}} M^{-1/2},$$

where even in this case,  $\sigma_{f-\tilde{f}} \rightarrow 0$  as  $t \rightarrow \infty$ .

Let now observe that a general variance reduction technique can be obtained by introducing the following control variate estimator [23]

$$(57) \quad \tilde{E}_M^\lambda[f](v, t) = \frac{1}{M} \sum_{k=1}^M f^k(v, t) - \lambda \left( \frac{1}{M} \sum_{k=1}^M \tilde{f}^k(v, t) - \tilde{\mathbf{f}}(v, t) \right).$$

In particular, for  $\lambda = 0$  we recover the standard MC estimator  $\tilde{E}_M^0[f] = E_M[f]$ , whereas for  $\lambda = 1$  we have the estimator  $\tilde{E}_M^1[f] = \mathbb{E}[\tilde{f}] + E_M[f - \tilde{f}]$  corresponding to (56). The following result holds true

**Lemma 3.1.** — *The control variate estimator (57) is unbiased and consistent for any  $\lambda \in \mathbb{R}$ .*

*Proof.* — The expected value of the control variate estimator  $\tilde{E}_M^\lambda[f]$  in (57) yields the unbiasedness for any choice of  $\lambda \in \mathbb{R}$

$$\mathbb{E}[\tilde{E}_M^\lambda[f]] = \frac{1}{M} \sum_{k=1}^M \mathbb{E}[f^k] - \lambda \left( \frac{1}{M} \sum_{k=1}^M \mathbb{E}[\tilde{f}^k] - \mathbb{E}[\tilde{\mathbf{f}}] \right) = \mathbb{E}[f],$$

since  $\mathbb{E}[f^k] = \mathbb{E}[f]$  and  $\mathbb{E}[\tilde{f}^k] = \mathbb{E}[\tilde{f}]$  for  $k = 1, \dots, M$ . Moreover, since  $f^k$  and  $\tilde{f}^k$  are i.i.d. random variables

$$\lim_{M \rightarrow \infty} \frac{1}{M} \sum_{k=1}^M f^k - \lambda \left( \frac{1}{M} \sum_{k=1}^M \tilde{f}^k - \mathbb{E}[\tilde{f}] \right) \stackrel{p}{=} \mathbb{E}[f],$$

from the consistency of the standard MC estimator and where the last identity has to be understood in probability sense [37, 56].  $\square$

If we now consider a new the random variable depending on  $\lambda$

$$f^\lambda(z, v, t) = f(v, z, t) - \lambda(\tilde{f}(z, v, t) - \tilde{\mathbf{f}}(v, t)),$$

we have that the expectation for this new random variable is such that  $\mathbb{E}[f^\lambda] = \mathbb{E}[f]$ ,  $E_M[f^\lambda] = \tilde{E}_M^\lambda[f]$ , i.e. it shares the same expectation of the distribution function  $f$  in terms of the random variable. Moreover, we can quantify its variance as

$$(58) \quad \text{Var}(f^\lambda) = \text{Var}(f) + \lambda^2 \text{Var}(\tilde{f}) - 2\lambda \text{Cov}(f, \tilde{f})$$

and we can prove the following result [23]

**Theorem 3.1.** — *The quantity*

$$(59) \quad \lambda^* = \frac{\text{Cov}(f, \tilde{f})}{\text{Var}(\tilde{f})}$$

*minimizes the variance of  $f^\lambda$  at the point  $(v, t)$  and gives*

$$(60) \quad \text{Var}(f^{\lambda^*}) = (1 - \rho_{f, \tilde{f}}^2) \text{Var}(f),$$

where  $\rho_{f,\tilde{f}} \in [-1, 1]$  is the correlation coefficient between  $f$  and  $\tilde{f}$ . In addition, we have

$$(61) \quad \lim_{t \rightarrow \infty} \lambda^*(v, t) = 1, \quad \lim_{t \rightarrow \infty} \text{Var}(f^{\lambda^*})(v, t) = 0 \quad \forall v \in \mathbb{R}^{d_v}.$$

*Proof.* — Equation (59) is readily found by direct differentiation of (58) with respect to  $\lambda$  and then observing that  $\lambda^*$  is the unique stationary point. The fact that  $\lambda^*$  is a minimum follows from the positivity of the second derivative  $2\text{Var}(f^\infty) > 0$ . Then, by substitution in (58) of the optimal value  $\lambda^*$  one finds (60) where

$$\rho_{f,f^\infty} = \frac{\text{Cov}(f, f^\infty)}{\sqrt{\text{Var}(f)\text{Var}(f^\infty)}}.$$

In addition, since as  $t \rightarrow \infty$  we have  $f \rightarrow f^\infty$ , asymptotically  $\lambda^* \rightarrow 1$  and  $\text{Var}(f^{\lambda^*}) \rightarrow 0$  independently of  $v$ .  $\square$

The above result permits in combination with a deterministic solver satisfying (45) to get the following error estimate [23, 60]

$$(62) \quad \|\mathbb{E}[f](\cdot, t) - \tilde{E}_M^{\lambda^*}[f]\|_{L^1_2(\mathbb{R}^{d_v}; L^2(\Omega))} \leq C \left\{ \sigma_{f^{\lambda^*}} M^{-1/2} + \Delta v^{q_1} \right\}$$

where  $\sigma_{f^{\lambda^*}} = \|(1 - \rho_{f,\tilde{f}}^2)^{1/2} \text{Var}(f)^{1/2}\|_{L^1_2(\mathbb{R}^{d_v})}$ , and  $C > 0$  depends on the final time and on the initial data. Let observe that in the above estimate, we ignored the statistical errors due to the approximation of the control variate expectation and the error in the estimate of  $\lambda^*$ . Note finally that, since  $\rho_{f,\tilde{f}}^2 \rightarrow 1$  as  $t \rightarrow \infty$  the statistical error will vanish for large times.

**Remark 3.2.** — *In practice,  $\text{Cov}(f, \tilde{f})$  appearing in  $\lambda^*$  is not known and has to be estimated. Starting from the  $M$  samples we have the following unbiased estimators*

$$(63) \quad \text{Var}_M(\tilde{f}) = \frac{1}{M-1} \sum_{k=1}^M (\tilde{f}^k - E_M[\tilde{f}])^2,$$

$$(64) \quad \text{Cov}_M(f, \tilde{f}) = \frac{1}{M-1} \sum_{k=1}^M (f^k - E_M[f])(\tilde{f}^k - E_M[\tilde{f}]),$$

which allow to estimate

$$(65) \quad \lambda_M^* = \frac{\text{Cov}_M(f, \tilde{f})}{\text{Var}_M(\tilde{f})}.$$

It can be verified easily that  $\lambda_M^* \rightarrow 1$  as  $f \rightarrow f^\infty$ .

---

**Algorithm 2:** Bi-fidelity MSCV method

---

1. **Sampling:** Sample  $M$  i.i.d. initial data  $f_0^k$ ,  $k = 1, \dots, M$  from the random initial data  $f_0$  and approximate these over the grid.
2. **Solving:** For each realization  $f_0^k$ ,  $k = 1, \dots, M$ 
  - (a) Compute the control variate  $\tilde{f}_{\Delta v}^{k,n}$ ,  $k = 1, \dots, M$  at time  $t^n$  using (54) and denote by  $\tilde{\mathbf{f}}_{\Delta v}^n$  an accurate estimate of  $\mathbb{E}[\tilde{f}_{\Delta v}^n]$  obtained from  $\tilde{\mathbf{f}}_{\Delta v}^0$  and  $\tilde{\mathbf{f}}_{\Delta v}^\infty$  using (55).
  - (b) Solve numerically the underlying kinetic equation (49) by the corresponding deterministic solvers. We denote the solution at time  $t^n$  by  $f_{\Delta v}^{k,n}$ ,  $k = 1, \dots, M$ .
3. **Estimating:**
  - (a) Estimate the optimal value of  $\lambda^*$  as

$$\lambda_M^{*,n} = \frac{\sum_{k=1}^M (f_{\Delta v}^{k,n} - E_M[f_{\Delta v}^n]) (\tilde{f}_{\Delta v}^{k,n} - E_M[\tilde{f}_{\Delta v}^n])}{\sum_{k=1}^M (\tilde{f}_{\Delta v}^{k,n} - E_M[\tilde{f}_{\Delta v}^n])^2}.$$

- (b) Compute the expectation of the random solution with the control variate estimator

$$(66) \quad \tilde{E}_M^{\lambda^*}[f_{\Delta v}^n] = \frac{1}{M} \sum_{k=1}^M f_{\Delta v}^{k,n} - \lambda_M^{*,n} \left( \frac{1}{M} \sum_{k=1}^M \tilde{f}_{\Delta v}^{k,n} - \tilde{\mathbf{f}}_{\Delta v}^n \right).$$


---

The resulting multi-scale control variate method based on a low-fidelity model is summarized in Algorithm 2.

In Figure 2, we show some results of the MSCV method in the space homogeneous case in comparison with standard MC approaches. In this test, we solve the homogeneous Boltzmann equation with Maxwellian kernel, i.e. equation (4) with  $\alpha = 0$ , for  $v \in [-V, V]^2$  through the fast spectral method [62] using  $V = 16$  and  $N_v = 64$  modes in each direction. The initial condition is a two bumps problem with uncertainty

$$(67) \quad f_0(z, v) = \frac{\rho_0}{2\pi} \left( \exp\left(-\frac{|v - (2 + sz)|^2}{\sigma}\right) + \exp\left(-\frac{|v + (1 + sz)|^2}{\sigma}\right) \right)$$

with  $s = 0.2$ ,  $\rho_0 = 0.125$ ,  $\sigma = 0.5$  and  $z$  uniform in  $[0, 1]$ . The figure shows the expectation of the distribution function together with the  $L_2$  error of the expected value of the solution.

The gain in accuracy obtained with the MSCV methods is of several orders of magnitudes larger with respect to standard Monte Carlo.

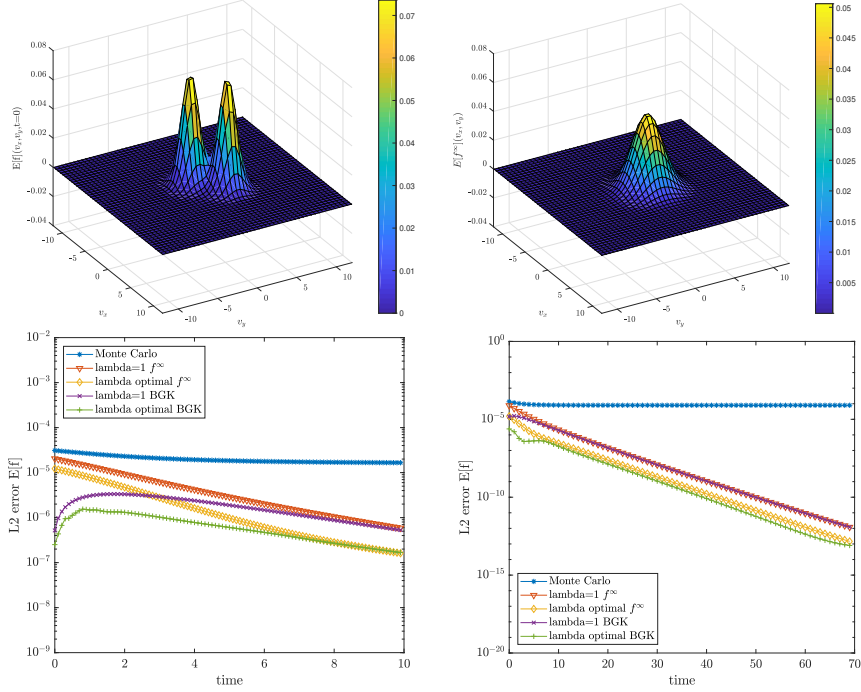


FIGURE 2. MSCV method - space homogeneous case. Expected value of the distribution function  $\mathbb{E}[f]$  (top) and  $L_2$  norm of the error for  $\mathbb{E}[f]$  (bottom) using the Monte Carlo and the MSCV methods with various control variates strategies with  $M = 100$  samples.

**3.3.2. The space non homogeneous case.** — We focus now on the full space non homogeneous problem (1). Generalizing the space homogeneous method based on the local equilibrium  $f^\infty$  as control variate, we consider here the Euler closure. If we denote by  $U_F = (\rho_F, u_F, T_F)^T$  the solution of the fluid model (10), for the same initial data, the corresponding equilibrium state  $f_F^\infty$  can be used as low fidelity model. In this case, the control variate estimate based on  $M$  i.i.d. samples reads

$$(68) \quad E_M^\lambda[f](x, v, t) = \frac{1}{M} \sum_{k=1}^M f^k(x, v, t) - \lambda \left( \frac{1}{M} \sum_{k=1}^M f_F^{\infty, k}(x, v, t) - \mathbf{f}_F^\infty(x, v, t) \right),$$

where  $\mathbf{f}_F^\infty(x, v, t)$  is an accurate approximation of  $\mathbb{E}[f_F^\infty(\cdot, x, v, t)]$ . Consistency and unbiasedness of (68) for any  $\lambda \in \mathbb{R}$  follows again from Lemma 3.1. The fundamental difference is that now the variance of

$$f^\lambda(z, x, v, t) = f(z, x, v, t) - \lambda(f_F^\infty(z, x, v, t) - \mathbb{E}[f_F^\infty](\cdot, x, v, t))$$

will not vanish asymptotically in time since  $f^\infty \neq f_F^\infty$ , unless the kinetic equation is close to the fluid regime, namely for small values of the Knudsen number. We can state the following

**Theorem 3.2.** — *If  $\text{Var}(f_F^\infty) \neq 0$  the quantity*

$$(69) \quad \lambda^* = \frac{\text{Cov}(f, f_F^\infty)}{\text{Var}(f_F^\infty)}$$

*minimizes the variance of  $f^\lambda$  at the point  $(x, v, t)$  and gives*

$$(70) \quad \text{Var}(f^{\lambda^*}) = (1 - \rho_{f, f_F^\infty}^2) \text{Var}(f),$$

*where  $\rho_{f, f_F^\infty} \in [-1, 1]$  is the correlation coefficient between  $f$  and  $f_F^\infty$ . In addition, we have*

$$(71) \quad \lim_{\varepsilon \rightarrow 0} \lambda^*(x, v, t) = 1, \quad \lim_{\varepsilon \rightarrow 0} \text{Var}(f^{\lambda^*})(x, v, t) = 0 \quad \forall (x, v) \in \mathcal{D} \times \mathbb{R}^{d_v}.$$

The proof follows the same lines of Theorem 3.1. Note that, since as  $\varepsilon \rightarrow 0$  we formally have  $Q(f, f) = 0$  which implies  $f = f^\infty$  and  $f_F^\infty = f^\infty$ , from (69) and (70) we obtain (71).

Similarly to the homogeneous case, the generalization to an improved control variate based on a suitable approximation of the kinetic solution by a low fidelity model can be done with the aid of a more accurate fluid approximation, like the compressible Navier-Stokes system, or a simplified kinetic model. In the latter case, we can solve a BGK model (14) for the same initial data and use its solution as control variate. More precisely, given  $M$  i.i.d. samples of the solution  $f^k(x, v, t)$  and of the control variate  $\tilde{f}^k(x, v, t)$  we define the new estimator

$$(72) \quad \tilde{E}_M^\lambda[f](x, v, t) = \frac{1}{M} \sum_{k=1}^M f^k(x, v, t) - \lambda \left( \frac{1}{M} \sum_{k=1}^M \tilde{f}^k(x, v, t) - \tilde{\mathbf{f}}(x, v, t) \right),$$

where  $\tilde{\mathbf{f}}(x, v, t)$  is an accurate approximation of  $\mathbb{E}[\tilde{f}(\cdot, x, v, t)]$ . As for the case of the compressible Euler equations in the space non homogeneous case the variance of

$$f^\lambda(z, x, v, t) = f(z, x, v, t) - \lambda(\tilde{f}(z, x, v, t) - \tilde{\mathbf{f}}(z, x, v, t))$$

will not vanish asymptotically in time since  $f^\infty \neq \tilde{f}$ , unless the two solutions are very close together, such as in the fluid regime. Thus, while the first part of Theorem 3.1 is still valid, the optimal value

$$(73) \quad \lambda^* = \frac{\text{Cov}(f, \tilde{f})}{\text{Var}(\tilde{f})}$$

and the variance

$$(74) \quad \text{Var}(f^{\lambda^*}) = (1 - \rho_{f, \tilde{f}}^2) \text{Var}(f)$$

now satisfy a different condition relating the low fidelity and the high fidelity models. In fact, one can prove that

$$(75) \quad \lim_{\varepsilon \rightarrow 0} \lambda^*(x, v, t) = 1, \quad \lim_{\varepsilon \rightarrow 0} \text{Var}(f^{\lambda^*})(x, v, t) = 0 \quad \forall (x, v) \in \mathbb{R}^{d_x} \times \mathbb{R}^{d_v}.$$

In fact, since as  $\varepsilon \rightarrow 0$  from (1) we formally have  $Q(f, f) = 0$  which implies  $f = f^\infty$  and  $\tilde{f} = f^\infty$ , from (73) and (74) we obtain (75).

Let notice now that even if simulating the control variate system is cheaper than the full model, however its computational cost is no more negligible and thus we cannot ignore it. In this respect, we assume then that the control variate model is computed over a fine grid of  $M_E \gg M$  samples. At the same time, we replace the exact computation of the expectation of the low fidelity BGK model with the approximation

$$\tilde{\mathbf{f}}(x, v, t) = E_{M_E}[\tilde{f}](x, v, t),$$

in the estimator (72) which we will denote now by  $\tilde{E}_{M, M_E}^\lambda[f]$ . This replacement has an impact on the optimal value of  $\lambda$ . In fact, using the independence of  $E_M[\cdot]$  and  $E_{M_E}[\cdot]$  by the central limit theorem [37, 56] we have

$$\text{Var}(E_M[f]) = M^{-1} \text{Var}(f), \quad \text{Var}(E_{M_E}[\tilde{f}]) = M_E^{-1} \text{Var}(\tilde{f}).$$

Thus, minimizing the variance now leads to the optimal value

$$(76) \quad \tilde{\lambda}^* = \frac{M_E}{M + M_E} \lambda^*,$$

with  $\lambda^*$  given by (73). As can be easily seen from the above formula, this correction may be relevant only in the cases when  $M$  and  $M_E$  do not differ too much. In many practical cases and in the simulations shown after, however,  $M_E \gg M$  so that  $\frac{M_E}{M + M_E} \approx 1$  and we consequently assume  $\tilde{\lambda}^* \approx \lambda^*$ .

Using the optimal value (73) for the control variate variable and a deterministic solver which satisfies (45), we obtain the error estimate [23, 60]

$$(77) \quad \begin{aligned} & \|E[f](\cdot, t) - \tilde{E}_{M, M_E}^{\lambda^*}[f]\|_{L^1_2(\mathcal{D} \times \mathbb{R}^{d_v}; L^2(\Omega))} \\ & \leq C \left\{ \sigma_{f^{\lambda^*}} M^{-1/2} + \tau_{f^{\lambda^*}} M_E^{-1/2} + \Delta x^{q_1} + \Delta v^{q_2} \right\} \end{aligned}$$

with  $\sigma_{f^{\lambda^*}} = \|(1 - \rho_{f, \tilde{f}}^2)^{1/2} \text{Var}(f)^{1/2}\|_{L^1_2(\mathcal{D} \times \mathbb{R}^{d_v})}$ ,  $\tau_{f^{\lambda^*}} = \|\rho_{f, \tilde{f}} \text{Var}(f)^{1/2}\|_{L^1_2(\mathcal{D} \times \mathbb{R}^{d_v})}$  and with a constant  $C > 0$  depending on the final time and on the initial data.

**Remark 3.3.** — *For space non homogeneous simulations, one is typically interested in the evolution of the moments  $\langle \phi f \rangle$  instead that on the evolution*



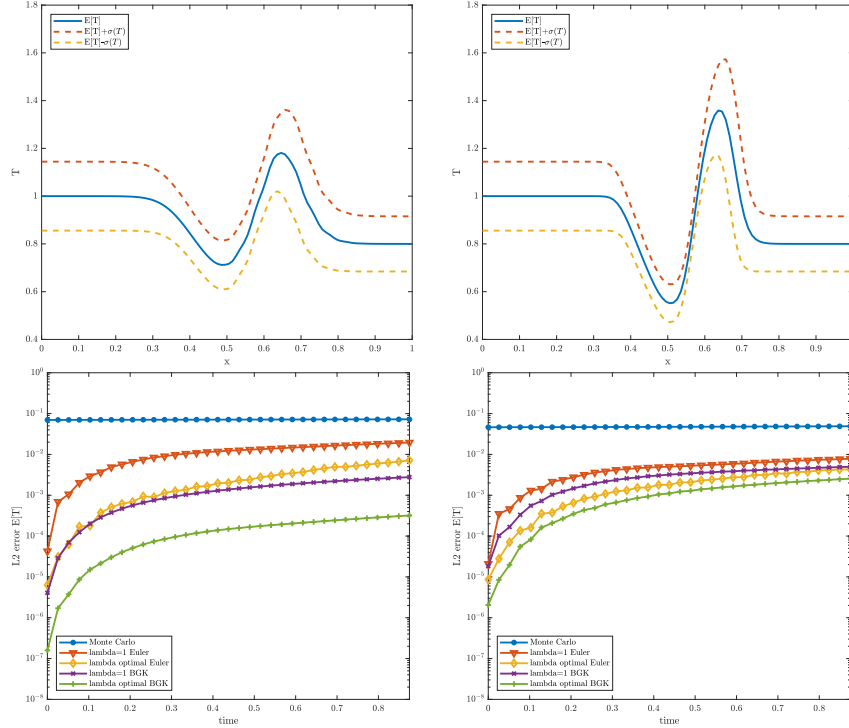


FIGURE 3. MSCV method - Sod test with uncertainty in the initial data and different low fidelity strategies. Expectation for the temperature  $\mathbb{E}[T]$  and confidence bands at final time (top) and  $L_2$  norm of the error for  $\mathbb{E}[T]$  (bottom) with  $M = 10$  and  $M_E = 10^4$ . Left:  $\varepsilon = 10^{-2}$ . Right:  $\varepsilon = 10^{-3}$ .

of the shape of the distribution function. More in general, one can compute the optimal value of  $\lambda$  with respect to any quantity of interest  $q[f]$  as

$$(78) \quad \lambda_q^* = \frac{\text{Cov}(q[f], q[\tilde{f}])}{\text{Var}(q[\tilde{f}])}.$$

In particular, in the case  $q[f] = \langle \phi f \rangle$ , we have  $\lambda_q^* = \lambda_q^*(x, t)$ . Note that, using (78) all estimates in this section for  $\mathbb{E}[f]$  translates into estimates for  $\mathbb{E}[q[f]]$ . This is particularly relevant when compressible Euler or Navier-Stokes equations are used as the low-fidelity model.

In Figure 3, we show the results of the MSCV method where the BGK or the compressible Euler equations are used as low fidelity models. The Boltzmann equation is solved for  $v \in [-V, V]^2$ ,  $x \in [0, L]$ , and  $\alpha = 0$  in (4). The fast spectral method [61] for  $V = 8$  with  $N_v = 32$  modes in each direction is

used combined with a fifth order WENO method [91] in space for  $L = 1$  with  $N_x = 100$  grid points.. The initial conditions are given by Sod problem with uncertain temperature

$$(79) \quad \begin{aligned} \rho_0(x) = 1, \quad T_0(z, x) = 1 + sz & \quad \text{if } 0 < x < L/2 \\ \rho_0(x) = 0.125, \quad T_0(z, x) = 0.8 + sz & \quad \text{if } L/2 < x < L \end{aligned}$$

with  $s = 0.25$ ,  $z$  uniformly distributed in  $[0, 1]$  and equilibrium initial distribution given by

$$f_0(z, x, v) = \frac{\rho_0(x)}{2\pi} \exp\left(-\frac{|v|^2}{2T_0(z, x)}\right).$$

We report the results for two different regimes, namely  $\varepsilon = 10^{-2}$  and  $\varepsilon = 10^{-3}$ . The images show on the top the expectation of the temperature at the final time together with the confidence bands  $\mathbb{E}[T] - \sigma_T, \mathbb{E}[T] + \sigma_T$  with  $\sigma_T$  the standard deviation. On the bottom, we report the various errors for the expected value of the temperature as a function of time. The number of samples used to compute the expected value of the solution is  $M = 10$  while the number of samples used to compute the control variate is  $M_E = 10^4$ . The optimal values of  $\lambda^*(x, t)$  have been computed with respect to the temperature.

In Figure 4 we show the results of the same MSCV approach where the Navier-Stokes equations (11) are used as low fidelity model. The setting is similar to the one shown in Figure 3 where now, however, uncertainty is also present in the initial density. We then have

$$(80) \quad \begin{aligned} \rho_0(x) = 1 + sz, \quad T_0(z, x) = 1 + sz & \quad \text{if } 0 < x < L/2 \\ \rho_0(x) = 0.125(1 + sz), \quad T_0(z, x) = 0.8 + sz & \quad \text{if } L/2 < x < 1, \end{aligned}$$

the other discretization parameters remaining unchanged. In this case, the optimal values of  $\lambda^*(x, t)$  have been computed both with respect to the density (left images) as well as with respect to the temperature (right images). We stress that the computation of the optimal values is done through an offline procedure. This employs, irrespectively of the quantity of interest, the same results of the deterministic simulations for the low and high fidelity models. These results are then combined to improve the estimation of the expectation of respectively the density and the temperature. For all situations reported the Navier-Stokes control variate approach improves the result of the compressible Euler case, especially when far from the thermodynamical equilibrium.

### 3.4. Multi-fidelity MSCV methods. —

**3.4.1. The space homogeneous case.** — In this section we extend the control variate strategy to the case in which several low-fidelity models are employed to

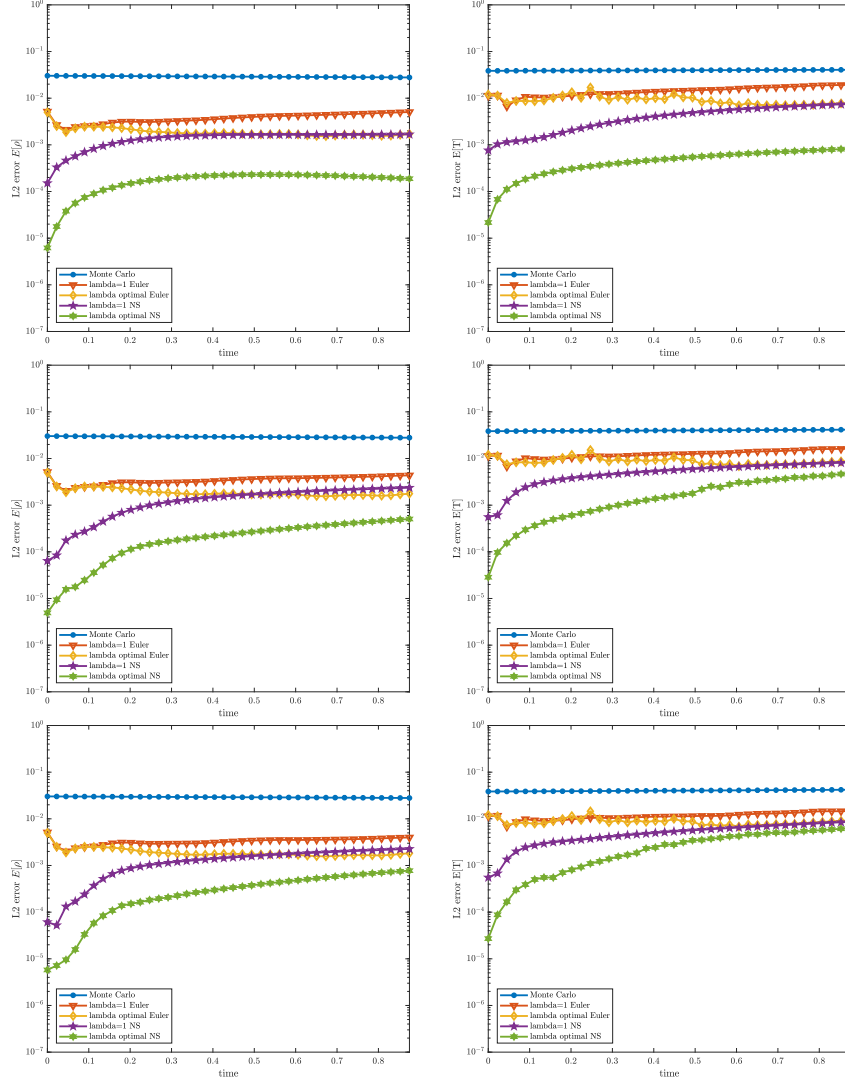


FIGURE 4. MSCV method - Sod test with uncertainty in the initial data. Comparison between the compressible Euler and the Navier-Stokes control variate models.  $L_2$  norm of the error for  $\mathbb{E}[\rho]$  (left) and  $\mathbb{E}[T]$  (right) with  $M = 10$ . Top:  $\varepsilon = 10^{-2}$ . Middle:  $\varepsilon = 10^{-3}$ . Bottom:  $\varepsilon = 5 \times 10^{-4}$ .

accelerate the statistical convergence. We start again from the space homogeneous equation (49) for sake of clarity. Let us consider  $f_1(z, v, t), \dots, f_L(z, v, t)$  approximations of  $f(z, v, t)$  furnished by a set of low fidelity models whose properties will be discussed later. We can then define a new random variable

as

$$(81) \quad f^{\lambda_1, \dots, \lambda_L}(z, v, t) = f(z, v, t) - \sum_{h=1}^L \lambda_h (f_h(z, v, t) - \mathbb{E}[f_h](v, t)).$$

Clearly (81) is such that  $\mathbb{E}[f^{\lambda_1, \dots, \lambda_L}] = \mathbb{E}[f]$  while the variance of this new variable is given by

$$(82) \quad \begin{aligned} \mathbb{V}ar(f^{\lambda_1, \dots, \lambda_L}) &= \mathbb{V}ar(f) + \sum_{h=1}^L \lambda_h^2 \mathbb{V}ar(f_h) + \\ &+ 2 \sum_{h=1}^L \lambda_h \left( \sum_{\substack{k=1 \\ k \neq h}}^L \lambda_k \mathbb{C}ov(f_h, f_k) - \mathbb{C}ov(f, f_h) \right). \end{aligned}$$

The above quantity can be rewritten in a more compact form by introducing the following notations

$$\Lambda = (\lambda_1, \dots, \lambda_L)^T, \quad b = (\mathbb{C}ov(f, f_1), \dots, \mathbb{C}ov(f, f_L))^T$$

giving then

$$(83) \quad \mathbb{V}ar(f^\Lambda) = \mathbb{V}ar(f) + \Lambda^T C \Lambda - 2\Lambda^T b$$

where  $C = (c_{ij})$ ,  $c_{ij} = \mathbb{C}ov(f_i, f_j)$  is the symmetric  $L \times L$  covariance matrix. Following the same path of the bi-fidelity case, one can now try to find the set  $\Lambda^*$  minimizing the variance of the new variable  $f^\Lambda$ . This is obtained thanks to the following Theorem (see [24] for a proof):

**Theorem 3.3.** — *Assuming the covariance matrix is not singular, the vector*

$$(84) \quad \Lambda^* = C^{-1}b,$$

*minimizes the variance of  $f^\Lambda$  at the point  $(v, t)$  and gives*

$$(85) \quad \mathbb{V}ar(f^{\Lambda^*}) = \left( 1 - \frac{b^T (C^{-1})^T b}{\mathbb{V}ar(f)} \right) \mathbb{V}ar(f).$$

Having the above result in mind, one can then introduce the control variate estimator based on (81) which takes the form

$$(86) \quad E_M^\Lambda[f](v, t) = E_M[f](v, t) - \sum_{h=1}^L \lambda_h (E_M[f_h](v, t) - \mathbf{f}_h(v, t)),$$

where  $\mathbf{f}_h(v, t)$  is an accurate approximation of  $\mathbb{E}[f_h](v, t)$ . In the above formula, we also assumed to have at disposal  $M$  i.i.d. samples from the solution  $f(z, v, t)$  and from the control variate functions  $f_h(z, v, t)$  for  $h = 1, \dots, L$ . Moreover, in practice, as done for the bi-fidelity case, to estimate the value of the vector

$\Lambda^*$  we can use directly the Monte Carlo samples as in the bi-fidelity case. The resulting multi-fidelity MSCV method is summarized in Algorithm 3.

---

**Algorithm 3:** Multi-fidelity MSCV method

---

1. **Sampling:** Sample  $M$  i.i.d. initial data from the random initial data  $f_0$  and approximate these over the grid  $\Delta v$ . Denote these samples by  $f_{\Delta v}^{k,0}$ ,  $k = 1, \dots, M$ .

2. **Solving:**

(a) For each control variate and for each realization of the random input data  $f_{\Delta v}^{k,0}$ ,  $k = 1, \dots, M$ , the resulting control variate model is solved with mesh width  $\Delta v$ . We denote the resulting ensemble of deterministic solutions for  $h = 1, \dots, L$  at time  $t^n$  by

$$f_{h,\Delta v}^{k,n}, \quad k = 1, \dots, M.$$

(b) For each realization  $f_{\Delta v}^{k,0}$ ,  $k = 1, \dots, M$  the underlying kinetic equation (49) is solved with mesh width  $\Delta v$ . We denote the solution at time  $t^n$  by  $f_{\Delta v}^{k,n}$ ,  $k = 1, \dots, M$ .

3. **Estimating:**

(a) Estimate the optimal vector of values  $\Lambda^*$  solving

$$(87) \quad C_M^n \Lambda^{*,n} = b_M^n,$$

where  $(C_M^n)_{ij} = \text{Cov}_M(f_{i,\Delta v}^n, f_{j,\Delta v}^n)$  and  $(b_M^n)_i = \text{Cov}_M(f_{i,\Delta v}^n, f_{i,\Delta v}^n)$ .

(b) Compute the expectation of the random solution with the control variate estimator

$$(88) \quad E_M^{\Lambda^*} [f_{\Delta v}^n] = \frac{1}{M} \sum_{k=1}^M f_{\Delta v}^{k,n} - \sum_{h=1}^L \lambda_h^{*,n} \left( \frac{1}{M} \sum_{k=1}^M f_{h,\Delta v}^{k,n} - \mathbf{f}_{h,\Delta v}^n \right).$$


---

An interesting result is obtained introducing the vector  $F = (F_1, \dots, F_L)^T$ , such that  $F_h = f_h - \mathbb{E}[f_h]$ . This gives  $\mathbb{E}[F_h] = 0$ ,  $h = 1, \dots, L$  and equation (81) reads

$$(89) \quad f^{\lambda_1, \dots, \lambda_L}(z, v, t) = f(z, v, t) - \sum_{h=1}^L \lambda_h F_h(z, v, t).$$

This permits to conclude that the variance of  $f^{\Lambda^*}$  is reduced to zero if  $f$  is in the span of the set of functions  $F_1, \dots, F_L$ . Using now Gram–Schmidt orthogonalization and observing that

$$\langle F_h, F_k \rangle = \text{Cov}(f_h, f_k) = \text{Cov}(F_h, F_k), \quad h, k = 1, \dots, L,$$

we can also construct the vector  $G = (G_1, \dots, G_L)^T$ , with orthogonal components,  $\langle G_h, G_k \rangle = 0$  for  $h \neq k$ , as follows [35]

$$(90) \quad g_h = f_h - \sum_{j=1}^{h-1} \frac{\text{Cov}(g_j, f_h)}{\text{Var}(g_j)} g_j, \quad h = 1, \dots, L,$$

and define  $G_h = g_h - \mathbb{E}[g_h]$ , such that  $\mathbb{E}[G_h] = 0$ ,  $h = 1, \dots, L$ . Then, we may try to minimize the variance of the random variable

$$(91) \quad f^{\gamma_1, \dots, \gamma_L}(z, v, t) = f(z, v, t) - \sum_{h=1}^L \gamma_h G_h(z, v, t),$$

which now using the orthogonality property reads

$$\text{Var}(f^{\gamma_1, \dots, \gamma_L}) = \text{Var}(f) + \sum_{h=1}^L \gamma_h^2 \text{Var}(g_h) - 2 \sum_{h=1}^L \gamma_h \text{Cov}(f, g_h).$$

Given the above arguments, one can prove the following result [24]:

**Theorem 3.4.** — *If the control variate vector  $G = (G_1, \dots, G_L)^T$  in (91) has orthogonal components,  $\langle G_h, G_k \rangle = 0$  for  $h \neq k$ , then if  $\langle G_h, G_h \rangle \neq 0$  the vector  $\Gamma^*$  with components*

$$(92) \quad \gamma_h^* = \frac{\text{Cov}(f, g_h)}{\text{Var}(g_h)}, \quad h = 1, \dots, L,$$

*minimizes the variance of  $f^\Gamma$  at the point  $(v, t)$  and gives*

$$(93) \quad \text{Var}(f^{\Gamma^*}) = \left( 1 - \sum_{h=1}^L \rho_{f, g_h}^2 \right) \text{Var}(f)$$

*where  $\rho_{f, g_h} \in [-1, 1]$  is the correlation coefficient between  $f$  and  $g_h$ .*

Finally, estimating the orthogonal set of control variates using  $M$  samples by

$$(94) \quad E_M^\Gamma[f](v, t) = E_M[f](v, t) - \sum_{h=1}^L \gamma_h (E_M[g_h](v, t) - \mathbf{g}_h(v, t)),$$

where  $\mathbf{g}_h(v, t) = \mathbb{E}[g_h](v, t)$  or its accurate approximation, in combination with a deterministic solver satisfying (45), one obtains the following result [23, 60]:

**Proposition 3.2.** — *Let consider (49) with random and sufficiently regular initial data  $f(z, v, 0) = f_0(z, v)$ . The multi-fidelity MSCV method (94) with the optimal values (92) satisfies the error bound*

$$(95) \quad \|\mathbb{E}[f](\cdot, t^n) - E_M^{\Gamma^*}[f_{\Delta v}^n]\|_{L_2^1(\mathbb{R}^{d_v}; L^2(\Omega))} \leq C \left\{ \sigma_{f^{\Gamma^*}} M^{-1/2} + \Delta v^{q_2} \right\}$$

where  $\sigma_{f\Gamma^*} = \left\| \left( 1 - \sum_{h=1}^L \rho_{f,g_h}^2 \right)^{1/2} \text{Var}(f)^{1/2} \right\|_{L_2^1(\mathbb{R}^{d_v})}$ , and  $C > 0$  depends on the final time and on the initial data.

**3.4.2. A leading example: two control variates.** — To better exemplify the multi-fidelity approach, here we give the details of the method in the case  $L = 2$ , where  $f_1 = f_0$ , the initial data, and  $f_2 = f^\infty$ , the stationary state. In this case we know that  $f$  is in the span of the control variates at  $t = 0$  and as  $t \rightarrow \infty$ . A straightforward computation shows that the optimal values  $\lambda_1^*$  and  $\lambda_2^*$  are given by

$$(96) \quad \begin{aligned} \lambda_1^* &= \frac{\text{Var}(f^\infty)\text{Cov}(f, f_0) - \text{Cov}(f_0, f^\infty)\text{Cov}(f, f^\infty)}{\Delta}, \\ \lambda_2^* &= \frac{\text{Var}(f_0)\text{Cov}(f, f^\infty) - \text{Cov}(f_0, f^\infty)\text{Cov}(f, f_0)}{\Delta}, \end{aligned}$$

where  $\Delta = \text{Var}(f_0)\text{Var}(f^\infty) - \text{Cov}(f_0, f^\infty)^2 \neq 0$ . Using  $M$  samples for both control variates, the optimal estimator reads

$$(97) \quad \begin{aligned} E_M^{\lambda_1^*, \lambda_2^*}[f](v, t) &= E_M[f](v, t) - \lambda_1^* (E_M[f_0](v) - \mathbf{f}_0(v)) + \\ &\quad - \lambda_2^* (E_M[f^\infty](v) - \mathbf{f}^\infty(v)). \end{aligned}$$

Now, at  $t = 0$  since  $f(z, v, 0) = f_0(z, v)$  we clearly have  $\lambda_1^* = 1$  and  $\lambda_2^* = 0$  so that the estimator (97) is exact

$$E_M^{1,0}[f](v, 0) = \mathbf{f}_0(v).$$

Moreover, by the same arguments as in Theorem 3.1, for large times since  $f(z, v, t) \rightarrow f^\infty(z, v)$  from (96) we get

$$\lim_{t \rightarrow \infty} \lambda_1^* = 0, \quad \lim_{t \rightarrow \infty} \lambda_2^* = 1,$$

and thus, the variance of the estimator vanishes asymptotically in time

$$\lim_{t \rightarrow \infty} E_M^{\lambda_1^*, \lambda_2^*}[f](v, t) = E_M^{0,1}[f](v) = \mathbf{f}^\infty(v).$$

We want now to emphasize the relation between this last example and the bi-fidelity case based on the BGK model discussed in (57). This latter can be rewritten in the form (97)

$$E_M^{\lambda^*}[f](v, t) = E_M[f](v, t) - \tilde{\lambda}_1^* (E_M[f_0](v) - \mathbf{f}_0(v)) - \tilde{\lambda}_2^* (E_M[f^\infty](v) - \mathbf{f}^\infty(v))$$

where

$$\tilde{\lambda}_1^* = e^{-t}\lambda^*, \quad \tilde{\lambda}_2^* = (1 - e^{-t})\lambda^*.$$

Therefore, the single control variate based on the BGK model can be understood as a suboptimal solution to the minimization problem for the control variates  $f_0$  and  $f^\infty$ . In particular, if the solution  $f$  has the form (54), namely

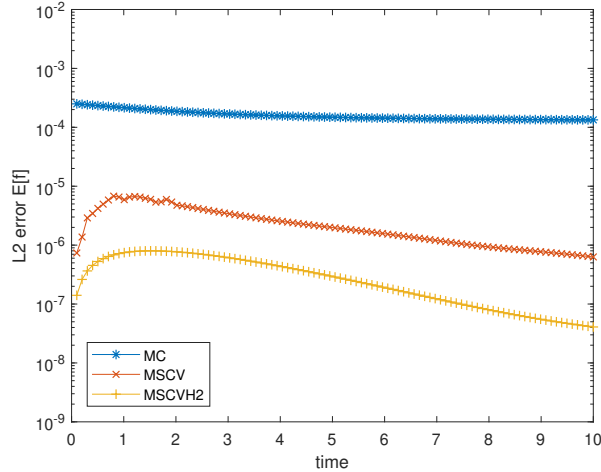


FIGURE 5. Multi-fidelity MSCV method - space homogeneous case.  $L_2$  norm of the error in time for the expectation of the distribution function for the MC method, the bi-fidelity MSCV method based on the BGK solution and the multi-fidelity MSCV2 method based on the two control variates  $f_0$  and  $f^\infty$ .

the full model is the BGK model, then it is in the span generated by  $f_0$  and  $f^\infty$  and we obtain  $\lambda_1^* = \tilde{\lambda}_1^*$  and  $\lambda_2^* = \tilde{\lambda}_2^*$ .

We now compare the case of the single control variate given by the BGK model discussed in 3.3 with the case of the two control variate approach discussed here. The number of samples used to compute the expected solution for the Boltzmann equation is  $M = 100$  while the expected values of the control variates can be evaluated offline as in the BGK case. The initial condition is the two bumps problem with uncertainty (67) and the same discretization parameters as in Figure 2 have been used. In Figure 5, we report the  $L_2$  error with respect to the random variable in the computation of the expected value for the distribution function  $\mathbb{E}[f](v, t)$  for the different methods. We observe that the multi-fidelity method with two control variates permits to gain one order of accuracy with respect to the standard bi-fidelity approach.

**3.4.3. The space non homogeneous case.** — For non homogeneous problems, as in the bi-fidelity case summarized in Section 3.3.2, we cannot assume to know offline the expectation of the control variate. Therefore, the control variates have a non-negligible computational cost. Each control variate, in fact, acts at a certain scale and requires the numerical solution of a suitable time dependent model in the phase space. The multi-fidelity MSCV estimator (86), based on the multi fidelity control variates  $f_1(z, x, v, t), \dots, f_L(z, x, v, t)$



for the solution  $f(z, x, v, t)$  to the space non homogeneous problem (1), reads

$$(98) \quad \begin{aligned} E_{M, M_E}^\Lambda[f](x, v, t) &= E_M[f](x, v, t) + \\ &\quad - \sum_{h=1}^L \lambda_h (E_M[f_h](x, v, t) - E_{M_E}[f_h](x, v, t)), \end{aligned}$$

where  $M_E \gg M$  samples have been used to estimate the expectations of the control variates  $\mathbb{E}[f_h(z, v, t)]$ . As in the bi-fidelity case, minimization of the variance of (98), leads to the optimal values

$$(99) \quad \tilde{\Lambda}^* = \frac{M_E}{M + M_E} \Lambda^*,$$

with  $\Lambda^*$  given by (84). In the sequel we assume  $M_E \gg M$  so that  $\tilde{\Lambda}^* \approx \Lambda^*$ .

We can apply the Gram–Schmidt orthogonalization (90) and estimate

$$(100) \quad \begin{aligned} E_{M, M_E}^\Gamma[f](v, t) &= E_M[f](x, v, t) + \\ &\quad - \sum_{h=1}^L \gamma_h (E_M[g_h](x, v, t) - E_{M_E}[g_h](x, v, t)), \end{aligned}$$

with the optimal vector of values  $\Gamma^*$  defined by (92). For the estimator (100) we have the following generalization of the error estimate (95).

**Proposition 3.3.** — *Consider a deterministic scheme which satisfies (45) for problem (1) with random and sufficiently regular initial data  $f(z, x, v, 0) = f_0(z, x, v)$ . Then, the multi-fidelity MSCV estimate defined in (100) with the optimal values given by (92) satisfies the error bound*

$$(101) \quad \begin{aligned} &\| \mathbb{E}[f](\cdot, t^n) - E_{M, M_E}^{\Gamma^*}[f_{\Delta x, \Delta v}^n] \|_{L_2^1(\mathcal{D} \times \mathbb{R}^{d_v}; L^2(\Omega))} \\ &\leq C \left\{ \sigma_{f\Gamma^*} M^{-1/2} + \tau_{f\Gamma^*} M_E^{-1/2} + \Delta x^p + \Delta v^q \right\} \end{aligned}$$

with

$$\begin{aligned} \sigma_{f\Gamma^*}^2 &= \left\| \left( 1 - \sum_{h=1}^L \rho_{f, g_h}^2 \right) \text{Var}(f) \right\|_{L_2^1(\mathcal{D} \times \mathbb{R}^{d_v})}, \\ \tau_{f\Gamma^*}^2 &= \left\| \sum_{h=1}^L \rho_{f, g_h}^2 \text{Var}(f) \right\|_{L_2^1(\mathcal{D} \times \mathbb{R}^{d_v})}, \end{aligned}$$

and  $C > 0$  depends on the final time and on the initial data.

### 3.5. Hierarchical multi-fidelity MSCV methods. —

**3.5.1. The space homogeneous case.** — We formulate in this part a recursive construction of the multiple control variate estimator (86) based on the use of several low-fidelity models.

To this aim, let us assume that the control variates  $f_1, \dots, f_L$  represent kinetic models with an increasing level of fidelity. Under this assumption the control variate  $f_1$  represents the less accurate model whereas the control variate  $f_L$  is the closer model to the high fidelity model  $f$ .

To start with, we estimate  $\mathbb{E}[f]$  with  $M_L$  samples using  $f_L$  as control variate

$$\mathbb{E}[f] \approx E_{M_L}[f] - \hat{\lambda}_L (E_{M_L}[f_L] - \mathbb{E}[f_L]).$$

Next, to estimate of  $\mathbb{E}[f_L]$  we use  $M_{L-1} \gg M_L$  samples and consider  $f_{L-1}$  as control variate

$$\mathbb{E}[f_L] \approx E_{M_{L-1}}[f_L] - \hat{\lambda}_{L-1} (E_{M_{L-1}}[f_{L-1}] - \mathbb{E}[f_{L-1}]).$$

Similarly, in a recursive way we can construct estimators for the remaining expectations of the control variates  $\mathbb{E}[f_{L-2}], \mathbb{E}[f_{L-3}], \dots, \mathbb{E}[f_2]$  using respectively  $M_{L-3} \ll M_{L-4} \ll \dots \ll M_1$  samples until

$$\mathbb{E}[f_2] \approx E_{M_1}[f_2] - \hat{\lambda}_1 (E_{M_1}[f_1] - \mathbb{E}[f_1]),$$

and we stop with the final estimate

$$\mathbb{E}[f_1] \approx E_{M_0}[f_1],$$

with  $M_0 \gg M_1$ . By combining the estimators of each stage together we obtain the hierarchical MSCV estimator

$$\begin{aligned} E_L^{r, \hat{\Lambda}}[f] &= E_{M_L}[f] - \hat{\lambda}_L (E_{M_L}[f_L] - E_{M_{L-1}}[f_L]) \\ &+ \hat{\lambda}_{L-1} (E_{M_{L-1}}[f_{L-1}] - E_{M_{L-2}}[f_{L-1}]) \\ &\dots \\ &+ \hat{\lambda}_1 (E_{M_1}[f_1] - E_{M_0}[f_1]) \dots \end{aligned} \quad (102)$$

Now, if we compute the optimal values  $\hat{\lambda}_h^*$  independently for each level by ignoring the errors due to the approximations of the various expectations, if  $\text{Var}(f_h) \neq 0$ , we obtain

$$\hat{\lambda}_h^* = \frac{\text{Cov}(f_{h+1}, f_h)}{\text{Var}(f_h)}, \quad h = 1, \dots, L \quad (103)$$

where we used the notation  $f_{L+1} = f$ . We refer to this set of values as quasi-optimal since they are obtained in the hypothesis in which the expectations are computed without any approximations. Note also that, since the control variates  $f_{h+1}$  and  $f_h$  are known on the same set of samples  $M_h$  the values  $\hat{\lambda}_h^*$  can be estimated using (63)-(64).

We now analyze the estimator (102) in more details. We can recast it in the form

$$\begin{aligned}
 E_L^{\hat{\Lambda}}[f] &= E_{M_L}[f_{L+1}] - \sum_{h=1}^L \lambda_h (E_{M_h}[f_h] - E_{M_{h-1}}[f_h]) \\
 (104) \qquad &= \lambda_1 E_{M_0}[f_1] + \sum_{h=1}^L (\lambda_{h+1} E_{M_h}[f_{h+1}] - \lambda_h E_{M_h}[f_h]),
 \end{aligned}$$

where we defined

$$(105) \qquad \lambda_h = \prod_{j=h}^L \hat{\lambda}_j, \quad h = 1, \dots, L, \quad \lambda_{L+1} = 1.$$

Since by the central limit theorem [37, 56] we have  $\text{Var}(E_M[f]) = M^{-1} \text{Var}(f)$ , using the independence of the estimators  $E_{M_h}[\cdot]$ ,  $h = 0, \dots, L$ , the total variance of the estimator (104) is

$$\begin{aligned}
 \text{Var}(E_L^{\hat{\Lambda}}[f]) &= \lambda_1^2 M_0^{-1} \text{Var}(f_1) \\
 &+ \sum_{h=1}^L M_h^{-1} \{ \lambda_{h+1}^2 \text{Var}(f_{h+1}) + \lambda_h^2 \text{Var}(f_h) - 2\lambda_{h+1}\lambda_h \text{Cov}(f_{h+1}, f_h) \}.
 \end{aligned}$$

Now, the first order optimality conditions

$$\frac{\partial \text{Var}(E_L^{\hat{\Lambda}}[f])}{\partial \lambda_h} = 0, \quad h = 1, \dots, L$$

lead to the tridiagonal system for  $h = 1, \dots, L$

$$\begin{aligned}
 (106) \qquad \lambda_h \text{Var}(f_h) - \lambda_{h-1} \frac{M_h}{M_{h-1} + M_h} \text{Cov}(f_h, f_{h-1}) \\
 - \lambda_{h+1} \frac{M_{h-1}}{M_{h-1} + M_h} \text{Cov}(f_{h+1}, f_h) = 0
 \end{aligned}$$

where we assumed  $\lambda_0 = 0$  and  $\lambda_{L+1} = 1$ . The system (106) can be rewritten as

$$\hat{\lambda}_h \text{Var}(f_h) - \text{Cov}(f_{h+1}, f_h) = \frac{M_h \left( \hat{\lambda}_h \hat{\lambda}_{h-1} \text{Cov}(f_h, f_{h-1}) + \text{Cov}(f_{h+1}, f_h) \right)}{M_{h-1} + M_h}.$$

The above expression permits to conclude that the quasi-optimal values computed in (103) solves the above system up to  $O(M_h/(M_{h-1} + M_h))$  error and thus they are a sufficiently good approximation in the case in which  $M_{h-1} \ll M_h$ . The following Theorem holds true [24]

**Theorem 3.5.** — *The vector  $\Lambda^* = (\lambda_1^*, \dots, \lambda_L^*)^T$  solution of (106) minimizes the variance of the estimator (104). In particular the vector  $\hat{\Lambda}^*$  (103) of quasi-optimal solutions is such that*

$$(107) \quad \prod_{j=h}^L \hat{\lambda}_j^* = \lambda_h^* + O(\bar{\mu}_h), \quad h = 1, \dots, L$$

$$\text{where } \bar{\mu}_h = \max_{h \leq k \leq L} \left\{ \frac{M_k}{M_{k-1} + M_k} \right\}.$$

We summarized in Algorithm 4 the details of the hierarchical MSCV method applied to the space homogeneous problem (49) in combination with a deterministic solver.

Regarding the error bound that we obtain using (104) with the values given by (103) let us observe that if, at each stage, we denote

$$E_{M_h}^{\hat{\lambda}_h} [f_h] = E_{M_h} [f_h] - \hat{\lambda}_h (E_{M_h} [f_{h-1}] - E_{M_{h-1}} [f_{h-1}^n])$$

then by the error bound (77) we have

$$\|\mathbb{E}[f_h](\cdot, t) - E_{M_h}^{\hat{\lambda}_h} [f_h](\cdot, t)\|_{L_2^1(\mathbb{R}^{d_v}; L^2(\Omega))} \leq C_h \left\{ \sigma_h M_h^{-1/2} + \tau_h M_{h-1}^{-1/2} \right\}$$

where  $C_h > 0$  is a suitable constant and we defined

$$(110) \quad \sigma_h = \left\| \left( 1 - \rho_{f_h, f_{h-1}}^2 \right)^{1/2} \text{Var}(f_h)^{1/2} \right\|_{L_2^1(\mathbb{R}^{d_v})},$$

$$(111) \quad \tau_h = \|\rho_{f_h, f_{h-1}} \text{Var}(f_h)^{1/2}\|_{L_2^1(\mathbb{R}^{d_v})}.$$

Thus one can prove the following result

**Proposition 3.4.** — *Consider a deterministic scheme which satisfies (45) for the solution of (49) with random sufficiently regular initial data  $f(z, v, 0) = f_0(z, v)$ . Then, the hierarchical MSCV estimate defined in (102) satisfies the error bound*

$$(112) \quad \begin{aligned} & \|\mathbb{E}[f](\cdot, t^n) - E_L^{\hat{\Lambda}^*} [f_{\Delta v}^n]\|_{L_2^1(\mathbb{R}^{d_v}; L^2(\Omega))} \\ & \leq C \left( \sum_{h=1}^L \xi_h \sigma_h M_h^{-1/2} + \xi_0 M_0^{-1/2} + \Delta v^{q_2} \right) \end{aligned}$$

where  $\xi_h = \prod_{j=h+1}^L \tau_j$ , and  $C > 0$  depends on the final time and on the initial data.

---

**Algorithm 4:** Hierarchical MSCV method

---

1. **Sampling:** For each control variate  $f_h$ , we draw a number  $M_h$  of i.i.d. samples from the random initial data  $f_0$  and approximate these over the mesh  $\Delta v$ . Denote these control variate dependent number of samples for  $h = 1, \dots, L$  by

$$f_{h,\Delta v}^{k,0}, \quad k = 1, \dots, M_h$$

and set  $f_{\Delta v}^{k,0} = f_{L,\Delta v}^{k,0}$ ,  $k = 1, \dots, M_L$ .

2. **Solving:**

- (a) For each control variate and for each realization of the random input data  $f_{h,\Delta v}^{k,0}$ ,  $k = 1, \dots, M_h$ , the resulting model is solved with mesh widths  $\Delta v$ . We denote the resulting ensemble of deterministic solutions for  $h = 1, \dots, L$  at time  $t^n$  by

$$f_{h,\Delta v}^{k,n}, \quad k = 1, \dots, M_h.$$

- (b) For each realization  $f_{\Delta v}^{k,0}$ ,  $k = 1, \dots, M_L$  the underlying kinetic equation (1) is solved with mesh widths  $\Delta v$ . We denote the solution at time  $t^n$  by  $f_{\Delta v}^{k,n}$ ,  $k = 1, \dots, M_L$ .

3. **Estimating:**

- (a) Estimate the quasi-optimal vector of values  $\hat{\Lambda}^*$  as

$$(108) \quad \hat{\lambda}_h^{*,n} = \frac{\text{Cov}_{M_h}(f_{h+1,\Delta v}^n, f_{h,\Delta v}^n)}{\text{Var}_{M_h}(f_{h,\Delta v}^n)}, \quad h = 1, \dots, L$$

where we used the notation  $f_{L+1,\Delta v}^{k,n} = f_{\Delta v}^{k,n}$ ,  $k = 1, \dots, M_L$ .

- (b) Compute the expectation of the random solution with the control variate estimator

$$(109) \quad E_L^{\hat{\Lambda}^*}[f_{\Delta v}^n] = \frac{1}{M_L} \sum_{k=1}^{M_L} f_{\Delta v}^{k,n} - \sum_{h=1}^L \lambda_h^{*,n} \left( \frac{1}{M_h} \sum_{k=1}^{M_h} f_{h,\Delta v}^{k,n} - \mathbf{f}_{h,\Delta v}^n \right),$$

where

$$\mathbf{f}_{h,\Delta v}^n = \frac{1}{M_{h-1}} \sum_{k=1}^{M_{h-1}} f_{h,\Delta v}^{k,n}, \quad \lambda_h^{*,n} = \prod_{j=h}^L \hat{\lambda}_j^{*,n}, \quad h = 1, \dots, L.$$


---

**3.5.2. The space non homogeneous case.** — In a space non homogeneous setting the hierarchical multi-fidelity MSCV estimator (104), based on the control variates  $f_1(z, x, v, t)$ ,  $\dots$ ,  $f_L(z, x, v, t)$  with increasing level of fidelity

for the solution  $f(z, x, v, t)$  to (1), is

$$(113) \quad \begin{aligned} E_L^\Lambda[f](x, v, t) &= E_{M_L}[f](x, v, t) \\ &- \sum_{h=1}^L \lambda_h (E_{M_h}[f_h](x, v, t) - E_{M_{h-1}}[f_h](x, v, t)), \end{aligned}$$

with  $M_{h-1} \gg M_h$  and where now the optimal values of  $\Lambda^* = (\lambda_1^*, \dots, \lambda_L^*)^T$  are obtained from the quasi-optimal solution (103) using (105) or by the correction introduced by the solution of the tridiagonal system (106) if relevant. In this case, the extension of algorithms 4 and estimate (112) to the non homogeneous case follows straightforwardly simply replacing  $f_{\Delta v}^{n,k}$  and  $f_{h,\Delta v}^{n,k}$  with  $f_{\Delta x, \Delta v}^{n,k}$  and  $f_{h,\Delta x, \Delta v}^{n,k}$ , and is omitted for brevity.

For sake of clarity and due to its importance in practical applications, we describe the details of the hierarchical method in the case  $L = 2$ . We consider  $f_1(z, x, v, t)$  as the equilibrium state  $f_F^\infty(z, x, v, t)$  associated to the system of Euler equations (10) with  $U_F = (\rho_F, u_F, T_F)^T$ , and corresponding to the limit case  $\varepsilon \rightarrow 0$  in (1). As a second control variate we consider  $f_2(z, x, v, t)$  as the solution of the BGK model (14). Both models are solved for the same initial data  $f_0(z, x, v)$ . Now, the Euler equations are used as control variate to improve the computation of the expectation in the BGK model, that in turn is used as control variate to improve the computation of the expectation in the full Boltzmann model.

The hierarchical two-level estimator reads

$$(114) \quad \begin{aligned} E_2^{\hat{\lambda}_1, \hat{\lambda}_2}[f] &= E_{M_2}[f] \\ &- \hat{\lambda}_2 (E_{M_2}[f_2] - E_{M_1}[f_2] + \hat{\lambda}_1 (E_{M_1}[f_1] - E_{M_0}[f_1])), \end{aligned}$$

where  $M_0 \gg M_1 \gg M_2$ . If we define  $\lambda_2 = \hat{\lambda}_2$  and  $\lambda_1 = \hat{\lambda}_1 \hat{\lambda}_2$  their optimal values are computed as solutions of system (106) for  $L = 2$

$$\begin{aligned} \lambda_1 \text{Var}(f_1) - \lambda_2 (1 - \mu_1) \text{Cov}(f_2, f_1) &= 0 \\ \lambda_2 \text{Var}(f_2) - \lambda_1 \mu_2 \text{Cov}(f_2, f_1) &= (1 - \mu_2) \text{Cov}(f, f_2). \end{aligned}$$

with  $\mu_h = M_h / (M_{h-1} + M_h)$ , which gives

$$\begin{aligned} \lambda_1^* &= \frac{(1 - \mu_1)(1 - \mu_2) \text{Cov}(f_2, f_1) \text{Cov}(f, f_2)}{\text{Var}(f_1) \text{Var}(f_2) - (1 - \mu_1) \mu_2 \text{Cov}(f_2, f_1)^2} \\ \lambda_2^* &= \frac{(1 - \mu_2) \text{Var}(f_1) \text{Cov}(f, f_2)}{\text{Var}(f_1) \text{Var}(f_2) - (1 - \mu_1) \mu_2 \text{Cov}(f_2, f_1)^2}. \end{aligned}$$

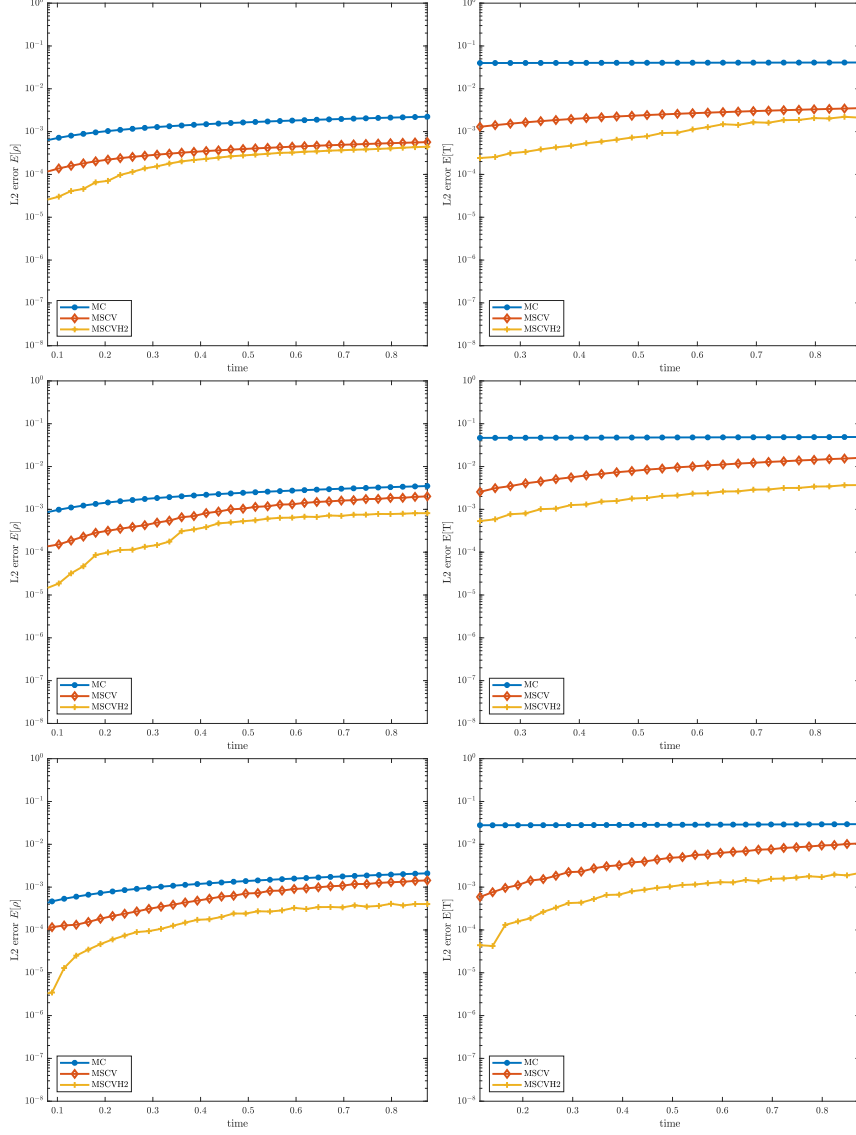


FIGURE 6. Hierarchical MSCV method - Sod test with uncertainty in the initial data.  $L_2$  norm of the error for the MC method, the MSCV method and the MSCVH2 method for  $\mathbb{E}[\rho]$  (left) and  $\mathbb{E}[T]$  (right). The number of samples is  $M = 10$ , for the BGK model  $M_{E_1} = 100$  and for the Euler system  $M_{E_2} = 10^5$ . From top to bottom:  $\varepsilon = 10^{-2}, 10^{-3}, 2 \times 10^{-4}$ .

The quasi-optimal values are instead obtained assuming  $\mu_1, \mu_2 \approx 0$  and are characterized by

$$(115) \quad \hat{\lambda}_1^* = \frac{\text{Cov}(f_2, f_1)}{\text{Var}(f_1)}, \quad \hat{\lambda}_2^* = \frac{\text{Cov}(f, f_2)}{\text{Var}(f_2)}.$$

In Figure 6 we compare the results of the MSCV approach with two hierarchical levels (MSCHVH2) against the standard MC and the bi-fidelity MSCV method based on the BGK model discussed in Section 3.3.2. The initial conditions are given by Sod problem with uncertainty (80). The Boltzmann equation has been solved with the same discretization parameters as in Figure 3. For this situation, we perform three different computations corresponding to  $\varepsilon = 10^{-2}$ ,  $\varepsilon = 10^{-3}$  and  $\varepsilon = 2 \times 10^{-4}$ . The  $L_2$  norms of the errors for the standard MC method, the MSCV approach and the MSCVH2 method for the expected value of the temperature and the density as a function of time are shown in the figure. The number of samples used for the BGK model is  $M_{E_1} = 100$  while for the compressible Euler system is  $M_{E_2} = 10^5$ . In all regimes the gain of the hierarchical two-level approach is remarkable and improves for smaller values of the Knudsen number.

**3.6. Mean-field control variate methods.** — In this section we discuss two important issues that have remained open since the previous presentation of the MSCV method. Namely, how to couple the MSCV strategy with particle-based solvers in physical space, and how to extend the range of applicability of the methods to other kinetic equations where an equilibrium state is not known and thus the classical closure of rarefied gas dynamics cannot be adopted.

As a prototype example to develop our arguments, we will consider the Boltzmann model for socio-economic interactions with uncertainty introduced in Section 2.2.

**3.6.1. The DSMC method for kinetic equations.** — Let us first recall the classical Direct Simulation Monte Carlo (DSMC) method for the solution of the Boltzmann equation [9, 65] in case without uncertainty. We are in particular interested in the evolution of the density  $f = f(w, t)$  solution of (18) with initial condition  $f(0, w) = f_0(w)$ . The DSMC method in the form originally proposed by Nanbu [65] is reported in Algorithm 5. We refer to [71, 74, 88] for an introduction to Monte Carlo methods for kinetic equations.

The kinetic distribution as well as its moments are then recovered from the empirical density function

$$(116) \quad f_N(t, w) = \frac{1}{N} \sum_{i=1}^N \delta(w - w_i(t)),$$



---

**Algorithm 5:** DSMC method

---

1. Let us consider a time interval  $[0, T]$ , and let us discretize it in  $n_t$  intervals of size  $\Delta t$ .
  2. Compute the initial sample particles  $\{w_i^0, i = 1, \dots, N\}$ , by sampling them from the initial density  $f_0(w)$
  3. for  $n = 0$  to  $n_t - 1$ 
    - given  $\{w_i^n, i = 1, \dots, N\}$ 
      - set  $N_c = \text{Sround}(N\Delta t/2)$  (stochastic rounding)
      - select  $N_c$  pairs  $(i, j)$  uniformly among all possible pairs,
        - perform the collision between  $i$  and  $j$ , and compute  $w'_i$  and  $w'_j$  according to the collision law (15)
        - set  $w_i^{n+1} = w'_i, w_j^{n+1} = w'_j$
      - set  $w_i^{n+1} = w_i^n$  for all the particles not selected
- end for
- 

where  $\delta(\cdot)$  is the Dirac delta and  $\{w_i(t), i = 1, \dots, N\}$  are the samples of particles at time  $t \geq 0$ . For any test function  $\varphi$ , if we now denote by

$$\langle \varphi, f \rangle(t) = \int_V \varphi(w) f(t, w) dw,$$

we have

$$(117) \quad \langle \varphi, f_N \rangle(t) = \frac{1}{N} \sum_{i=1}^N \varphi(w_i(t)).$$

Hence, by assuming that  $\int_V f(t, w) dw = 1$  we have that  $\langle \varphi, f \rangle = \mathbb{E}_V[\varphi]$ , where  $\mathbb{E}_V[\cdot]$  is the expectation of the observable quantity  $\varphi$  with respect to the density  $f$  to be distinguished from  $\mathbb{E}[\cdot]$  used to denote the expectation in the random space of uncertainties. Thanks to the central limit theorem we have [12]

**Lemma 3.2.** — *The root mean square error is such that for each  $t \geq 0$*

$$(118) \quad \mathbb{E}_V \left[ (\langle \varphi, f \rangle - \langle \varphi, f_N \rangle)^2 \right]^{1/2} = \frac{\sigma_\varphi}{N^{1/2}},$$

where  $\sigma_\varphi^2 = \text{Var}_V[\varphi]$  with

$$(119) \quad \text{Var}_V[\varphi](t) = \int_V (\varphi(w) - \langle \varphi, f \rangle(t))^2 f(t, w) dw.$$

While the moments of the distribution can be easily computed via (117) if one is interested in the shape of the distribution function one must do an appropriate reconstruction. For example, one can operate as follows: set up a

uniform grid in  $V \subseteq \mathbb{R}$  where each cell has width  $\Delta w > 0$  and subsequently define a smoothing function  $S_{\Delta w} \geq 0$  such that

$$\Delta w \int_V S_{\Delta w}(w) dw = 1.$$

Then, the approximation of the empirical density (116) is obtained by

$$(120) \quad f_{N,\Delta w}(t, w) = \frac{1}{N} \sum_{i=1}^N S_{\Delta w}(w - w_i(t)).$$

In the simplest case,  $S_{\Delta w}(w) = \chi(|w| \leq \Delta w/2)/\Delta w$ , where  $\chi(\cdot)$  is the indicator function, (120) corresponds to the standard histogram reconstruction. Then, the numerical error of the reconstructed DSMC solution (120), can be estimated from

$$\|g\|_{L^p(V, L^2(V))} = \|\mathbb{E}_V [g^2]\|_{L^p(V)}^{1/2},$$

as [76]

**Theorem 3.6.** — *The error introduced by the reconstruction function (120) satisfies*

$$(121) \quad \|f(t, \cdot) - f_{N,\Delta w}(t, \cdot)\|_{L^p(V, L^2(V))} \leq \frac{\|\sigma_S\|_{L^p(V)}}{N^{1/2}} + C_f(\Delta w)^q,$$

where  $C_f$  depends on the  $q$  derivative in velocity of  $f$  and  $\sigma_S^2$  is given by

$$(122) \quad \sigma_S^2(w, t) = \mathbb{V}ar_V[S_{\Delta w}(w - \cdot)](t).$$

**3.6.2. The combined MC-DSMC method for uncertainty quantification.** —

Let assume  $f(t, w, z)$ ,  $w \in V$ , solution of a PDE with uncertainties only in the initial distribution  $f_0(w, z)$ ,  $z \in \Omega \subseteq \mathbb{R}^{d_z}$ . The MC sampling method for the uncertainty quantification has been formulated in Section 3.2. The only difference with respect to (46) is the way in which the deterministic kinetic equation is solved since here a DSMC method is used.

The empirical kinetic distribution in presence of uncertainty is given by

$$f_N(t, w, z) = \frac{1}{N} \sum_{i=1}^N \delta(w - w_i(t, z)),$$

being  $\{w_i(t, z), i = 1, \dots, N\}$  the samples of the particles at time  $t \geq 0$  such that  $w_i \in L^2(\Omega)$ .

While the algorithm is similar to the deterministic case, the error analysis is different and the following result holds true [76]

**Lemma 3.3.** — *The root mean square error of the MC-DSMC method satisfies*

$$\mathbb{E} \left[ \mathbb{E}_V [(\mathbb{E}[\langle \varphi, f \rangle] - E_M[\langle \varphi, f_N \rangle])^2] \right]^{1/2} \leq \frac{\nu_{\langle \varphi, f \rangle}}{M^{1/2}} + \frac{\sigma_{\varphi, M}}{N^{1/2}},$$

where  $\nu_{\langle \varphi, f \rangle}^2 = \text{Var}[\langle \varphi, f \rangle]$  and  $\sigma_{\varphi, M}^2 = E_M[\sigma_\varphi^2]$  with  $\sigma_\varphi^2 = \text{Var}_V[\varphi]$ .

Let us now consider the reconstructed distribution with uncertainty

$$(123) \quad f_{N, \Delta w}(t, w, z) = \frac{1}{N} \sum_{i=1}^N S_{\Delta w}(w - w_i(t, z)),$$

and let us focus on the accuracy of the expectation of the solution  $\mathbb{E}[f]$ . One can give, using

$$\|g\|_{L^p(V, L^2(\Omega, L^2(V)))} = \|\mathbb{E}[\mathbb{E}_V[g^2]]^{1/2}\|_{L^p(V)},$$

the following estimate [76]

**Theorem 3.7.** — *The error introduced by the reconstruction function (123) in the MC-DSMC method satisfies*

$$(124) \quad \begin{aligned} & \|\mathbb{E}[f](t, \cdot) - E_M[f_{N, \Delta w}](t, \cdot)\|_{L^p(V, L^2(\Omega, L^2(V)))} \\ & \leq \frac{\|\nu_{\langle S, f \rangle}\|_{L^p(V)}}{M^{1/2}} + \frac{\|\sigma_{S, M}\|_{L^p(V)}}{N^{1/2}} + C_{\mathbb{E}[f]}(\Delta w)^q \end{aligned}$$

where  $\nu_{\langle S, f \rangle}^2$  is defined as

$$(125) \quad \nu_{\langle S, f \rangle}^2 = \text{Var}[(S_{\Delta w}(w - \cdot), f)].$$

and  $\sigma_{S, M}^2 = E_M[\sigma_S^2]$  with  $\sigma_S^2$  defined in (122).

**3.6.3. Mean Field Control Variate DSMC methods.** — In order to improve the accuracy of standard MC sampling methods, we introduce a class of mean field control variate methods playing the role of the low-fidelity model. The key idea is to take advantage of the reduced cost of the mean field model which approximates the asymptotic behavior of the original Boltzmann model. More precisely we consider two different control variates strategies obtained by the mean field approximation: the direct numerical solution of the mean field model and its corresponding steady state. In the sequel most of the analysis is reported for a general quantity of interest  $q[f]$ .

Let us denote by  $\tilde{f} = \tilde{f}(t, w, z)$  the solution of the mean field model (19) complemented by the same initial distribution  $\tilde{f}(0, w, z) = f_0(w, z)$  of the high fidelity model. As discussed in Section 2.2 for small values of the scaling parameter  $\varepsilon$  we have

$$\lim_{\varepsilon \rightarrow 0} f_\varepsilon(t, w, z) = \tilde{f}(t, w, z),$$

being  $f_\varepsilon$  solution of the high-fidelity Boltzmann model (18). Therefore, also the equilibrium distribution is such that

$$\lim_{t \rightarrow \infty} \lim_{\varepsilon \rightarrow 0} f_\varepsilon(t, w, z) = \tilde{f}^\infty(w, z).$$

In this setting, the parameter dependent control variate method with  $\lambda \in \mathbb{R}$  can be formulated introducing the quantity

$$(126) \quad q^\lambda[f_\varepsilon] = q[f_\varepsilon] - \lambda(q[\tilde{f}] - \mathbb{E}[q[\tilde{f}]]).$$

By the same arguments as in Section 3.3 we can state also the following

**Theorem 3.8.** — *The optimal value  $\lambda^*$  which minimizes the variance of (126) is given by*

$$(127) \quad \lambda^* := \frac{\text{Cov}[q[f_\varepsilon], q[\tilde{f}]]}{\text{Var}[q[\tilde{f}]]},$$

where  $\text{Cov}[\cdot, \cdot]$  denotes the covariance. The corresponding variance of  $q^{\lambda^*}[f_\varepsilon]$  is then

$$(128) \quad \text{Var}[q^{\lambda^*}[f_\varepsilon]] = \left(1 - \rho_{q[f_\varepsilon], q[\tilde{f}]}^2\right) \text{Var}[q[f_\varepsilon]],$$

where

$$\rho_{q[f_\varepsilon], q[\tilde{f}]} := \frac{\text{Cov}[q[f_\varepsilon], q[\tilde{f}]]}{\sqrt{\text{Var}[q[f_\varepsilon]] \text{Var}[q[\tilde{f}]]}} \in (-1, 1),$$

is the correlation coefficient between  $q[f_\varepsilon]$  and  $q[\tilde{f}]$ . In particular, we have

$$\lim_{\varepsilon \rightarrow 0} \frac{\text{Cov}[q[f_\varepsilon], q[\tilde{f}]]}{\text{Var}[q[\tilde{f}]]} = 1, \quad \lim_{\varepsilon \rightarrow 0} \text{Var}[q^{\lambda^*}[f_\varepsilon]] = 0.$$

Of course, the control variate formulation in (126) can be modified using the steady state  $\tilde{f}_\infty(w, z)$  of the mean-field model (19)

$$(129) \quad q^\lambda[f_\varepsilon] = q[f_\varepsilon] - \lambda(q[\tilde{f}_\infty] - \mathbb{E}[q[\tilde{f}_\infty]]).$$

Then, for the mean field control variate steady state (129), a similar results holds in the large time limit, as the ones shown in Theorem 3.8.

Let us now give the details of the Mean Field Control Variate (MFCV) algorithm. To that aim, we recall that using  $M$  realizations of our random variable  $z$  to define the Mean Field Control Variate (MFCV) estimator, we have

$$\mathbb{E}[q^{\lambda^*}[f_\varepsilon]] \approx E_M[q^{\lambda^*}[f_\varepsilon]] = E_M[q[f_\varepsilon]] - \frac{C_M[q[f_\varepsilon], q[\tilde{f}]]}{V_M[q[\tilde{f}]]} (E_M[q[\tilde{f}]] - \mathbb{E}[q[\tilde{f}]]),$$

where  $\mathbb{E}[q[\tilde{f}]]$  denotes the exact value of the expectation of the quantity of interest or its numerical approximation with negligible error. Furthermore, we have the following notations

$$\begin{aligned} E_M[q[f_\varepsilon]] &:= \frac{1}{M} \sum_{k=1}^M q[f_\varepsilon^k], & E_M[q[\tilde{f}]] &:= \frac{1}{M} \sum_{k=1}^M q[\tilde{f}^k] \\ V_M[q[\tilde{f}]] &:= \frac{1}{M-1} \sum_{k=1}^M (q[\tilde{f}^k] - E_M[q[\tilde{f}]])^2, \\ C_M[q[f_\varepsilon], q[\tilde{f}]] &:= \frac{1}{M-1} \sum_{k=1}^M (q[f_\varepsilon^k] - E_M[q[f_\varepsilon]]) (q[\tilde{f}^k] - E_M[q[\tilde{f}]]), \end{aligned}$$

being  $f_\varepsilon^k$  and  $\tilde{f}^k$  the solutions of the Boltzmann-type and the mean-field models, respectively, relative to  $k$ th realization of the random variable  $z$ . The corresponding MFCV algorithm based on a DSMC method is reported in Algorithm 6.

Concerning the evaluation of moments, by ignoring the error term due to the approximation of  $\lambda_*$ , we have the following [76]

**Lemma 3.4.** — *The root mean square error of the MFCV-DSMC method satisfies*

$$(130) \quad \begin{aligned} &\mathbb{E} \left[ \mathbb{E}_V \left[ \left( \mathbb{E}[\langle \varphi, f_\varepsilon \rangle] - E_M^{\lambda_*}[\langle \varphi, f_{\varepsilon, N} \rangle] \right)^2 \right] \right]^{1/2} \\ &\leq \left( 1 - \rho_{\langle \varphi, f_\varepsilon \rangle, \langle \varphi, \tilde{f} \rangle}^2 \right)^{1/2} \frac{\nu_{\langle \varphi, f_\varepsilon \rangle}}{M^{1/2}} + \frac{\sigma_{\varphi, M}}{N^{1/2}}, \end{aligned}$$

where  $\nu_{\langle \varphi, f_\varepsilon \rangle}^2 = \text{Var}[\langle \varphi, f_\varepsilon \rangle]$  and  $\sigma_{\varphi, M}^2 = E_M[\sigma_\varphi^2]$  with  $\sigma_\varphi^2 = \text{Var}_V[\varphi]$ .

In the case of the reconstruction function (123), we have

$$\begin{aligned} &\left\| \mathbb{E}[f_\varepsilon](t, \cdot) - E_M^{\lambda_*}[f_{\varepsilon, N, \Delta w}](t, \cdot) \right\|_{L^p(V, L^2(\Omega, L^2(V)))} \\ &\leq \left\| \mathbb{E}[f_\varepsilon](t, \cdot) - \mathbb{E}[f_{\varepsilon, \Delta w}](t, \cdot) \right\|_{L^p(V)} \\ &\quad + \left\| \mathbb{E}[f_{\varepsilon, \Delta w}](t, \cdot) - E_M^{\lambda_*}[f_{\varepsilon, N, \Delta w}](t, \cdot) \right\|_{L^p(V, L^2(\Omega, L^2(V)))}, \end{aligned}$$

where the first term is bounded as in Theorem 3.7 and the second term can be bounded using Lemma 3.4 with  $\phi(\cdot) = S_{\Delta w}(w - \cdot)$ . Thus we have the following result.

---

**Algorithm 6:** Bi-fidelity MFCV-DSMC method
 

---

1. **Sampling:** Sample  $M$  independent identically distributed (i.i.d.) samples of the initial distribution  $f^{k,0} = f_0(w, z^k)$ ,  $k = 1, \dots, M$  from the random initial data  $f_0(w, z)$ .
2. **Solving:** For each realization  $f^{0,k}$ ,  $k = 1, \dots, M$ 
  - (a) Compute the control variate  $\tilde{f}^{k,n}$ ,  $k = 1, \dots, M$  at time  $t^n$  solving with a suitable deterministic method the mean field model (19) (or using the steady state  $\tilde{f}_\infty$ ) and compute  $\mathbb{E}[q[\tilde{f}^n]]$  (or  $\mathbb{E}[q[\tilde{f}_\infty]]$ ) with negligible error.
  - (b) Solve the kinetic equation (18) by a MC solver with sample size  $N$ . We denote the solution at time  $t^n$  by  $f_{\varepsilon,N}^{k,n}$ ,  $k = 1, \dots, M$ .

**3. Estimating:**

- (a) Estimate the optimal value of  $\lambda^*$  at time  $t^n$  by

$$\lambda_M^{*,n} = \frac{C_M[q[f_{\varepsilon,N}^n], q[\tilde{f}^n]]}{V_M[q[\tilde{f}^n]]},$$

which in the mean field steady state control variate case becomes

$$\lambda_M^{*,n} = \frac{C_M[q[f_{\varepsilon,N}^n], q[\tilde{f}_\infty]]}{V_M[q[\tilde{f}_\infty]]}.$$

- (b) Compute the the expectation of any quantity of interest  $q[f_{\varepsilon,N}]$  of the random solution field with the mean-field control estimator

$$E_M^{\lambda^*}[g[f_{\varepsilon,N}]] = E_M[q[f_{\varepsilon,N}]] - \lambda_M^{*,n}(E_M[q[\tilde{f}^n]] - \mathbb{E}[q[\tilde{f}^n]]).$$


---

**Theorem 3.9.** — *The error introduced by the reconstruction function (123) in the MFCV-DSMC method satisfies*

$$(131) \quad \left\| \mathbb{E}[f_\varepsilon](t, \cdot) - E_M^{\lambda^*}[f_{\varepsilon,N,\Delta w}](t, \cdot) \right\|_{L^p(V, L^2(\Omega, L^2(V)))} \\ \leq \frac{\left\| \left(1 - \rho_{\langle S, f_\varepsilon \rangle, \langle S, \tilde{f} \rangle}^2\right)^{1/2} \nu_{\langle S, f_\varepsilon \rangle} \right\|_{L^p(V)}}{M^{1/2}} + \frac{\|\sigma_{S,M}\|_{L^p(V)}}{N^{1/2}} + C_{\mathbb{E}[f]}(\Delta w)^q$$

where and  $\nu_{\langle S, f_\varepsilon \rangle}^2$  is defined as in (125) and  $\sigma_{S,M}^2$  is defined in Theorem 3.7.

As a consequence when the solution of the high-fidelity model is close to the solution of the control variate the statistical error due to the uncertainty vanishes. This justifies the use of a large number of samples in the velocity

space in agreement with the reconstruction used in order to balance the last two error terms in (131).

**3.6.4. Application to socio-economic sciences.** — We present two numerical examples concerning kinetic models in socio-economic sciences. We will denote by MFCV-S the case where the steady state  $\tilde{f}_\infty(w, z)$  of the mean-field model is analytically known and is used off line as control variate and by MFCV the case where the Fokker-Planck equation (19) is numerically solved and used as a time dependent control variate. The mean field model is solved by the second order structure preserving method for nonlocal Fokker-Planck equations developed in [77]. The solutions are averaged over 50 runs to reduce statistical fluctuations. In order to compute with negligible error  $\mathbb{E}[\tilde{f}_\infty]$  we adopt a stochastic collocation approach with 20 collocation nodes.

We first consider the kinetic model for opinion formation (20) with uncertainties present on the initial distribution or on the interaction strength. We assume that  $z \sim \mathcal{U}([0, 1])$  and the initial distribution  $f_0(w, z)$  is given by

$$(132) \quad f_0(w, z) = \begin{cases} 1 & w \in \left[ \frac{1}{4}(z-2), \frac{1}{4}(z+2) \right] \\ 0 & \text{otherwise.} \end{cases}$$

We also assume

$$(A) \quad p(|v-w|, z) = 1, \quad D(v) = \sqrt{1-v^2},$$

and thus we obtain a steady state of the Fokker-Planck equation of the form  $\tilde{f}_\infty(w, z)$  given by (22). The Boltzmann equation is solved with  $N = 2 \times 10^4$  particles. The number of grid points of the mean field model is set to  $N_{MF} = 20$  and the number of samples we have chosen is  $M_{MF} = 10^4$  which correspond to a computational cost comparable to  $M = 10$  for the Boltzmann solver. In Figure 7 (left) we report the  $L^2$  error of the expected density obtained by the standard MC and MFCV-S methods for increasing number of samples at time  $t = 5$ . We obtain an improvement in accuracy for the MFCV-S between one and two orders of magnitude using the same number of samples.

As a further case for opinion dynamics we consider the kinetic model (20) with

$$(B) \quad p(|w-v|, z) = \frac{3}{4} + \frac{z}{4}, \quad z \sim \mathcal{U}([-1, 1]), \quad D(w) = 1 - w^2,$$

so that the resulting steady state of the Fokker-Planck model is the Maxwellian-like distribution (21). The initial data in this case is (132) in the deterministic setting  $z = 0$ . In Figure 7 (right), we report the  $L^2$  error of expected probability distribution function computed by the MC and MFCV-S method at the final time for different number of samples. As in case (A) we obtain an improvement

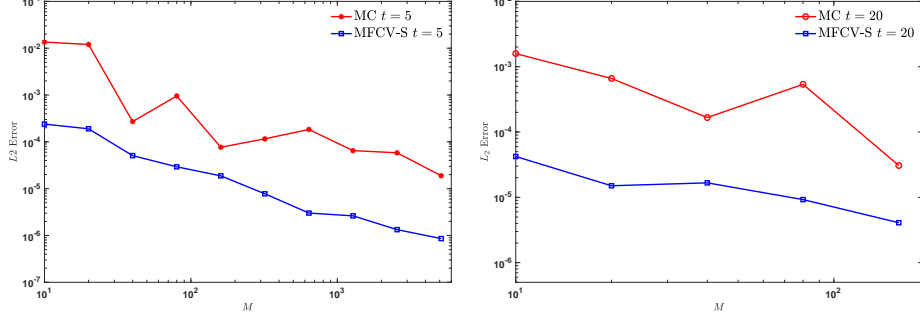


FIGURE 7. MFCV method for opinion dynamics. Error of the MFCV-S estimate and classical MC method for increasing number of samples  $M$ . We considered  $N = 2 \times 10^4$  in the DSMC solver. (Left) Solution at  $t = 5$  of case (A) with uncertain initial data; (Right) Solution at  $t = 20$  of case (B) with uncertain interaction parameters.

between one and two orders of accuracy for the MFCV-S method compared to the classical MC method.

We study now two test cases related to the wealth exchange CPT model defined by (23). First, we consider uncertainty in the initial condition and secondly in the saving propensity. The computational domain is the interval  $[0, 10]$ . Let us first consider  $z \in \mathcal{U}([0, 1])$  and the initial distribution  $f_0(w, z)$  defined by

$$(133) \quad f_0(w, z) = \begin{cases} \frac{1}{2} & w \in \left[\frac{z}{5}, 2 + \frac{z}{5}\right] \\ 0 & \text{otherwise.} \end{cases}$$

Furthermore, we consider

$$(C) \quad \lambda(z) = 1, \quad D(w) = w,$$

so that the large time behavior of the Fokker-Planck model  $\tilde{f}_\infty(w, z)$  is given by (24) with  $m(z) = 1 + \frac{z}{5}$ . As a second case, we consider uncertainty in the interaction

$$(D) \quad \lambda(z) = \frac{1}{2} + \frac{z}{4}, \quad z \sim \mathcal{U}([-1, 1]), \quad D(w) = w.$$

The initial condition is uniformly distributed on  $[0, 2]$ , so that the large time behavior of the Fokker-Planck model is given by (24) with  $m_{\tilde{f}} \equiv 1$ . The DSMC solver for the Boltzmann model uses  $N = 5 \times 10^4$  particles. For the mean field scheme instead we consider  $N_{MF} = 100$  and we choose  $M_{MF} = 5 \times 10^3$  which gives a comparable cost of the full Boltzmann solver for  $M = 10$ . In Figure 8, we compare the  $L^2$  error of  $\mathbb{E}[f_\varepsilon]$  computed by the MFCV or MFCV-S method



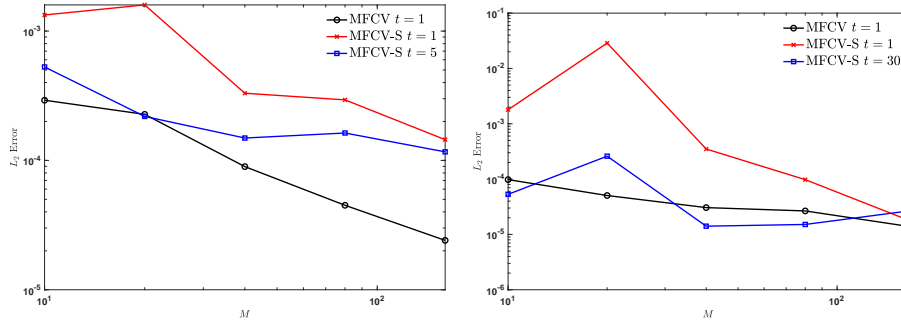


FIGURE 8. MFCV method for a wealth exchange model. The  $L^2$  error of  $\mathbb{E}[f]$  computed by the MFCV-S and the MFCV methods for different number of samples  $M$  at  $t = 1$  and  $t = 5$ . The left hand side corresponds to the setting of case (C) and the right to case (D).

at fixed times but for different number of samples  $M$ . We obtain that the  $L^2$  error of the expected probability distribution function of the MFCV-S method is considerably smaller at larger times. In comparison to the MFCV-S method, MFCV method is able to be more accurate even at early times.

#### 4. Bi-fidelity stochastic collocation methods

In the examples of multi-fidelity models that were discussed in the previous section, high-fidelity samples are not selected based on any criteria other than the fact that they are small in number compared to low-fidelity samples. Here, following [6,30,54,55] we explore a different direction and we focus on stochastic collocation methods based on bi-fidelity algorithms. The main idea is that within the bi-fidelity approximation, one employs the cheap low-fidelity model to explore the random parameter space and to select the most important parameter points in this space. After that, by applying exactly the same approximation rule learnt from the low-fidelity model, one solves the high-fidelity model. Following the above idea, we first review the BFSC methods in its generality. After we focus on its application to efficient uncertainty quantification for the Boltzmann equation of Section 2.1, the linear transport equation of Section 2.3 and finally the epidemic transport models of Section 2.4.

**4.1. A Bi-fidelity stochastic collocation (BFSC) algorithm.** — To set the stage for the discussion, we first introduce basic notions in the following. We let  $u(x, t; z)$  be the solution of a complex system subject to uncertainty, where  $x \in \mathcal{D}$  and  $t$  are the spatial and temporal variables.  $z \in \Omega \subset \mathbb{R}^{d_z}$

is a  $d_z$ -dimensional random variable. Here  $\Omega$  is the support of  $z$ , where the probability distribution  $p(z)$  is defined. For the sake of simplicity, we denote  $u(x, t; z)$  by  $u(z)$  when from the context the dependence on the other variables will be clear. Let us assume now the high-fidelity solutions  $u^H(z)$  and low-fidelity solutions  $u^L(z)$  are available. Let also  $N$  be the number of affordable low-fidelity simulation runs, which, in principle, is very large due to the reduced complexity of the model. On the other hand,  $M$  denotes the number of high-fidelity simulation runs that can be afforded and it is typically very small, i.e. the setting is such that  $N \gg M$ . Note that in this section, to simplify notations, we will use  $N$  to denote the number of samples used by the low-fidelity model instead of  $M_E$  as in Section 3.3. Let finally  $\gamma_k = \{z_1, \dots, z_k\}$ ,  $k \geq 1$  be a set of sample points in  $\Omega$ .

We denote by  $u^L(\gamma_k) = [u^L(z_1), \dots, u^L(z_k)]$  the low-fidelity snapshot matrix corresponding to the solution of the low fidelity model for the sample point  $z_k$ . To this matrix we can associate a corresponding low-fidelity approximation space, i.e. the space spanned by the set of sample points  $\gamma_k$ ,

$$U^L(\gamma_k) = \text{span}\{u^L(\gamma_k)\} = \text{span}\{u^L(z_1), \dots, u^L(z_k)\}.$$

Similarly, the high-fidelity snapshot matrix, i.e. the matrix obtained from the sample set  $\gamma_k$ , and the corresponding high-fidelity approximation space, i.e. the space spanned by the solutions computed at nodes  $z_k$ , are defined as follows:

$$u^H(\gamma_k) = [u^H(z_1), \dots, u^H(z_k)], \quad U^H(\gamma_k) = \text{span}\{u^H(\gamma_k)\}.$$

The main idea of the BFSC method is to construct an inexpensive surrogate  $u^B(z; \gamma_M)$  of the high-fidelity solution in the following non-intrusive manner

$$(134) \quad u^H(z) \approx u^B(z; \gamma_M) = \sum_{k=1}^M c_k(z) u^H(z_{i_k})$$

where  $M$  is expected to be the number of high-fidelity samples and where correspondingly  $z_{i_k} \in \gamma_M$  is a subset of size  $M$  of the sample space of size  $M_E$ . In other words, we approximated the solution of the high fidelity model in the space spanned by  $u^H(z_{i_k})$ ,  $k = 1, \dots, M$ . When constructing such algorithm one seeks for  $M$  to be as small as possible, since large  $M$  means more high-fidelity simulations and consequently prohibitive computational efforts. Thus, the central idea of the BFSC algorithm is to use cheap low-fidelity models to learn the coefficients  $c_i(z)$  in (134), and then apply the same approximation rule to a limited number, but selected, of high-fidelity samples to construct the bi-fidelity approximations of high-fidelity samples.

The BFSC algorithm for approximating the high-fidelity solution consists of offline and online stages. In the offline stage, we employ the cheap low-fidelity model to explore the parameter space to find the most important

parameter points, i.e. a small number of samples permitting to give a suitable approximate solution. During the online stage, we learn the approximation rule from the low-fidelity model for any given  $z$ , and apply it to construct the bi-fidelity approximation. Thus, to construct the BFSC approximation in (134), one essentially needs to answer the following two questions:

- How to choose a good collocation nodal set that results in a good approximation of the high fidelity solution in the random space?
- How to recover the coefficients  $\{c_i\}$  in an efficient manner? In other words, what is the efficient reconstruction algorithms that can be realized without resorting to an intensive use of the high-fidelity solver?

These two questions, if properly addressed, constitute the key to the efficiency and accuracy of the algorithm. We outline the key ideas in Algorithm 7.

---

**Algorithm 7:** BFSC method

---

**1. Offline stage**

- (a) Select a sample set  $\Gamma_N = \{z_1, z_2, \dots, z_N\} \subset \Omega$ .
- (b) Run the low-fidelity model  $u_l(z_j)$  for each  $z_j \in \Gamma_N$ .
- (c) Select  $M$  "important" points from  $\Gamma_N$  and denote it by  $\gamma_M = \{z_{i_1}, \dots, z_{i_M}\} \subset \Gamma_N$ . Construct the low-fidelity approximation space  $U^L(\gamma_M)$ .

**2. Online**

- (a) Run high-fidelity simulations at each sample point of the selected sample set  $\gamma_M$ . Construct the high-fidelity approximation space  $U^H(\gamma_M)$ .
- (b) For any given  $z$ , run the low-fidelity model to get the corresponding low-fidelity solution  $u^L(z)$  and compute the low-fidelity coefficients by projection:

$$u^L(z) \approx \mathcal{P}_{U^L(\gamma_M)} u^L = \sum_{k=1}^M c_k(z) u^L(z_{i_k}).$$

- (c) Construct the bi-fidelity approximation by applying the sample approximation rule learned from the low-fidelity model:

$$u^B(z) = \sum_{k=1}^M c_k(z) u^H(z_{i_k}).$$


---

We address in the following the two main questions permitting to construct an efficient and accurate BFSC method: the proper point selection in the random space and the efficient construction of the bi-fidelity approximation.

**4.1.1. Point selection.** — To select the subset  $\gamma_M$ , we search the parameter space by the greedy algorithm proposed in [66, 106]: we gradually select the important point set from a candidate set  $\Gamma_N \in \Omega$ . The method works as follows.

- Start with a trivial subspace  $\gamma_0 = \emptyset$ , and assume that the first  $k - 1$  important points  $\gamma_{k-1} = \{z_{i_1}, \dots, z_{i_{k-1}}\} \subset \Gamma_N$  have been selected.
- We choose the next point  $z_{i_k} \in \Gamma$  as the point that maximizes the distance between its corresponding low-fidelity solution and the approximation space  $U^L(\gamma_{k-1})$ , spanned by the low-fidelity solutions on the existing point set  $\gamma_{k-1}$ , i.e.,

$$(135) \quad z_{i_k} = \arg \max_{z \in \Gamma} \text{dist}(u^L(z), U^L(\gamma_{k-1})), \quad \gamma_k = \gamma_{k-1} \cup z_{i_k},$$

where  $\text{dist}(v, W)$  is the distance function between  $v \in u^L(\Gamma)$  and subspace  $W \subset U^L(\Gamma_N)$ .

Thus, the greedy procedure essentially serves the purpose of searching the linear independent basis set in the parameterized low-fidelity solution space until all  $M$  important points are selected. Let us remark that the whole algorithm allows an efficient implementation by standard linear algebra operations, if  $\text{dist}(v, W)$  is chosen as squared Euclidean distance. Let  $\mathbf{G}$  be the Gramian matrix of the low-fidelity solution  $u^L(\Gamma_N)$ , i.e.,

$$(136) \quad \mathbf{G} = \langle u^L(z_i), u^L(z_j) \rangle^L, \quad 1 \leq i, j \leq N.$$

where  $\langle \cdot \rangle^L$  be an inner product space corresponding to the high-fidelity solution. Similar definition holds for  $\langle \cdot \rangle^H$ . We then apply the pivoted Cholesky decomposition to the matrix  $\mathbf{G}$ ,

$$(137) \quad \mathbf{G} = \mathbf{P}^T \mathbf{L} \mathbf{L}^T \mathbf{P},$$

where  $\mathbf{L}$  is lower-triangular and  $\mathbf{P}$  is a permutation matrix due to pivoting. This will produce an ordered permutation vector  $P = (i_1, \dots, i_N)$ , from which we choose the first  $M$  points to define  $\gamma_M = \{z_{i_1}, \dots, z_{i_M}\}$ . This procedure guaranteed that  $u^L(\gamma)$  can form a linearly independent collection [66]. More details and properties of the algorithm can be found in [66, 106]. We remark that other point selections strategies can be used in this setting [81].

**4.1.2. Bi-fidelity approximation.** — Once the important point set  $\gamma_M$  is selected, we can construct the low- and high-fidelity approximation space,  $U^L(\gamma_M)$  and  $U^H(\gamma_M)$ , respectively. For any given new sample point  $z \in \Omega$ ,

we project the corresponding low-fidelity solution  $u^L(z)$  onto the low-fidelity approximation space  $U^L(\gamma_M)$ :

$$u^L(z) \approx \mathcal{P}_{U^L(\gamma_M)}[u^L(z)] = \sum_{k=1}^M c_k(z) u^L(z_{i_k}),$$

where  $\mathcal{P}_V$  is the projection operator onto a Hilbert space  $V$  and the corresponding projection coefficients  $\{c_k\}$  are computed by the following projection:

$$(138) \quad \mathbf{G}^L \mathbf{c} = \mathbf{f}^L, \quad \mathbf{f}^L = (f_k^L)_{1 \leq k \leq M}, \quad f_k^L = \langle u^L(z), u^L(z_{i_k}) \rangle^L,$$

where  $\mathbf{G}^L$  is the Gramian matrix of  $u^L(\gamma_M)$ , defined by

$$(139) \quad (\mathbf{G}^L)_{ij} = \langle u^L(z_{i_k}), u^L(z_{j_k}) \rangle^L, \quad 1 \leq k \leq M, \quad i_k, j_k \in \gamma_M.$$

These low-fidelity coefficients  $\{c_k\}$  serve as the surrogate of the corresponding high-fidelity coefficients of  $u^H(z)$ . Therefore, the sought bi-fidelity approximation of  $u^H(z)$  can be constructed via (134). We emphasize that if the low-fidelity model can mimic the variations of the high-fidelity model in the parameter space, the low-fidelity coefficients can be a good approximation of the corresponding high-fidelity coefficients for a given sample  $z$ . The whole procedure of the bi-fidelity algorithm for a given  $z$  is summarized in Algorithm 7. It is worth noting that since the number of low-fidelity basis is typically small, the cost of computing the low-fidelity projection coefficients by solving the linear system (138) is negligible. Therefore, the dominant cost of the on-line step is one low-fidelity simulation run. If the low-fidelity solver is much cheaper than the high-fidelity solver, the speedup during the online stage can be significant as we will demonstrate with some examples in the rest of the survey.

**4.1.3. An empirical error bound estimation.** — An error bounds analysis for the bi-fidelity method was derived in [66, 105] in a rather general setting. Nonetheless, the results presented are largely theoretical. For practical applications of the BFSC approach, it is important to answer the following two questions:

- Given a low-fidelity model, is this model good enough to build a reasonably accurate BFSC approximation for practical purposes?
- How to efficiently estimate a reasonably good error bound on the entire parameter space?

In other words, an inexpensive but effective quality indicator (EQI) of the approximation is of practical importance. In realistic applications, *a priori* assessment of the model quality and prediction errors is very important. In this direction, a previous study [32] introduced a novel empirical error bound estimation approach with ease of implementation to evaluate the performance of the bi-fidelity surrogates *a priori*. We will briefly describe the methodology

here. In [32], two important quantities have been identified which are useful to build the approximation quality indicator for the BFSC approximation:

- $R_s$ , model similarity which characterizes the similarity between the low/high-fidelity models:

$$(140) \quad R_s(z) = \frac{d^H(u^H(z), U^H(\gamma_M))}{\|u^H(z)\|} / \frac{d^L(u^L(z), U^L(\gamma_M))}{\|u^L(z)\|},$$

If  $R_s(z) \approx 1$ , the low-fidelity model is informative for the point selection.

- $R_e$ , the ratio between the projection error and the distance error,

$$(141) \quad R_e(z) = \frac{\|\mathcal{P}_{U^H(\gamma_M)} u^H(z) - u^B(z; \gamma_M)\|}{d^H(u^H(z), U^H(\gamma_M))}.$$

when  $R_e(z)$  is too large, it indicates the greedy algorithm is less effective for point selection of high-fidelity samples. This suggests that one should stop collecting new high fidelity samples since the improvement in the result is likely marginal.

Empirically, one can then fix thresholds for  $R_s \approx 1$  and  $R_e < 10$  in such a way that the BFSC approximation can usually deliver results which are reasonably accurate, i.e. better than the low-fidelity solutions.

Using  $R_s$  and the observation in [32, Theorem 1], for any given new point  $z_*$ , one has

$$(142) \quad \frac{\|u^H(z_*) - u^B(z_*)\|}{\|u^H(z_*)\|} \leq \frac{d^L(u^L(z_*), U^L(\gamma_M))}{\|u^L(z_*)\|} R_s(z_*) \times \left(1 + \frac{\|\mathcal{P}_{U^H(\gamma_M)} u^H(z_*) - u^B(z_*)\|}{d^H(u^H(z_*), U^H(\gamma_M))}\right).$$

To remove the dependency of the new HF sample  $u^H(z_*)$  on the above right-hand side, one uses  $z_{M+1} \in \gamma_{M+1}$  as the testing points served as an error surrogate for the BFSC approximation in the entire parameter space. If the LF and HF models are similar (i.e.,  $R_s \approx 1$ ), one can choose some proper constants  $c_1$  and  $c_2$ , such that for the first  $M+1$  pre-selected important points  $\gamma_{M+1}$ ,

$$(143) \quad \begin{aligned} \frac{\|u^H(z_*) - u^B(z_*)\|}{\|u^H(z_*)\|} &\leq \frac{d^L(u^L(z_*), U^L(\gamma_M))}{\|u^L(z_*)\|} \\ &\times \left[ c_1 + c_2 \frac{\|\mathcal{P}_{U^H(\gamma_M)} u^H(z_{M+1}) - u^B(z_{M+1})\|}{d^H(u^H(z_{M+1}), U^H(\gamma_M))} \right] \\ &= \frac{d^L(u^L(z_*), U^L(\gamma_M))}{\|u^L(z_*)\|} (c_1 + c_2 R_e(z_{M+1})). \end{aligned}$$

Notably, in the right-hand side of the inequality, the first term only depends on the inexpensive low-fidelity data and the second term needs the high-fidelity solution at  $z_{M+1}$  – the  $(M + 1)$ -th point of the pre-selected important points  $\gamma_{M+1}$  without the need of the high-fidelity sample  $u^H(z)$  for a new given  $z$ . Essentially,  $z_{M+1}$  can be regarded as a test point to serve as an error/quality indicator of the BFSC approximation in the entire parameter space. This can be advantageous if the high-fidelity solver is very expensive.

We acknowledge that the above error bound estimation, though not rigorous, is a useful quantity to access the quality of the BFSC approximation in practical applications. In the following numerical experiments, our empirical results suggest that this error bound estimation is effective if the constants  $c_1$  and  $c_2$  are set to be 1 [32, 54].

**4.2. A BFSC method for the Boltzmann equation.** — In this section, we consider the application of the bi-fidelity algorithm to the study of the Boltzmann equation under the hydrodynamic scaling and with multi-dimensional random parameters presented in Section 2.1 and already analyzed in Section 3 using MSCV method.

To examine the performance of the bi-fidelity method, numerical errors are computed in the following way: we choose a fixed set of points  $\{\hat{z}_k\}_{k=1}^M \subset \Omega$  that is independent of the point sets  $\Gamma$ , then evaluate the following error between the bi-fidelity and high fidelity solutions at a final time  $t$ :

$$(144) \quad \|u^H(t) - u^B(t)\|_{L^2(D \times \Omega)} \approx \frac{1}{n} \sum_{k=1}^n \|u^H(\hat{z}_k, t) - u^B(\hat{z}_k, t)\|_{L^2(D)},$$

where  $\|\cdot\|_{L^2(D)}$  is the  $L^2$  norm in the physical domain  $D = \Omega \times \mathbb{R}^2$ . In the following two examples, the spatial domain is chosen to be  $[0, 1]$  with  $N_x$  grid points. The velocity domain is chosen as  $[-L_v, L_v]^2$  with  $L_v = 8.4$ . We denote  $N_v^l$  and  $N_v^h$  as the number of grid points used in velocity discretization of the low-fidelity and high-fidelity solver respectively. The  $d_z$ -dimensional random variable  $z$  is assumed to follow the uniform distribution on  $[-1, 1]^{d_z}$ . Let also the size of training set  $\Gamma$  be  $N = 1000$ . We examine the error of bi-fidelity approximation with respect to the number of high-fidelity runs by computing the norm defined in (144).

First, we consider a benchmark Sod shock tube test. Assume the random cross section

$$b(z^b) = 1 + 0.5 \sum_{k=1}^{d_1+1} \frac{z_k^b}{2k},$$

and the uncertain initial distribution given by

$$f^0(x, v, z) = \frac{\rho^0}{2\pi T^0} e^{-\frac{|v-u^0|^2}{2T^0}},$$

where the initial data for  $\rho^0$ ,  $u^0$  and  $T^0$  is

$$\left\{ \begin{array}{l} \rho_l = 1, \quad u_l = (0, 0), \quad T_l(z^T) = 1 + 0.4 \sum_{k=1}^{d_1} \frac{z_k^T}{2k}, \quad x \leq 0.5, \\ \rho_r = \frac{1}{8}, \quad u_r = (0, 0), \quad T_r(z^T) = \frac{1}{8} \left( 1 + 0.4 \sum_{k=1}^{d_1} \frac{z_k^T}{2k} \right), \quad x > 0.5. \end{array} \right.$$

Here  $z^b$  and  $z^T$  represent the random variables in the collision kernel and initial temperature, with  $\{z_i^b\}_{i=1}^{d_1+1}$  and  $\{z_i^T\}_{i=1}^{d_1+1}$  following the uniform distribution on  $[-1, 1]$ . We then set  $d_1 = 7$ , and the total dimension  $d_z$  of the random space to be 15. We solve the Boltzmann (high-fidelity) equation by using the asymptotic-preserving scheme developed in [28], with the second-order MUSCL scheme [50] for the spatial discretization, and fast spectral method [62] for the collision operator implementation. Here we set  $\Delta x = 0.01$ ,  $N_v^h = 24$ , and the final time  $t = 0.15$ . We employ the Euler equation as the low-fidelity model, and solve it with the same spatial and temporal resolution as that for the Boltzmann, while using  $N_v^l = 12$ . In this test, the fluid regime, i.e.  $\varepsilon = 10^{-4}$  is chosen. The Figure 9 suggests a fast convergence of  $L^2$  errors between the high-fidelity and bi-fidelity solutions. With 10 high-fidelity runs, the bi-fidelity approximation reaches an accuracy level of  $\mathcal{O}(10^{-3})$ , which is remarkable for a 15-dimensional random variable problem. To further illustrate the performance of our bi-fidelity method, we compare the high-fidelity, low-fidelity and the bi-fidelity solutions for a randomly selected sample point  $z$  by using  $M = 10$ . One observes that the high-fidelity and bi-fidelity solutions match really well, whereas the low-fidelity solutions are quite off at some spatial points.

Regarding the moments quantities in the random space, Figure 10 shows that the mean and standard deviation of bi-fidelity approximations for  $\rho$ ,  $u$  and  $T$  match well with the high-fidelity solutions with 10 high-fidelity runs. These results indicate that even though the Euler model may not be accurate in the physical space, it still can capture well the solution behavior of the Boltzmann equation in the random space. Besides, a significant speedup and memory savings are quite noticeable in this case.

We now consider a mixed regime problem with the Knudsen number  $\varepsilon$  varying in space, see Figure 11, defined by

$$(145) \quad \varepsilon(x) = 10^{-3} + \frac{1}{2} \left[ \tanh \left( 1 - \frac{11}{2}(x - 0.5) \right) + \tanh \left( 1 + \frac{11}{2}(x - 0.5) \right) \right].$$



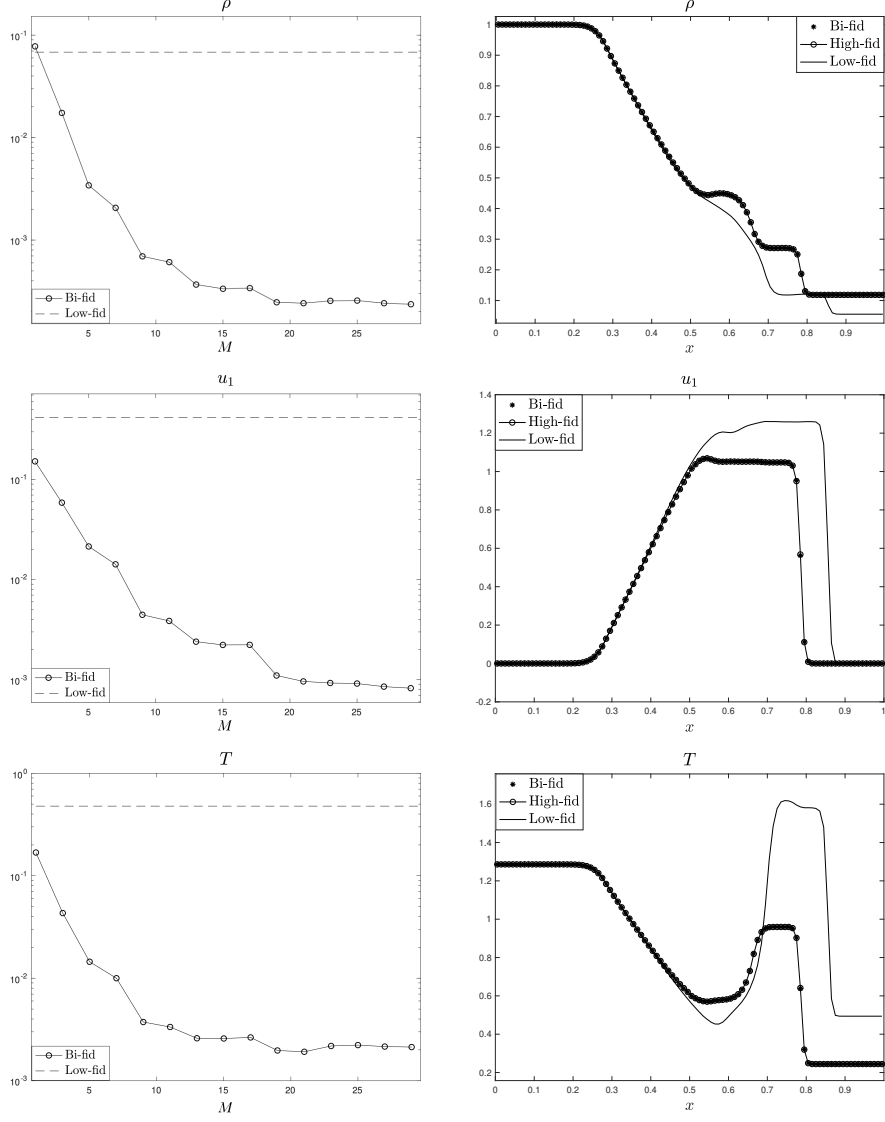


FIGURE 9. BFSC method for the Boltzmann equation. Results of the Sod shock tube test. (Left) The mean  $L^2$  errors between high-fidelity and low-fidelity or bi-fidelity solutions with respect to the number of high-fidelity runs; (Right) Comparison of the low-fidelity solution ( $N_v^l = 12$ ), high-fidelity solutions ( $N_v^l = 24$ ), and the corresponding bi-fidelity approximations  $M = 10$  for a fixed  $z$ .

Let initial data mimic the Karhunen-Loeve expansion of the random field:

$$(146) \quad \begin{cases} \rho_0(x, z^\rho) = \frac{1}{3} \left( 2 + \sin(2\pi x) + 0.2 \sum_{k=1}^{d_1} \sin[2\pi(k+1)x] \frac{z_k^\rho}{2k} \right), \\ u_0 = (0.2, 0), \\ T_0(x, z^T) = \frac{1}{4} \left( 3 + \cos(2\pi x) + 0.2 \sum_{k=1}^{d_1} \cos[2\pi(k+1)x] \frac{z_k^T}{2k} \right), \\ f_0(x, v, z) = \frac{\rho_0}{4\pi T_0} \left( \exp\left(-\frac{|v - u_0|^2}{2T_0}\right) + \exp\left(-\frac{|v + u_0|^2}{2T_0}\right) \right), \end{cases}$$

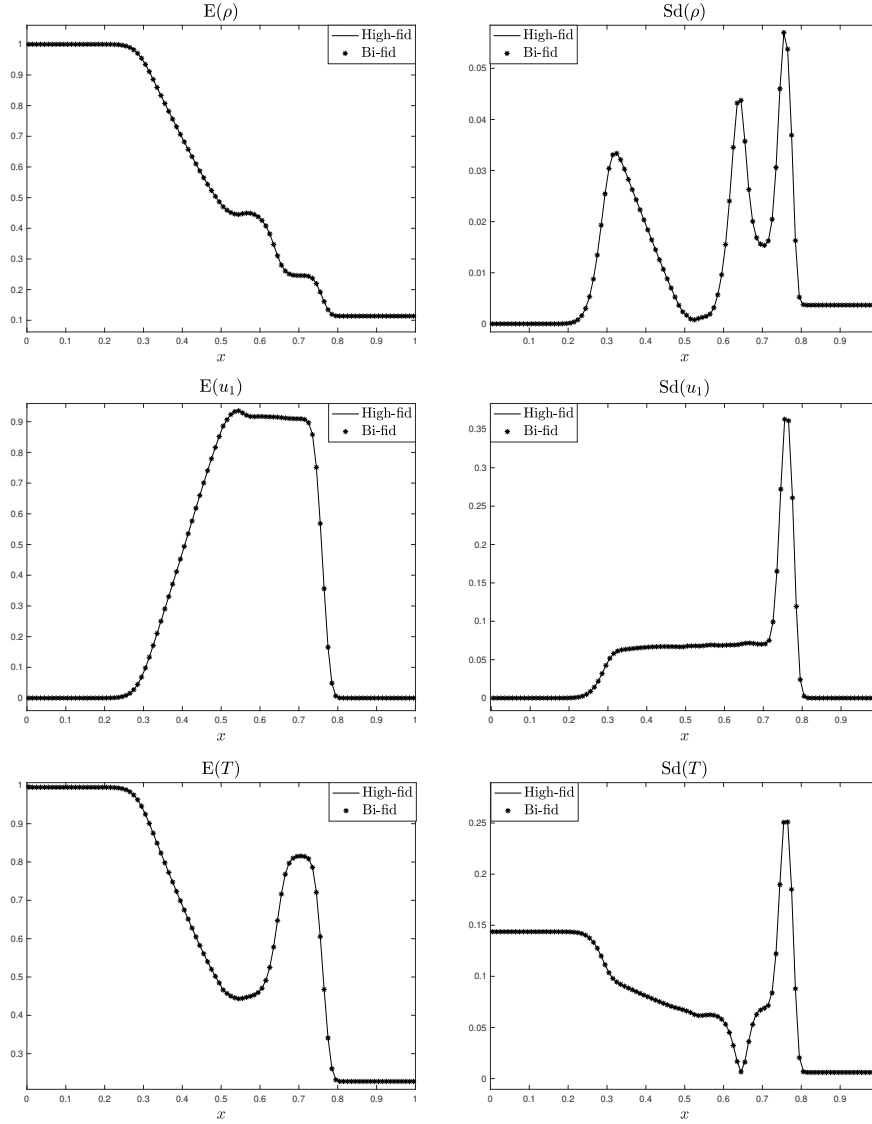


FIGURE 10. BFSC method for the Boltzmann equation. Results of the Sod shock tube test. The mean and standard deviation of  $\rho$ ,  $u_1$ ,  $T$  of high-fidelity and bi-fidelity solutions with  $M = 10$ .

where  $d_1 = 7$ . The collisional cross section is also assumed random,

$$(147) \quad b(z) = 1 + 0.5z_1^b.$$

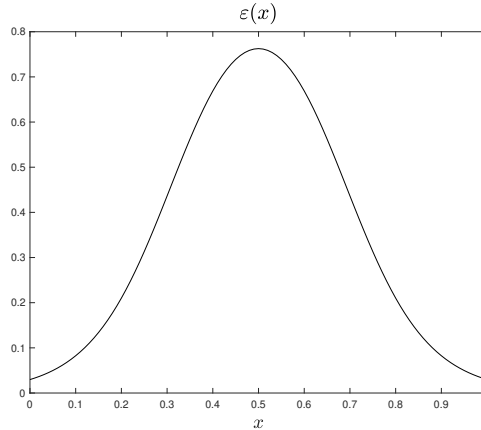


FIGURE 11. BFSC method for the Boltzmann equation. The distribution of  $\varepsilon(x)$  in (145) for the mixed regime problem.

We let  $N_v^h = 24$  and  $N_v^l = 8$  in the high-fidelity and low-fidelity solvers. From Figure 12, we observe a fast convergence of  $L^2$  errors between the high-fidelity and bi-fidelity solutions, which saturate quickly when  $M$  reaches around 25. The dotted lines which represent the errors between the high-fidelity and low-fidelity solutions are much larger than that between the high-fidelity and bi-fidelity solutions. This indicates that even though the low-fidelity solutions alone are relatively inaccurate in the spatial domain, it seems to still behave similarly in the random space. As a result the bi-fidelity approximation based on a small number of high-fidelity runs can reach a reasonable level of accuracy.

The right column of Figure 12 presents the high-fidelity, low-fidelity and bi-fidelity solutions at a randomly chosen sample point  $z$ . One can see that the high-fidelity and bi-fidelity solutions match really well, whereas the low-fidelity solutions are not accurate. With  $N = 1000$  low-fidelity runs of the Euler model, by only 25 implementation runs of the AP solver for the Boltzmann equation, the bi-fidelity approximation is able to capture the Boltzmann solution behaviors well in the random space, up to an accuracy of  $10^{-3}$ ; on the other hand, using the low-fidelity model (Euler equation) alone can not achieve this result, especially under the multiple scaling where  $\varepsilon$  ranges from  $10^{-3}$  to 1. This observation highlights the advantages of the bi-fidelity method. Figure 13 shows the mean and standard deviation of  $\rho$ ,  $u$ ,  $T$  by using 25 high-fidelity runs. The high-fidelity and bi-fidelity solutions match well, indicating that the bi-fidelity solutions have captured well the characteristics of the macroscopic quantities in the random space. Once we construct the bi-fidelity model, the online computational cost can be significantly reduced. In this example, the

high-fidelity model (Boltzmann) with  $N_v^h = 16$  takes about 50 times computation time of the low-fidelity model on a sequential machine. Since the dominant cost of the bi-fidelity reconstruction lies in the corresponding low-fidelity run, a significant amount of computational cost is reduced in this case.

**4.2.1. Accuracy and convergence analysis.** — We discuss now some accuracy and convergence results for the bi-fidelity method applied to the Boltzmann equation. We first give a summary of the hypocoercivity framework studied in [53], then we introduce the relation between the quantities of interests obtained from the Boltzmann and the compressible Euler system. The rough idea on which the analysis relies is that the bi-fidelity error can be split into two parts: the projection error and the remainder part. We mention that the error estimate of the bi-fidelity method for more general kinetic problems with multiple scales and uncertainties has been discussed in [30].

We first show that for each fixed  $z \in \Omega$ , the error between macroscopic quantities obtained from the Boltzmann equation and the compressible Euler system containing consistent initial data, is small and of order  $\varepsilon$  as shown later in (150). Let us recall some useful notations for the norms as used in [53]. Let  $f$  be the classical solution to the Boltzmann equation (1). Consider a linearization around the global equilibrium together with a perturbation of  $f$ :

$$f = \mathcal{M} + \varepsilon\sqrt{\mathcal{M}}h,$$

with

$$\mathcal{M}(v) = \frac{1}{(2\pi)^{\frac{d_x}{2}}} e^{-\frac{|v|^2}{2}}.$$

In this setting,  $h$  satisfies the perturbed equation

$$(148) \quad \partial_t h + v \cdot \nabla_x h = \frac{1}{\varepsilon} \mathcal{L}(h) + \mathcal{F}(h, h),$$

where the linearized operator  $\mathcal{L}$  and the nonlinear operator  $\mathcal{F}$  are given by

$$\begin{aligned} \mathcal{L}(h) &= \left(\sqrt{\mathcal{M}}\right)^{-1} \left[ \mathcal{Q}(\sqrt{\mathcal{M}}h, \mathcal{M}) + \mathcal{Q}(\mathcal{M}, \sqrt{\mathcal{M}}h) \right], \\ \mathcal{F}(h, h) &= 2 \left(\sqrt{\mathcal{M}}\right)^{-1} \mathcal{Q}(\sqrt{\mathcal{M}}h, \sqrt{\mathcal{M}}h). \end{aligned}$$

Let denote  $\partial_l^j := \partial/\partial v_j \partial/\partial x_l$  for multi-indices  $j$  and  $l$  and let introduce the following Sobolev norms:

$$(149) \quad \begin{aligned} \|h\|_{H_{x,v}^s}^2 &= \sum_{|j|+|l|\leq s} \|\partial_l^j h\|_{L_{x,v}^2}, & \|h\|_{H_{x,v}^{s,r}} &= \sum_{|\nu|\leq r} \|\partial^\nu h\|_{H_{x,v}^s}, \\ \|h\|_{H_{x,v}^s H_z^r} &= \int_{I_z} \|h\|_{H_{x,v}^{s,r}} \pi(z) dz, & \|h\|_{H_{x,v}^{s,r} L_z^\infty} &= \sup_{z \in I_z} \|h\|_{H_{x,v}^{s,r}}. \end{aligned}$$

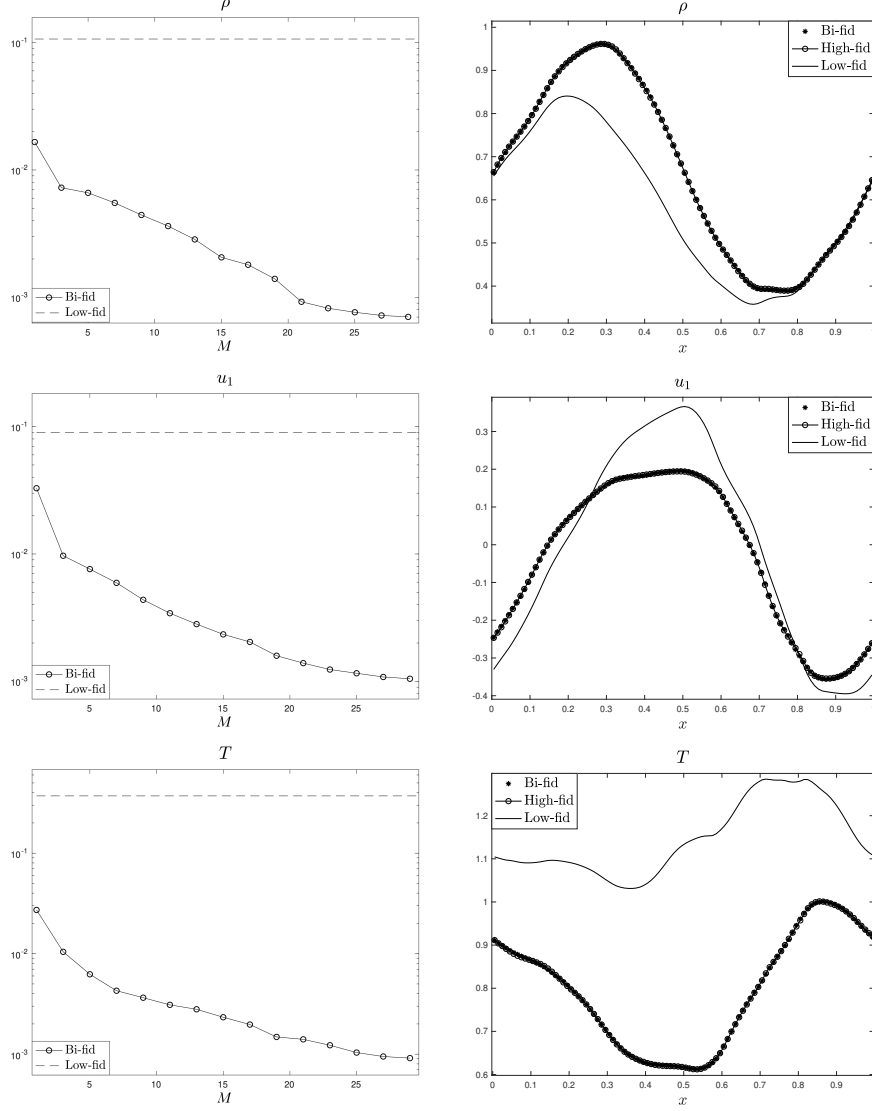


FIGURE 12. BFSC method for the Boltzmann equation. Results of the mixed regime test. (Left) The mean  $L^2$  errors between high-fidelity and low- or bi-fidelity solutions with respect to the number of high-fidelity runs; (Right) Comparison of the low-fidelity solution ( $N_v^l = 8$ ), high-fidelity solutions ( $N_v^l = 16$ ), and the corresponding bi-fidelity approximations  $M = 25$  for a fixed  $z$ .

We refer to [11, Theorem 2.5] for details. Let  $h_\varepsilon$  be the perturbed solution to the linearized equation (148). Suppose the initial data for (148) and (10) are

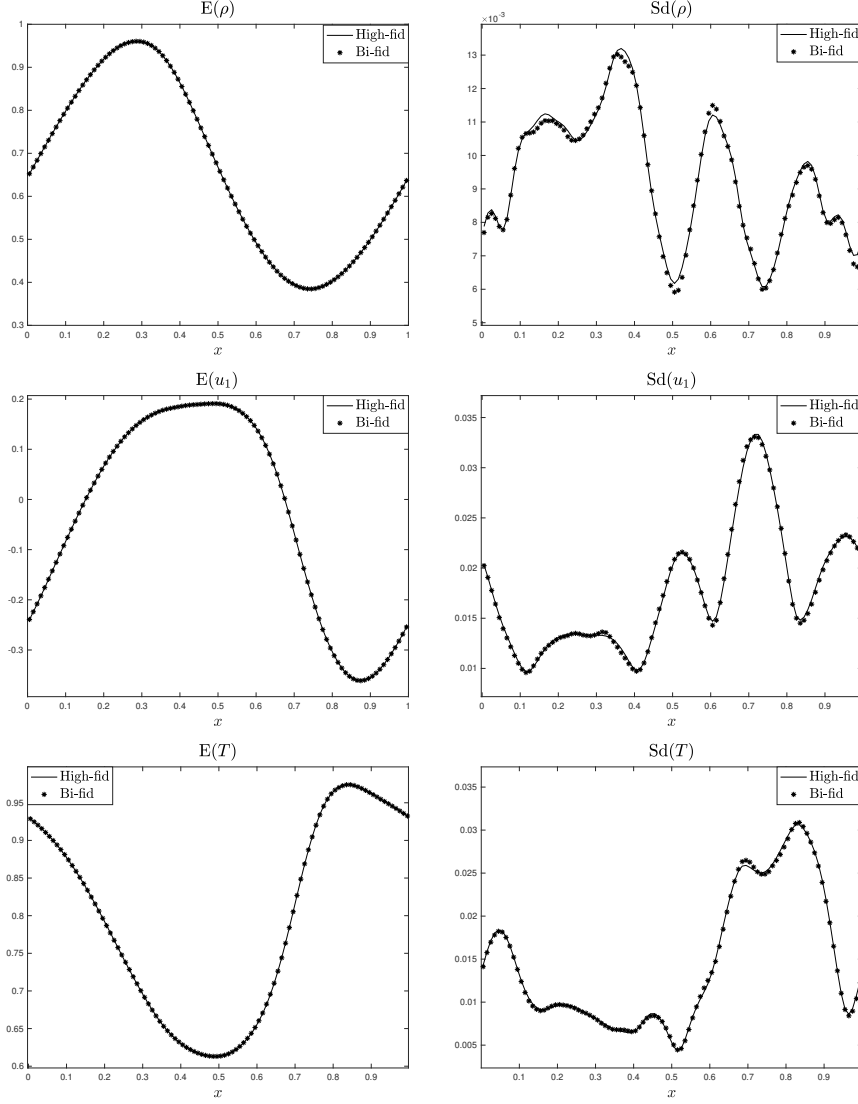


FIGURE 13. BFSC method for the Boltzmann equation. Results of the mixed regime test. The mean and standard deviation of  $\rho$ ,  $u_1$ ,  $T$  of high-fidelity solutions and bi-fidelity solutions with  $M = 25$ .

consistent for each  $z$ . If the initial distribution  $h_{in} \in \text{Null}(\mathcal{L})$  and  $h_{in} \in H_{x,v}^s$ , then for each  $z$ ,  $(h_\varepsilon)_{\varepsilon>0}$  converges strongly to

$$h(t, x, v, z) = \left[ \rho(t, x, z) + v \cdot u(t, x, z) + \frac{1}{2}(|v|^2 - d_v)T(t, x, z) \right] \mathcal{M}(v)$$

in  $L^2_{[0,T]} H_x^s L_v^2$  as the Knudsen number  $\varepsilon \rightarrow 0$ , where  $\rho, u, T$  satisfy the Euler system (10). Then, for all  $z \in \Omega$ , if  $h_{in}$  belongs to  $H_x^s L_v^2$ , we have

$$(150) \quad \begin{aligned} & \sup_{t \in [0, \infty]} \|h(t, z) - h_\varepsilon(t, z)\|_{L_{x,v}^2} \leq \\ & \sup_{t \in [0, \infty]} \|h(t, z) - h_\varepsilon(t, z)\|_{H_x^s L_v^2} \leq C \max\{\varepsilon, \varepsilon V_T(\varepsilon)\}, \end{aligned}$$

where  $\forall T > 0$ ,  $V_T(\varepsilon)$  is defined as

$$V_T(\varepsilon) = \sup_{t \in [0, T]} \|h(t, z) - h_\varepsilon(t, z)\|_{L_x^\infty L_v^2} \rightarrow 0, \quad \text{as } \varepsilon \rightarrow 0.$$

For each  $z$ , we can split the total error  $\|u^H(z) - u^B(z)\|^H$  into two parts:

$$(151) \quad \begin{aligned} & \|u^H(z) - u^B(z)\|^H \leq \\ & \|u^H(z) - P_{U^H(\gamma_M^L)} u^H(z)\|^H + \|P_{U^H(\gamma_M^L)} u^H(z) - u^B(z)\|^H, \end{aligned}$$

where  $u^H$  and  $u^B$  denote the high-fidelity and bi-fidelity solutions.  $\gamma_M^L = \{z_1^L, \dots, z_M^L\}$ . Also, [66, the Lemma 4.3] shows that the estimate for the second term can be written as:

$$(152) \quad \begin{aligned} & \|P_{U^H(\gamma_M^L)} u^H(z) - u^B(z)\|^H \leq \\ & c \|P_{U^H(\gamma_M^L)} u^H(z)\|^H + \|\sqrt{\mathbf{G}^H} (\mathbf{G}^L)^{-1} \mathbf{Q} \mathbf{f}^L\|, \end{aligned}$$

where  $c$  is a small constant such that  $c = \varepsilon_1 + \varepsilon_2 + \varepsilon_1 \varepsilon_2$ . Moreover  $\mathbf{G}^L$  (or  $\mathbf{G}^H$ ) is the Gramian matrix of  $u^L(\gamma)$  (or  $u^H(\gamma)$ ) given by (139) and the vector  $\mathbf{f}^L$  has entries

$$f_i^L = \langle u^L(z_i), u^L(z) \rangle^L,$$

with  $\mathbf{Q} := \mathbf{I} - \mathbf{P}$ , the orthogonal projection onto its kernel (with  $\mathbf{P}$  the orthogonal projection matrix onto its range), see [66] for details. Thus, the last term in (152) is related to the non-invertibility of high-fidelity Gramian matrix and it can be proven to be usually negligible. In addition, since

$\|P_{U^H(\gamma_M^L)} u^H(z)\|^H \leq \|u^H(z)\|^H$ , we can write

$$(153) \quad \|P_{U^H(\gamma_M^L)} u^H(z) - u^B(z)\|^H \leq c \|u^H(z)\|^H + \|\sqrt{\mathbf{G}^H} (\mathbf{G}^L)^{-1} \mathbf{Q} \mathbf{f}^L\|.$$

We study now the smoothness of the high-fidelity solution  $u^H : \Omega \mapsto V^H$ , where  $z$  is a multivariate random parameter and  $V^H$  is a Hilbert space with the usual inner product  $\langle \cdot, \cdot \rangle^H$ . Successively, we establish an estimate bound for the Kolmogorov width to show the convergence result of our bi-fidelity method. To that aim, let us recall the standard multivariate notation in [55].

We denote the countable set of finitely supported sequences of nonnegative integers by

$$\mathcal{F} := \{\nu = (\nu_1, \nu_2, \dots) : \nu_j \in \mathbb{N}, \text{ and } \nu_j \neq 0 \text{ for only a finite number of } j\},$$

with  $|\nu| := \sum_{j \geq 1} |\nu_j|$ . For  $\nu \in \mathcal{F}$  supported in  $\{1, \dots, J\}$ , one defines the partial derivative in  $z$

$$(154) \quad \partial^\nu u = \frac{\partial^{|\nu|} u}{\partial^{\nu_1} z_1 \cdots \partial^{\nu_J} z_J},$$

and the multi-factorial  $\nu! := \prod_{j \geq 1} \nu_j!$ , where  $0! := 0$ . If the initial distribution of the high-fidelity model satisfies

$$(155) \quad \|h_\varepsilon^{in}(z)\|_{H_{x,v}^{1,r} L_z^\infty} \leq C_I,$$

then for a fixed time  $t > 0$  and  $|\nu| \leq r$ ,

$$(156) \quad \sup_{z \in \Omega} \|\partial^\nu u^H(t, z)\|^H \leq C' e^{-\varepsilon \tau t} + \xi,$$

where  $\xi$  depends on the order and discretization parameters  $\Delta t, \Delta x, \Delta v$ . Thus for all  $z \in \Omega$ , one gets

$$\|\partial^\nu u^H(t, z)\|^H \leq C' e^{-\varepsilon \tau t} + \xi.$$

Here note that  $C_I, C, C'$  and  $\tau$  are all positive generic constants independent of  $\varepsilon$ . We recall now the assumption on the random collision kernel:

**Assumption 4.1.** — Assume the collision kernel take the form

$$(157) \quad \begin{aligned} B(|v - v^*|, \cos z, z) &= \Phi(|v - v^*|) b(\cos z, z), \\ \Phi(|v - v^*|) &= C |v - v^*|^m, \quad m \in [0, 1], \end{aligned}$$

and  $(\psi_j)_{j \geq 1}$  be an affine representer [17] of the cross section  $b$ , that is,

$$(158) \quad b(\eta, z) = \bar{b}(\eta) + \sum_{j \geq 1} z_j \psi_j(\eta), \quad z := (z_j)_{j \geq 1}, \quad \eta = \cos z,$$

where the sequence  $(\|\psi_j\|_{L^\infty(\eta)})_{j \geq 1} \in \ell^p$  for  $0 < p < 1$ . In addition, one assumes that

$$(159) \quad |b(\eta, z)| \leq C_0, \quad |\partial_\eta b(\eta, z)| \leq C_1, \quad |\partial^\nu b(\eta, z)| \leq C_2,$$

for all  $\eta \in [-1, 1]$  and  $|\nu| \leq r$  with  $C, C_0, C_1, C_2$  are all positive constants.

We now review the main result on convergence analysis in [55]:

**Theorem 4.1.** — If the assumptions for the random initial data, random collision kernel, namely (155) and Assumption 4.1 are satisfied, for fixed time



$t > 0$  and fixed numerical discretization parameters  $\Delta t$ ,  $\Delta x$  and  $\Delta v$ , for all  $z \in \Omega$ , are chosen, then

$$(160) \quad \begin{aligned} & \|u^H(t, z) - u^B(t, z)\|^H \leq \\ & C_1 \frac{e^{-\frac{\varepsilon\tau t}{2}}}{(N/2 + 1)^{q/2}} + C_2 e^{-\varepsilon\tau t} + \chi + \left\| \sqrt{\mathbf{G}^H} (\mathbf{G}^L)^{-1} \mathbf{Q} \mathbf{f}^L(z) \right\|, \end{aligned}$$

where  $N$  is the size of the subspace  $\gamma_M$  in Algorithm 7, with  $q = \frac{1}{p} - 1$  and  $p$  dependent on the  $\ell^p$ -summability assumption of  $(\psi_j)_{j \geq 1}$ . Moreover,  $C_1$ ,  $C_2$  and  $\tau$  are all constants dependent on the initial data  $u^{in}$  and Assumption 4.1 about the collision kernel while  $\delta_1$ ,  $\delta_2$  are both sufficiently small.

For details and the proof refer to [55]. This Theorem indicates that the error between the bi-fidelity and high-fidelity solutions decays algebraically with respect to the number of high-fidelity runs. The convergence rate  $q/2$  is independent of dimension of the random parameters and regularity of the initial data, and only relates to the  $\ell^p$  summability of the affine representative  $(\psi_j)_{j \geq 1}$  shown in Assumption 4.1.

**4.3. BFSC method in the diffusion limit.** — The linear transport equation in the diffusion scaling (25) introduced in Section 2 will be here employed in the framework of the bi-fidelity method. After the even and odd parity formulation of the transport equation (28), we have shown that the general linear transport equation degenerates to a diffusion equation in the limit  $\varepsilon \rightarrow 0$ . The idea we explore here is to use the so-called Goldstein-Taylor (GT) model—which is a discrete velocity approximation of the underlying kinetic equation with only two velocities—as the low-fidelity model. We show that the GT model share the same diffusive limit behavior of the original kinetic model (25). However, the clear advantage of the GT model is that it is significantly less computationally expensive than the original kinetic equation. This permits to better explore the space spanned by the solution of the GT model in a random framework and successively to choose the best random points to be used in the high fidelity method.

The one-dimensional Goldstein-Taylor (GT) model [34, 94] with random inputs is given by

$$(161) \quad \begin{cases} \partial_t u + \frac{1}{\varepsilon} \partial_x u = \frac{\sigma(x, z)}{2\varepsilon^2} (v - u), \\ \partial_t v - \frac{1}{\varepsilon} \partial_x v = \frac{\sigma(x, z)}{2\varepsilon^2} (u - v). \end{cases}$$

Here we assume a random scattering coefficient  $\sigma(x, z)$  as for the original high fidelity model (25). It is worth mentioning that the Goldstein-Taylor model (161) can be regarded as a discrete-velocity kinetic counterpart of the linear

transport equation where  $u$  defines the density of particles traveling with velocity 1, whereas  $v$  that of particles traveling in the reverse direction with velocity  $-1$ . Besides, the GT model has significantly cheaper computational cost, yet shares the same limiting diffusion equations with the linear transport model as  $\varepsilon \rightarrow 0$ . We refer to [52] for rigorous results concerning the diffusion limit of two-velocity models and extensions to nonlinear diffusion coefficients. This low-fidelity model is shown to be used in many interesting applications [36]. We introduce now the macroscopic variables: the mass density  $\rho$  and the flux  $s$ ,

$$\rho = u + v, \quad s = \frac{u - v}{\varepsilon},$$

then the GT model (161) is equivalent to the following system:

$$(162) \quad \begin{cases} \partial_t \rho + \partial_x s = 0, \\ \partial_t s + \frac{1}{\varepsilon^2} \partial_x \rho = -\frac{\sigma(x, z)}{\varepsilon^2} s. \end{cases}$$

The above system as said shares the same limit of the high fidelity model (28). In fact, in the diffusion limit  $\varepsilon \rightarrow 0$ , the system (162) can be approximated by the heat equation to the leading order, with random diffusion coefficient  $\sigma(x, z)$ ,

$$(163) \quad \begin{cases} s = -\frac{1}{\sigma(x, z)} \partial_x \rho, \\ \partial_t \rho = \partial_x \left[ \frac{1}{\sigma(x, z)} \partial_x \rho \right]. \end{cases}$$

Comparing (30) and (163), the two systems look similar except for the magnitude of the diffusion coefficient on the right hand-side which is different. However, if one defines the diffusion coefficient in (163) as  $\sigma_{\text{GT}}$  and that in (30) as  $\sigma_{\text{LTE}}$ , then by assuming  $\sigma_{\text{GT}} = \frac{1}{3} \sigma_{\text{LTE}}$  the two models share precisely the same diffusion limit.

Motivated by the above observations, we employ the equivalent formulation of the GT equation, that is, system (162) as our low-fidelity model. Without loss of generality, the  $d_z$ -dimensional random variable  $z = \{z_1, \dots, z_d\}$  is assumed to follow the uniform distribution on  $[-1, 1]^{d_z}$ , and the dimension of the random parameter is chosen as  $d = 5$ . To compute the reference solutions for the mean and standard deviation of the high-fidelity quantities of interests, we use the high-order stochastic collocation method over 5-dimensional sparse quadrature points with 5-level Clenshaw-Curtis rules, i.e., evaluated on 2243 quadrature points (cf., [103]). For the high-fidelity solver, at each given sample we employ the AP scheme [48] developed for the deterministic linear transport

equation (25) under the diffusive scaling. The standard 16-points Gauss-Legendre quadrature set is used for the velocity space to compute  $\rho$  in (29). For the low-fidelity (LF) solver, we use the deterministic AP method [47] to solve the linear Goldstein-Taylor model (162). Periodic boundary conditions are considered.

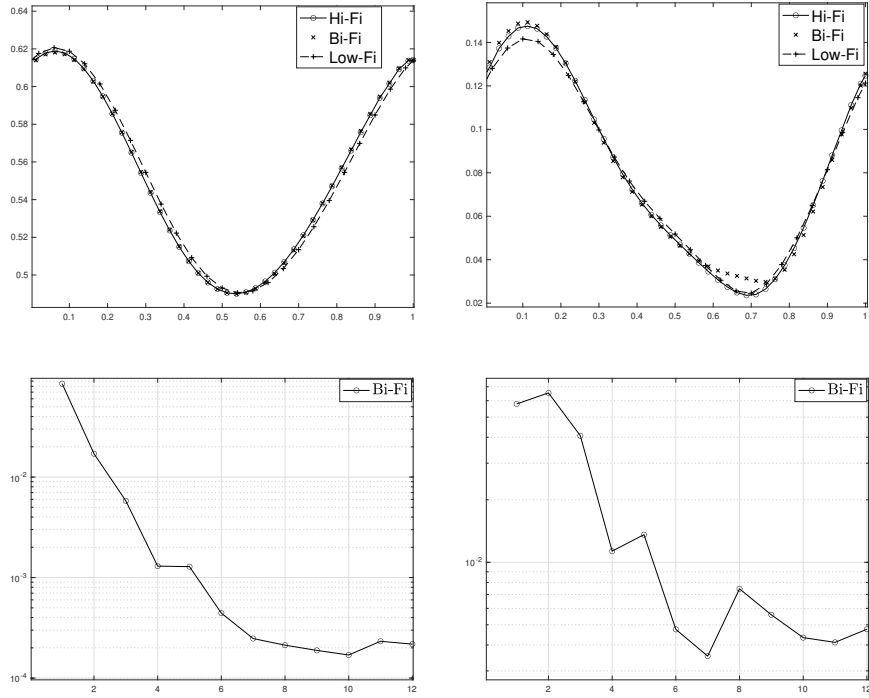


FIGURE 14. BFSC method for the linear transport. Test results of the uncertain cross-section and initial data in the diffusive scaling. The mean (left) and standard deviation (right) of the density  $\rho$ , obtained by  $M = 12$  high-fidelity runs and the sparse grid method with 2243 quadrature points (crosses, first row). The corresponding errors are reported in the second row,  $\varepsilon = 10^{-2}$ .

In the first test reported, we assume the random cross-section coefficient given by

$$(164) \quad \sigma(x, z) = 1 + 4 \sum_{i=1}^{d_z} \frac{1}{(i\pi)^2} \cos(2\pi i x) z_i,$$

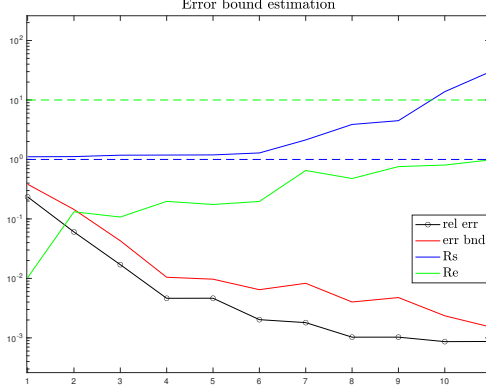


FIGURE 15. BFSC method for the linear transport. Error bound estimation in the diffusive scaling with uncertain cross-section and initial data.

with  $d = 5$ . Let also the uncertain initial data be

$$(165) \quad f_0(x, v, z) = \rho_0 \exp\left(-\left(\frac{v - 0.5}{T_0}\right)^2\right) + \rho_1 \exp\left(-\left(\frac{v + 0.75}{T_1}\right)^2\right),$$

where

$$\rho_0(x, z) = 1 + 3 \sum_{k=1}^{d_z} \frac{\sin(2\pi kx) z_k}{(k\pi)^2}, \quad T_0(x, z) = \frac{5 + 2 \cos(2\pi x)}{20} (1 + 0.6z_1),$$

$$\rho_1(x, z) = 1 + 2 \sum_{k=1}^{d_z} \frac{\cos(2\pi kx) z_k}{(k\pi)^2}, \quad T_1(x, z) = 0.5 + 0.2 \cos(2\pi x) z_2.$$

We use  $\Delta x = 0.025$ ,  $\Delta t = 10^{-4}$  for the high-fidelity solver, and  $\Delta x = 0.04$ ,  $\Delta t = 2 \times 10^{-4}$  for the low-fidelity solver. Numerical solutions and bi-fidelity errors at output time  $T = 0.02$  are shown in Figure 14. We observe that while the low-fidelity solution may miss details of the high-fidelity solution near the peaks, the mean and standard deviation of the bi-fidelity approximation agree well with the high-fidelity solution globally, when using  $M = 12$ . A fast exponential decay of bi-fidelity errors is suggested from Figure 15. With only 12 simulations for the high-fidelity AP solver, the bi-fidelity mean can reach the accuracy level of less than  $\mathcal{O}(10^{-4})$ . In Figure 15, the error estimators bound well the true bi-fidelity errors, with the values of both metrics  $R_e$  and  $R_s$  around less than 10.

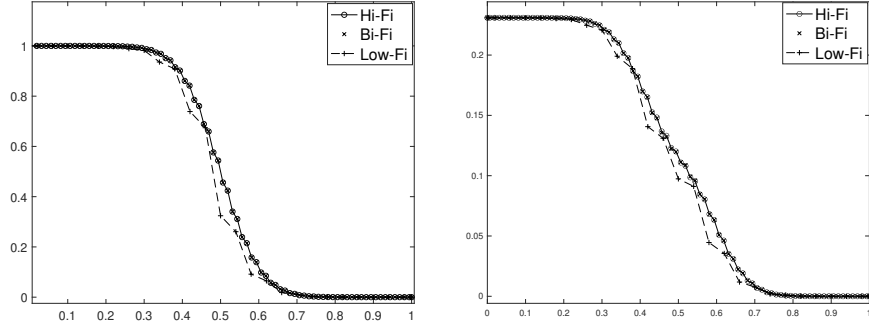


FIGURE 16. BFSC method for the linear transport. Results of the Riemann problem in the diffusive scaling. The mean (left) and standard deviation (right) of the density  $\rho$ , obtained by  $M = 12$  high-fidelity runs and the sparse grid method using 2243 quadrature points (crosses). Here  $\varepsilon = 10^{-8}$ .

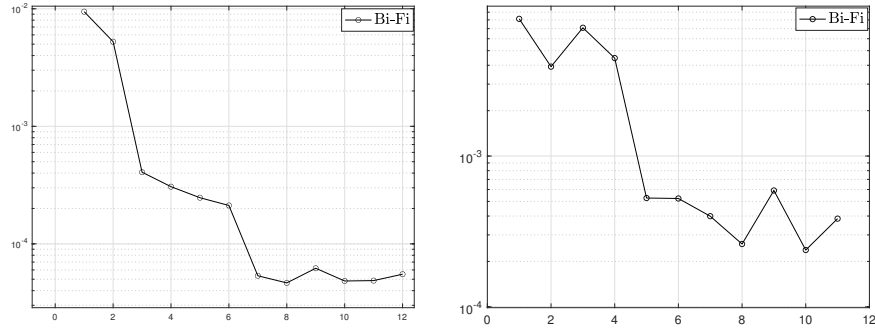


FIGURE 17. BFSC method for the linear transport. Results of the Riemann problem in the diffusive scaling. Errors of the bi-fidelity approximation mean (left) and standard deviation (right) of the density  $\rho$  with respect to the number of high-fidelity runs.

We now consider a Riemann problem. Let assume the same random coefficient (164) with boundary conditions

$$f(x = 0, t, v, z) = 1 + 0.4z_1, \quad \text{if } v \geq 0,$$

$$f(x = 1, t, v, z) = 0, \quad \text{if } v \leq 0,$$

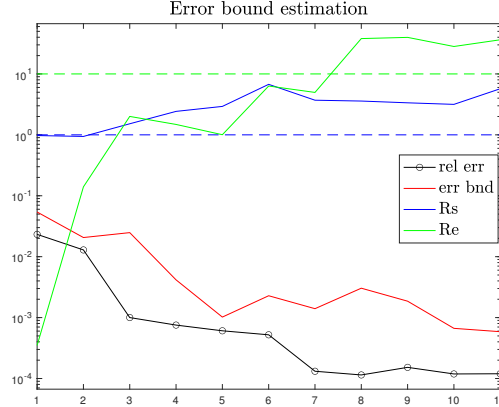


FIGURE 18. BFSC method for the linear transport. Error bound estimation for the Riemann problem in the diffusive scaling.

with uncertain initial distribution given by

$$f(x, t = 0, v, z) = 1 + 0.4z_1, \quad 0 \leq x < 0.5,$$

$$f(x, t = 0, v, z) = 0, \quad 0.5 \leq x \leq 1.$$

In this example, we let the output time  $T = 0.01$  and  $\varepsilon = 10^{-8}$ . We set  $\Delta t = 2 \times 10^{-4}$ ,  $\Delta x = 0.04$  in the low-fidelity solver, and  $\Delta t = 5 \times 10^{-5}$ ,  $\Delta x = 0.0125$  in the high-fidelity solver. The Figure 16 shows the numerical mean and standard deviation of the density  $\rho$  for  $\varepsilon = 10^{-8}$ . While the low-fidelity solutions are not able to capture the detailed information around the transition region, the bi-fidelity approximation agrees with the high-fidelity  $\rho$  at a quite satisfactory level. From Figure 17, it is obvious that the bi-fidelity errors decay fast with respect to the selected high-fidelity runs. With only  $M = 12$  high-fidelity simulation runs, the bi-fidelity errors for the mean and standard deviation of the density  $\rho$  reach as small as  $\mathcal{O}(10^{-4})$ . Based on Figure 18, the error estimators bound well the true bi-fidelity errors, with both metrics  $R_e$  and  $R_s$  around or less than 10. We also remark that further increasing the high-fidelity samples after  $M = 8$  will not help improving the quality of bi-fidelity approximation.

**4.4. BFSC method for kinetic epidemic models.** — We consider in this last example the quantification of uncertainty by using the bi-fidelity approach for the kinetic model of disease spread (32) introduced in Section 2.4.

The low-fidelity model, is based on considering individuals moving in two opposite directions (indicated by signs “+” and “-”), with velocities  $\pm\lambda_S$  for susceptible,  $\pm\lambda_I$  for infected and  $\pm\lambda_R$  for removed. This dynamics of the

population through the two-velocity epidemic model [7] is given by

$$(166) \quad \begin{aligned} \frac{\partial S^\pm}{\partial t} + \lambda_S \frac{\partial S^\pm}{\partial x} &= -F(S^\pm, I) \mp \frac{1}{2\tau_S} (S^+ - S^-) \\ \frac{\partial I^\pm}{\partial t} + \lambda_I \frac{\partial I^\pm}{\partial x} &= F(S^\pm, I) - \gamma I^\pm \mp \frac{1}{2\tau_I} (I^+ - I^-) \\ \frac{\partial R^\pm}{\partial t} + \lambda_R \frac{\partial R^\pm}{\partial x} &= \gamma I^\pm \mp \frac{1}{2\tau_R} (R^+ - R^-). \end{aligned}$$

In the above system, individuals  $S(x, t, z)$ ,  $I(x, t, z)$  and  $R(x, t, z)$  are defined as

$$S = S^+ + S^-, \quad I = I^+ + I^-, \quad R = R^+ + R^-.$$

The transmission of infection is governed by the same incidence function as in the high-fidelity model, defined by (33). The definition of the basic reproduction number  $R_0$  is the same as introduced in (34). The fluxes are now given by

$$(167) \quad J_S = \lambda_S (S^+ - S^-), \quad J_I = \lambda_I (I^+ - I^-), \quad J_R = \lambda_R (R^+ - R^-).$$

Then we derive a hyperbolic model equivalent to (166), while presenting a macroscopic description of propagation of the epidemic at finite speeds. In this system the fluxes satisfy

$$(168) \quad \begin{aligned} \frac{\partial J_S}{\partial t} + \lambda_S^2 \frac{\partial S}{\partial x} &= -F(J_S, I) - \frac{J_S}{\tau_S} \\ \frac{\partial J_I}{\partial t} + \lambda_I^2 \frac{\partial I}{\partial x} &= \frac{\lambda_I}{\lambda_S} F(J_S, I) - \gamma J_I - \frac{J_I}{\tau_I} \\ \frac{\partial J_R}{\partial t} + \lambda_R^2 \frac{\partial R}{\partial x} &= \frac{\lambda_R}{\lambda_I} \gamma J_I - \frac{J_R}{\tau_R}. \end{aligned}$$

Let us now consider the behavior of the low-fidelity model in the diffusive regime. To this aim, we introduce the diffusion coefficients

$$(169) \quad D_S = \lambda_S^2 \tau_S, \quad D_I = \lambda_I^2 \tau_I, \quad D_R = \lambda_R^2 \tau_R.$$

Its diffusion limit can be formally recovered by letting the relaxation times  $\tau_{S,I,R} \rightarrow 0$ . Under this scaling, (168) leads again to the parabolic reaction-diffusion system (38). We remark that the motivation of choosing (166) as our low-fidelity model in the bi-fidelity approximation is that it shares the same diffusion limit as the high-fidelity model. The only difference lies in the definition of two diffusion coefficients, as shown in (37) and (169).

In the following tests, we consider a 2-dimensional random vector  $\mathbf{z} = (z_1, z_2)^T$ , with independent random parameters  $z_1$  and  $z_2$  following a uniform distribution on  $[-1, 1]$ . To compute the reference solutions, we adopt a 3-rd level sparse grid quadrature based on Clenshaw-Curtis rules for the choice of

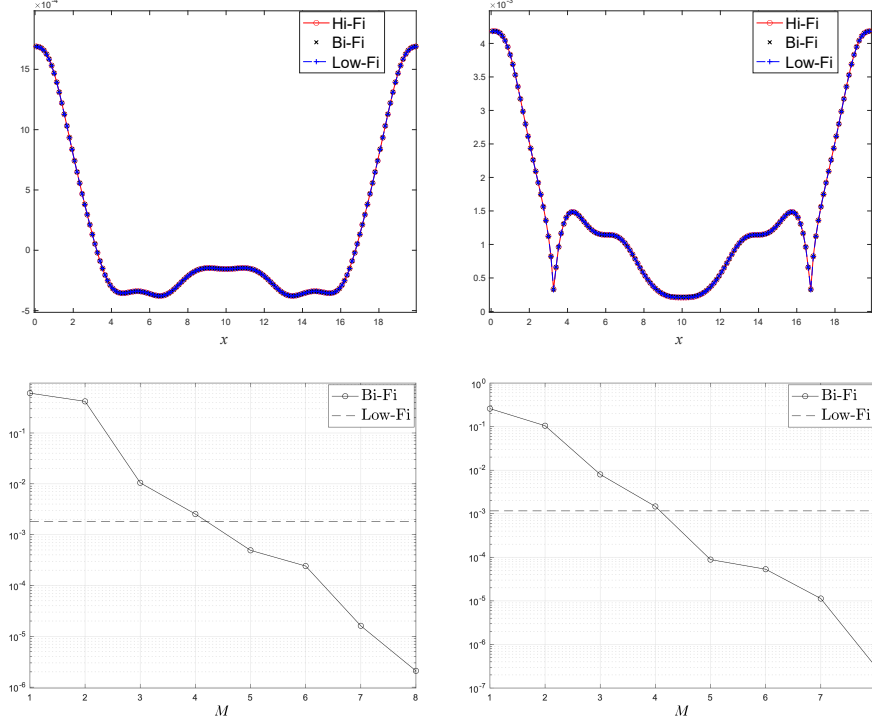


FIGURE 19. BFSC method for the kinetic SIR model. Results in the diffusive regime. First row: mean (left) and standard deviation (right) for the density  $I$ , by using  $M = 8$  high-fidelity runs. Second row: relative  $L^2$  errors of the bi-fidelity approximation.

the stochastic collocation nodes, with a total of 29 points, for both the high-fidelity and low-fidelity models. Let assume the initial distributions of the high-fidelity kinetic SIR model (32) as follows:

$$(170) \quad f_i(x, v, 0) = c i(x, 0) e^{-\frac{v^2}{2}}, \quad i \in \{S, I, R\}$$

where  $c = \frac{1}{2} \sum_{i=1}^{N_v} w_i e^{-\frac{\zeta_i^2}{2}}$  is a re-normalization constant, with  $N_v$  the number of Gauss-Legendre quadrature points used in velocity discretization. Let also the initial densities to be

$$S(x, 0) = 1 - I(x, 0), \quad I(x, 0) = 0.01e^{-(x-10)^2}, \quad R(x, 0) = 0,$$

with a physical domain  $L = [0, 20]$ . Let finally the initial fluxes  $J_S(x, 0)$ ,  $J_I(x, 0)$  and  $J_R(x, 0)$  be zeros and consider periodic boundary conditions. The same initial conditions for  $S, I, R$  and  $J_S, J_I, J_R$  are imposed in the low-fidelity SIR model (36)-(168), to make the two models consistent.



Concerning spatially heterogeneous environments, we assume the contact rate [7, 100] depends on space and contains uncertainties

$$\beta(x, z) = \beta^0(z) \left( 1 + 0.05 \sin \left( \frac{13\pi x}{20} \right) \right),$$

where

$$\beta^0(z) = 11(1 + 0.6z_1).$$

The uncertain recovery rate is given by

$$\gamma(z) = 10(1 + 0.4z_2).$$

In the incidence function, we set  $\kappa = 0$  and  $p = 1$ . For spatial and velocity discretizations we use  $N_x = 150$  in both the high-fidelity and low-fidelity models and  $N_v = 8$  for the high-fidelity model. In the first test, a parabolic configuration of speeds and relaxation parameters is considered. We let  $\lambda_i^2 = 10^5$ ,  $i \in \{S, I, R\}$ , and  $\tau_i = 10^{-5}$  in the low-fidelity model and  $\tau_i = 3 \times 10^{-5}$  in the high-fidelity model, to maintain consistency of the two simulations.

In the first row of Figure 19, the mean and standard deviation of the solution of compartment  $I$  for the high-fidelity model, the low-fidelity model and the bi-fidelity approximation at time  $t = 5$  are shown. Since the high-fidelity and low-fidelity model share the same diffusive limit, a perfect agreement of the solutions are observed. In the second row, we plot the relative  $L^2$  errors of the mean and standard deviation between the bi-fidelity and high-fidelity solutions at  $t = 5$ , with respect to the number of selected important points of the bi-fidelity algorithm. A fast error decay is clearly observed. One can conclude that with only 8 hi-fidelity sample points, bi-fidelity approximation is able to achieve a relative error of  $\mathcal{O}(10^{-6})$  for both the mean and standard deviation. In the second test case, we consider the hyperbolic regime for  $\lambda_i = 1$ ,  $i \in \{S, I, R\}$ , with  $\tau_i = 1$  in the low-fidelity model and  $\tau_i = 3$  in the high-fidelity model. We plot the results in Figure 20. Similar conclusions can be drawn as in the previous case.

## 5. Conclusions

In this survey we have discussed some recent developments in the field of multi-fidelity methods for kinetic equations with uncertain factors. To emphasize the wide range of applicability of the various techniques we adopted a model oriented presentation ranging from classical rarefied gas dynamics and transport theory to socio-economic modelling and epidemiology. Here we have focused essentially on two main classes of methods for uncertainty propagation: multi-fidelity methods based on control variates and bi-fidelity stochastic collocation methods. The main guideline in the development of the corresponding low-fidelity models is given by the classical legacy of fluid-dynamic and diffusive

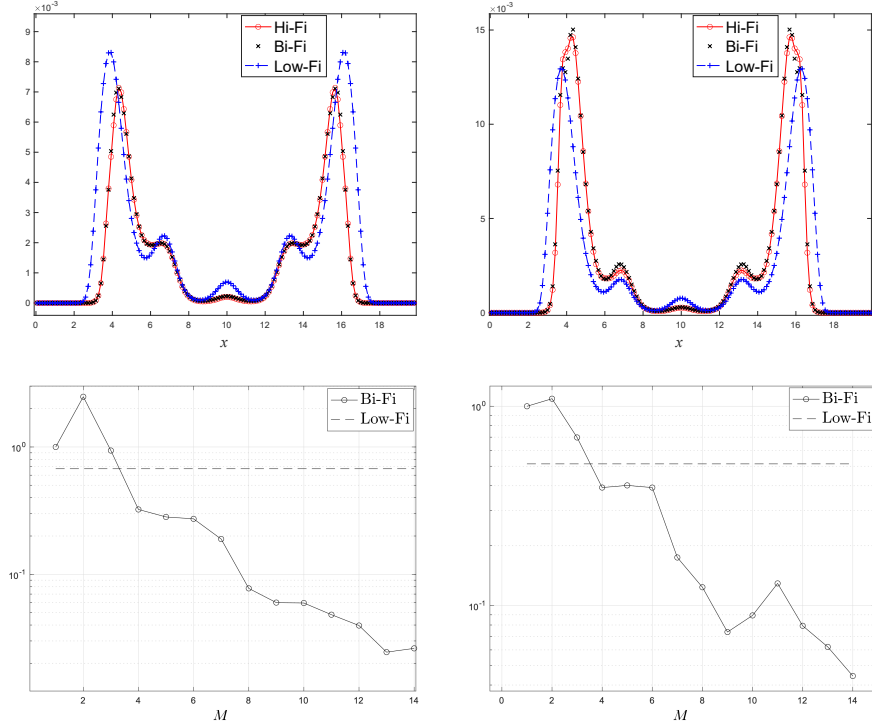


FIGURE 20. BFSC method for the kinetic SIR model. Results in the hyperbolic regime. First row: mean (left) and standard deviation (right) for the density  $I$ , by using  $M = 8$  high-fidelity runs. Second row: relative  $L^2$  errors of the bi-fidelity approximation.

limits in kinetic theory. In particular, this allows appropriate error estimates to be placed alongside the various methods and to identify regimes in which the statistical error vanishes.

There are numerous open problems of great interest for future research. Among these we mention the use of low-fidelity models capable of covering a broader spectrum than classical fluid dynamics, such as the moment equations of extended thermodynamics in gasdynamics [95]. In addition to the problem of determining appropriate low-fidelity models in other areas of application where kinetic equations play a relevant role, e.g. plasma physics [101], an important challenge is to move beyond methods that focus exclusively on models. Among these, the inclusion of information from experimental data and other information sources, and their fusion with computational models is certainly one of the main challenges [51, 80].

**Acknowledgements.** — This work has been written within the activities of GNCS and GNFM groups of INdAM (National Institute of High Mathematics). G.D. and L.P. acknowledge the partial support of MIUR-PRIN Project 2017, No. 2017KKJP4X “Innovative numerical methods for evolutionary partial differential equations and applications”. L.L. holds the Direct Grant for Research supported by Chinese University of Hong Kong and Early Career Scheme 2021/22, No. 24301021, from Research Grants Council of Hong Kong. X. Zhu was supported by the Simons Foundation (504054).

### References

- [1] G. ALBI, G. BERTAGLIA, W. BOSCHERI, G. DIMARCO, L. PARESCHI, G. TOSCANI, AND M. ZANELLA, *Kinetic modelling of epidemic dynamics: social contacts, control with uncertain data, and multiscale spatial dynamics*, in Predicting Pandemics in a Globally Connected World, Vol.1 (to appear), N. Bellomo and M. Chaplain, eds., Modeling and Simulation in Science, Engineering, and Technology, Birkhäuser-Springer, New York, 2022.
- [2] G. ALBI, L. PARESCHI, G. TOSCANI, AND M. ZANELLA, *Recent advances in opinion modeling: control and social influence*, in Active Particles, Volume 1: Advances in Theory, Models, and Applications, N. Bellomo, P. Degond, and E. Tadmor, eds., Birkhäuser, Cham, 2017, pp. 49–98.
- [3] G. ALBI, L. PARESCHI, AND M. ZANELLA, *Uncertainty quantification in control problems for flocking models*, Math. Probl. Eng., (2015), pp. 1–14.
- [4] C. BARDOS, R. SANTOS, AND R. SENTIS, *Diffusion approximation and computation of the critical size*, Trans. Amer. Math. Soc., 284 (1984), pp. 617–649.
- [5] G. BERTAGLIA, W. BOSCHERI, G. DIMARCO, AND L. PARESCHI, *Spatial spread of COVID-19 outbreak in Italy using multiscale kinetic transport equations with uncertainty*, Math. Biosci. Eng., 18 (2021), pp. 7028–7059.
- [6] G. BERTAGLIA, L. LIU, L. PARESCHI, AND X. ZHU, *Bi-fidelity stochastic collocation methods for epidemic transport models with uncertainties*, preprint arXiv:2110.14579, (2021).
- [7] G. BERTAGLIA AND L. PARESCHI, *Hyperbolic models for the spread of epidemics on networks: kinetic description and numerical methods*, ESAIM Math. Model. Numer. Anal., 55 (2021), pp. 381–407.
- [8] P. BHATNAGAR, E. GROSS, AND M. KROOK, *A model for collision processes in gases I: Small amplitude processes in charged and neutral one-component systems*, Phys. Rev., 94 (1954).
- [9] G. BIRD, *Direct simulation and the Boltzmann equation*, The Physics of Fluids, 13 (1970), pp. 2676–2681.
- [10] W. BOSCHERI, G. DIMARCO, AND L. PARESCHI, *Modeling and simulating the spatial spread of an epidemic through multiscale kinetic transport equations*, Math. Mod. Meth. App. Scie., 31 (2021), pp. 1059–1097.

- [11] M. BRIANT, *From the Boltzmann equation to the incompressible Navier-Stokes equations on the torus: a quantitative error estimate*, J. Differential Equations, 259 (2015), pp. 6072–6141.
- [12] R. E. CAFLISCH, *Monte Carlo and Quasi Monte Carlo methods*, Acta Numerica, 7 (1998), pp. 1–49.
- [13] J. A. CARRILLO, J. HU, L. WANG, AND J. WU, *A particle method for the homogeneous Landau equation*, J. Comput. Phys. X, 7 (2020), pp. 100066, 24.
- [14] J. A. CARRILLO, L. PARESCHI, AND M. ZANELLA, *Particle based gPC methods for mean-field models of swarming with uncertainty*, Comm. Comp. Phys, 25 (2018), pp. 508–531.
- [15] C. CERCIGNANI, *The Boltzmann Equation and its applications*, Springer-Verlag, New York Inc, (1988).
- [16] ———, *Rarefied Gas Dynamics: From Basic Concepts to Actual Calculations*, Cambridge Texts in Applied Mathematics, Cambridge University Press, 2000.
- [17] A. COHEN AND R. DEVORE, *Approximation of high-dimensional parametric PDEs*, Acta Numer., 24 (2015), pp. 1–159.
- [18] S. CORDIER, L. PARESCHI, AND G. TOSCANI, *On a kinetic model for a simple market economy*, J. Stat. Phys., 120 (2005), pp. 253–277.
- [19] E. S. DAUS, S. JIN, AND L. LIU, *On the multi-species Boltzmann equation with uncertainty and its stochastic Galerkin approximation*, ESAIM Math. Model. Numer. Anal., 55 (2021), pp. 1323–1345.
- [20] P. DEGOND, L. PARESCHI, AND G. RUSSO, eds., *Modeling and computational methods for kinetic equations*, Modeling and Simulation in Science, Engineering and Technology, Birkhäuser Boston Inc., Boston, MA, 2004.
- [21] G. DIMARCO, R. LOUBÉRE, J. NARSKI, AND T. REY, *An efficient numerical method for solving the Boltzmann equation in multidimensions*, J. Comp. Phys, 353 (2018), pp. 46–81.
- [22] G. DIMARCO AND L. PARESCHI, *Numerical methods for kinetic equations*, Acta Numerica 23, (2014), pp. 369–520.
- [23] ———, *Multi-scale control variate methods for uncertainty quantification in kinetic equations*, J. Comput. Phys, 388 (2019), pp. 63–89.
- [24] ———, *Multi-scale variance reduction methods based on multiple control variates for kinetic equations with uncertainties*, Multiscale Model Simul., 18 (2020), pp. 351–382.
- [25] ———, *A Navier-Stokes based control variate method for the Boltzmann equation*, private report, unpublished, 2021.
- [26] G. DIMARCO, L. PARESCHI, AND M. ZANELLA, *Uncertainty quantification for kinetic models in socio-economic and life sciences*, in Uncertainty quantification for hyperbolic and kinetic equations, vol. 14 of SEMA SIMAI Springer Ser., Springer, Cham, 2017, pp. 151–191.
- [27] M. G. FERNÁNDEZ-GODINO, C. PARK, N.-H. KIM, AND R. T. HAFTKA, *Review of multi-fidelity models*, arXiv preprint arXiv:1609.07196, (2016).

- [28] F. FILBET AND S. JIN, *A class of asymptotic-preserving schemes for kinetic equations and related problems with stiff sources*, J. Comput. Phys., 229 (2010), pp. 7625–7648.
- [29] F. FILBET, C. MOUHOT, AND L. PARESCHI, *Solving the Boltzmann equation in  $N \log_2 N$* , SIAM J. Sci. Comput., 28 (2006), pp. 1029–1053.
- [30] I. M. GAMBA, S. JIN, AND L. LIU, *Error estimate of the bi-fidelity method for kinetic equations with random parameters and different scalings*, Int. J. Uncertainty. Quant., 11 (2021), pp. 57–75.
- [31] I. M. GAMBA AND S. H. THARKABHUSHANAM, *Spectral-Lagrangian methods for collisional models of non-equilibrium statistical states*, J. Comput. Phys., 228 (2009), pp. 2012–2036.
- [32] H. GAO, X. ZHU, AND J. WANG, *A bi-fidelity surrogate modeling approach for uncertainty propagation in three-dimensional hemodynamic simulations*, Comput. Methods Appl. Mech. Engrg., 366:113047 (2020), p. 23.
- [33] M. B. GILES, *Multilevel Monte Carlo methods*, Acta Numerica 23, 24 (2015), pp. 259–328.
- [34] S. GOLDSTEIN, *On diffusion by discontinuous movements, and on the telegraph equation*, Quart. J. Mech. Appl. Math, 4 (1951), pp. 129–156.
- [35] G. H. GOLUB AND C. F. V. LOAN, *Matrix computations*, 3rd ed., Johns Hopkins, (1996).
- [36] D. GOTTLIEB AND D. XIU, *Galerkin method for wave equations with uncertain coefficients*, Commun. Comput. Phys, 3 (2008), pp. 505–518.
- [37] J. M. HAMMERSLEY AND D. C. HANDSCOMB, *Monte Carlo methods*, Methuen & Co., London, and John Wiley & Sons, New York, (1964).
- [38] H. W. HETHCOTE, *The mathematics of infectious diseases*, SIAM Rev., 42 (2000), pp. 599–653.
- [39] L. H. HOLWAY, *New statistical models for kinetic theory: methods of construction*, Phys Fluid, 9 (1966), pp. 1658–1673.
- [40] J. HU AND S. JIN, *A stochastic Galerkin method for the Boltzmann equation with uncertainty*, J. Comp. Phys, 315 (2016), pp. 150–168.
- [41] J. HU, L. PARESCHI, AND Y. WANG, *Uncertainty quantification for the BGK model of the Boltzmann equation using multilevel variance reduced Monte Carlo methods*, SIAM/ASA J. Uncertain. Quantif., 9 (2021), pp. 650–680.
- [42] J. HU AND K. QI, *A fast Fourier spectral method for the homogeneous Boltzmann equation with non-cutoff collision kernels*, J. Comput. Phys., 423 (2020), pp. 109806, 21.
- [43] J. HU, J. SHEN, AND Y. WANG, *A Petrov-Galerkin spectral method for the inelastic Boltzmann equation using mapped Chebyshev functions*, Kinet. Relat. Models, 13 (2020), pp. 677–702.
- [44] G. JIANG AND C.-W. SHU, *Efficient implementation of weighted eno schemes*, J. Comp. Phys, 126 (1996), pp. 202–228.

- [45] S. JIN, H. LU, AND L. PARESCHI, *Efficient stochastic asymptotic-preserving implicit-explicit methods for transport equations with diffusive scalings and random inputs*, SIAM J Sci. Comput., 40 (2018), pp. 671–696.
- [46] S. JIN AND L. PARESCHI, eds., *Uncertainty quantification for hyperbolic and kinetic equations*, vol. 14 of SEMA-SIMAI Springer Series, Springer, 2017.
- [47] S. JIN, L. PARESCHI, AND G. TOSCANI, *Diffusive relaxation schemes for multiscale discrete-velocity kinetic equations*, SIAM J. Numer. Anal, 35 (1998), pp. 2405–2439.
- [48] ———, *Uniformly accurate diffusive relaxation schemes for multiscale transport equations*, SIAM J. Numer. Anal, 38 (2000), pp. 913–936.
- [49] E. W. LARSEN AND J. B. KELLER, *Asymptotic solution of neutron transport problems for small mean free paths*, J. Mathematical Phys, 15 (1974), pp. 75–81.
- [50] R. J. LEVEQUE, *Numerical Methods for Conservation Laws*, Birkhäuser, 1992.
- [51] Y. LI, F. P. ZHANG, Y. YAN, J. H. ZHOU, AND Y. F. LI, *Multi-source uncertainty considered assembly process quality control based on surrogate model and information entropy*, Struct. Multidiscip. Optim., 59 (2019), pp. 1685–1701.
- [52] P. L. LIONS AND G. TOSCANI, *Diffusive limit for finite velocity Boltzmann kinetic models*, Rev. Mat. Iberoamericana, 13 (1997), pp. 473–513.
- [53] L. LIU AND S. JIN, *Hypocoercivity based sensitivity analysis and spectral convergence of the stochastic Galerkin approximation to collisional kinetic equations with multiple scales and random inputs*, Multiscale Model. Simul., 16 (2018), pp. 1085–1114.
- [54] L. LIU, L. PARESCHI, AND X. ZHU, *A bi-fidelity stochastic collocation method for transport equations with diffusive scaling and multi-dimensional random inputs*, preprint, (2021).
- [55] L. LIU AND X. ZHU, *A bi-fidelity method for the Boltzmann equation with random parameters and multiple scales*, J. Comput. Phys, 402 (2020), p. 108914.
- [56] M. LOËVE, *Probability theory i*, 4th edition, Springer Verlag, (1977).
- [57] O. L. MAITRE AND O. M. KNIO, *Spectral methods for uncertainty quantification: with applications to computational fluid dynamics*, Scientific Computation, Springer Netherlands, (2010).
- [58] L. MIEUSSENS, *Discrete velocity model and implicit scheme for the BGK equation of rarefied gas dynamics*, Math Mod. Meth. Appl Sci, 10 (2000), pp. 1121–1149.
- [59] S. MISHRA AND C. SCHWAB, *Monte-Carlo finite-volume methods in uncertainty quantification for hyperbolic conservation laws*, in Uncertainty quantification for hyperbolic and kinetic equations, vol. 14 of SEMA SIMAI Springer Ser., Springer, Cham, 2017, pp. 231–277.
- [60] S. MISHRA, C. SCHWAB, AND J. ŠUKYS, *Multi-level Monte Carlo finite volume methods for nonlinear systems of conservation laws in multi-dimensions*, J. Comp. Phys., 231 (2012), pp. 3365–3388.

- [61] C. MOUHOT AND L. PARESCHI, *Fast algorithms for computing the Boltzmann collision operator*, Math Comp., 75 (2006), pp. 1833–1852.
- [62] C. MOUHOT AND L. PARESCHI, *Fast algorithms for computing the Boltzmann collision operator*, Math. Comp., 75 (2006), pp. 1833–1852.
- [63] R. MUNIPALLI, J. HAMILTON, AND X. ZHU, *A multifidelity approach to parameter dependent modeling of combustion instability*, 2018 Joint Propulsion Conference, (2018), p. 4557.
- [64] G. NALDI, L. PARESCHI, AND G. TOSCANI, eds., *Mathematical Modeling of Collective Behavior in Socio-Economic and Life Sciences*, Modeling and Simulation in Science, Engineering and Technology, Springer, 2010.
- [65] K. NANBU, *Direct simulation scheme derived from the Boltzmann equation I: Monocomponent gases*, Journal of the Physical Society of Japan, 49 (1980), pp. 2042–2049.
- [66] A. NARAYAN, C. GITTELSON, AND D. XIU, *A stochastic collocation algorithm with multifidelity models*, SIAM J. Sci. Comput., 36 (2014), p. 2.
- [67] F. NOBILE, R. TEMPONE, AND C. G. WEBSTER, *A sparse grid stochastic collocation method for partial differential equations with random input data*, SIAM J. Num. Anal., 46 (2008), pp. 2309–2345.
- [68] L. PARESCHI, *Hybrid multiscale methods for hyperbolic and kinetic problems*, ESAIM: Proc., 15 (2005), pp. 87–120.
- [69] L. PARESCHI, *An introduction to uncertainty quantification for kinetic equations and related problems*, in Trails in kinetic theory, vol. 25 of SEMA SIMAI Springer Ser., Springer, Cham, 2021, pp. 141–181.
- [70] L. PARESCHI AND G. RUSSO, *Numerical solution of the Boltzmann equation. I. Spectrally accurate approximation of the collision operator*, SIAM J. Numer. Anal., 37 (2000), pp. 1217–1245.
- [71] —, *An introduction to Monte Carlo method for the Boltzmann equation*, ESAIM: Proceedings, EDP Sciences, 10 (2001), pp. 35–75.
- [72] —, *An introduction to the numerical analysis of the Boltzmann equation*, Riv. Mat. Univ. Parma (7), 4\*\* (2005), pp. 145–250.
- [73] L. PARESCHI AND G. TOSCANI, *Self-similarity and power-like tails in nonconservative kinetic models*, Journal of statistical physics, 124 (2006), pp. 747–779.
- [74] —, *Interacting Multiagent Systems: Kinetic Equations and Monte Carlo Methods*, Oxford University Press, 2013.
- [75] L. PARESCHI, G. TOSCANI, A. TOSIN, AND M. ZANELLA, *Hydrodynamic models of preference formation in multi-agent societies*, J. Nonlin. Sci, 29 (2019), pp. 2761–2796.
- [76] L. PARESCHI, T. TRIMBORN, AND M. ZANELLA, *Mean-field control variate methods for kinetic equations with uncertainties and applications to socio-economic sciences*, Int. J. Uncertainty. Quant., 2021. to appear.

- [77] L. PARESCHI AND M. ZANELLA, *Structure-preserving schemes for nonlinear Fokker-Planck equations and applications*, Journal of Scientific Computing, 74 (2018), pp. 1575–1600.
- [78] ———, *Monte Carlo stochastic Galerkin methods for the Boltzmann equation with uncertainties: Space-homogeneous case*, Journal of Computational Physics, (2020), p. 423:109822.
- [79] C. PARK, R. T. HAFTKA, AND N. H. KIM, *Remarks on multi-fidelity surrogates*, Structural and Multidisciplinary Optimization, 55 (2017), pp. 1029–1050.
- [80] B. PEHERSTORFER, K. WILLCOX, AND M. GUNZBURGER, *Survey of multifidelity methods in uncertainty propagation, inference, and optimization*, SIAM Review, 60 (2018), pp. 550–591.
- [81] D. J. PERRY, R. M. KIRBY, A. NARAYAN, AND R. T. WHITAKER, *Allocation strategies for high fidelity models in the multifidelity regime*, SIAM/ASA J. Uncertain. Quantif., 7 (2019), pp. 203–231.
- [82] B. PERTHAME AND M. PULVIRENTI, *Weighted  $L_\infty$  bounds and uniqueness for the Boltzmann BGK model*, Arch. Rat. Mech. Anal., 125 (1993), pp. 289–295.
- [83] P. PETTERSSON, G. IACCARINO, AND J. NORDSTRÖM, *Polynomial Chaos Methods for Hyperbolic Partial Differential Equations: Numerical Techniques for Fluid Dynamics Problems in the Presence of Uncertainties*, Mathematical Engineering, Springer, 2015.
- [84] G. POËTTE, *A gPC-intrusive Monte-Carlo scheme for the resolution of the uncertain linear Boltzmann equation*, J. Comput. Phys., 385 (2019), pp. 135–162.
- [85] ———, *A gPC-intrusive Monte-Carlo scheme for the resolution of the uncertain linear Boltzmann equation*, J. Comput. Phys., 385 (2019), pp. 135–162.
- [86] ———, *Spectral convergence of the generalized polynomial chaos reduced model obtained from the uncertain linear Boltzmann equation*, Math. Comput. Simulation, 177 (2020), pp. 24–45.
- [87] G. POËTTE, B. DESPRÉS, AND D. LUCOR, *Uncertainty quantification for systems of conservation laws*, J. Comp. Phys, 228 (2009), pp. 2443–2467.
- [88] S. RJASANOW AND W. WAGNER, *Stochastic Numerics for the Boltzmann Equation*, vol. 37 of Computational Mathematics, Springer, 2005.
- [89] W. RUDIN, *Real and complex analysis*, Mladinska Knjiga, McGraw-Hill, (1970).
- [90] G. RUSSO, P. SANTAGATI, AND S. YUN, *Convergence of a semi-lagrangian scheme for the BGK model of the Boltzmann equation*, SIAM J. Numer. Anal, 50 (2012), pp. 1111–1135.
- [91] C.-W. SHU, *Essentially non-oscillatory and weighted essentially non-oscillatory schemes*, Acta Numerica, 29 (2020), p. 701–762.
- [92] R. SHU, J. HU, AND S. JIN, *A stochastic Galerkin method for the Boltzmann equation with multi-dimensional random inputs using sparse wavelet bases*, Num. Math.: Theory, Methods and Applications (NMTMA), 10 (2017), pp. 465–488.



- [93] E. SONNENDRUCKER, *Numerical methods for Vlasov equations*, Technical report, MPI TU Munich, (2013).
- [94] G. I. TAYLOR, *Diffusion by continuous movements*, Proc. London Math, 20 (1921), pp. 196–212.
- [95] M. TORRILHON, *Modeling nonequilibrium gas flow based on moment equations*, in Annual review of fluid mechanics. Vol. 48, vol. 48 of Annu. Rev. Fluid Mech., Annual Reviews, Palo Alto, CA, 2016, pp. 429–458.
- [96] G. TOSCANI, *Entropy production and the rate of convergence to equilibrium for the Fokker-Planck equation*, Quarterly of Applied Mathematics, LVII(3) (1999), pp. 521–541.
- [97] G. TOSCANI AND C. VILLANI, *Sharp entropy dissipation bounds and explicit rate of trend to equilibrium for the spatially homogeneous Boltzmann equation*, Communications in Mathematical Physics, 203(3) (1999), pp. 667–706.
- [98] I. TRISTANI, *Exponential convergence to equilibrium for the homogeneous Boltzmann equation for hard potentials without cut-off*, Journal of Statistical Physics, 157(3) (2014), pp. 474–496.
- [99] C. VILLANI, *A review of mathematical topics in collisional kinetic theory*, in S. D. S. E. Friedlander, ed., Handbook of Mathematical Fluid Mechanics, Vol. I, p., North-Holland, 2002, pp. 71–305.
- [100] J. WANG, F. XIE, AND T. KUNIYA, *Analysis of a reaction-diffusion cholera epidemic model in a spatially heterogeneous environment*, Commun. Nonlinear Sci. Numer. Simul., 80 (2020), p. 104951.
- [101] T. XIAO AND M. FRANK, *A stochastic kinetic scheme for multi-scale plasma transport with uncertainty quantification*, J. Comput. Phys., 432 (2021), pp. Paper No. 110139, 32.
- [102] D. XIU, *Numerical methods for stochastic computations*, Princeton University Press, (2010).
- [103] D. XIU AND J. S. HESTHAVEN, *High-order collocation methods for differential equations with random inputs*, SIAM J. Sci. Comput., 27 (2005).
- [104] C. ZHANG AND I. M. GAMBA, *A conservative discontinuous Galerkin solver for the space homogeneous Boltzmann equation for binary interactions*, SIAM J. Numer. Anal., 56 (2018), pp. 3040–3070.
- [105] X. ZHU, E. LINEBARGER, AND D. XIU, *Multi-fidelity stochastic collocation method for computation of statistical moments*, Journal of Computational Physics, 341 (2017), pp. 386–396.
- [106] X. ZHU, A. NARAYAN, AND D. XIU, *Computational aspects of stochastic collocation with multifidelity models*, SIAM/ASA J. Uncertain. Quantif., 2 (2014), pp. 444–463.
- [107] X. ZHU AND D. XIU, *A multi-fidelity collocation method for time-dependent parameterized problems*, In 19th AIAA Non-Deterministic Approaches Conference, 1094 (2017).

- [108] Y. ZHU AND S. JIN, *The Vlasov-Poisson-Fokker-Planck system with uncertainty and a one-dimensional asymptotic-preserving method*, SIAM Multiscale Model Simul., 15 (2017), pp. 1502–1529.

---

GIACOMO DIMARCO, Department of Mathematics and Computer Science, University of Ferrara, Via Machiavelli 30, Ferrara, 44121, Italy  
*E-mail* : `giacomo.dimarco@unife.it`

LIU LIU, Department of Mathematics, The Chinese University of Hong Kong, Shatin, N.T., Hong Kong SAR • *E-mail* : `lliu@math.cuhk.edu.hk`

LORENZO PARESCHI, Department of Mathematics and Computer Science, University of Ferrara, Via Machiavelli 30, Ferrara, 44121, Italy  
*E-mail* : `lorenzo.pareschi@unife.it`

XUEYU ZHU, Department of Mathematics, University of Iowa, Iowa City, IA 52242, USA  
*E-mail* : `xueyuzhu@uiowa.edu`